Ectopic expression of the sialic acid modifying enzyme CMAH in human THP1 macrophages

Dissertation

zur

Erlangung des Doktorgrades (Dr. rer. nat.)

der

Mathematisch-Naturwissenschaftlichen Fakultät

der

Rheinischen Friedrich-Wilhelms-Universität Bonn

vorgelegt von

Ozkan Is

aus

Tekirdag, Turkei

Bonn, February 2018

Angefertigt mit Genehmigung der Mathematisch-Naturwissenschaftlichen Fakultät der
Rheinischen Friedrich-Wilhelms-Universität Bonn

1. Gutachter*: Prof. Dr. Harald Neumann*

2. Gutachter*: Prof. Dr. Walter Witke*

Tag der Promotion: 21.08.2018

Erscheinungsjahr: 2018

Table of Contents

ABBREVIATIONS

AD	Alzheimer's disease
Aβ	Amyloid β
APP	Amyloid precursor protein
ARPE	Retinal pigment epithelial cells
$CaCl_2$	Calcium chloride
CD	Cluster of differentiation
CD33KO	CD33 knockout macrophages
CD33KO GFP	Empty vector transduced CD33KO macrophages
CD33KO CMAH	CMAH expressing CD33KO macrophages
CD64	Fcγ receptor I alpha chain
CMAH	Cytidine monophosphate N-acetylneuraminic acid hydroxylase
CNS	Central nervous system
CR1	Complement receptor 1
CSF	Cerebrospinal fluid
DHE	Dihydroethidium
DMSO	Dimethyl sulfoxide
dNTP	Nucleoside triphosphates containing deoxyribose
E	Embryonic
EDTA	Ethylenediaminetetraacetic acid
FCS	Fetal calf serum
GM-CSF	Granulocyte-macrophage colony stimulating factor
GWAS	Genome-wide association studies
HCl	Hydrochloric acid
H_2SO_4	Sulfuric acid
Ig	Immunoglobulin
IL	Interleukin
ITAM	Immunoreceptor tyrosine-based activatory motif
ITIM	Immunoreceptor tyrosine-based inhibitory motif
KCl	Potassium chloride
Kdn	Ketodeoxynonulosonic acid
LPS	Lipopolysaccharide
LB	Lysogeny broth
ManNAc	N-acetylmannosamine
MS	Multiple sclerosis
NaCl	Sodium chloride
$NaH_2PO_4*H_2O$	Sodiumhydrogenphosphate
$NaH_2PO_4*7H_2O$	Sodiumhydrogenphosphate

NaOH	Sodium hydroxide
Neu5Ac	N-acetlyneuraminic acid
Neu5Gc	N-glycolylneuraminic acid
OH	Hydroxyl
P	Postnatal
Pen/Strep	Penicilin/streptomycin
PLL	Poly-L-lysine
PMA	Phorbol-12-myristate-13-acetate
PS	Parkinson's disease
PS1	Presenilin
RAGE	Receptor for advanced glycosylation end products
ROS	Reactive oxygen species
SHP	SH2-containing tyrosine phosphatase
SIGLEC	Sialic acid-binding immunoglobulun-like lectins
TLR	Toll-like receptors
TNFα	Tumor necrosis factor α
TREM2	Triggering receptor expressed on myeloid cells 2
TRIS	Trisaminomethane
WT	Wild type
WT GFP	Empty vector transduced wild type macrophages
WT CMAH	CMAH expressing wild type macrophages

FIGURES AND TABLES

1. INTRODUCTION

1.1 Human Brain and Central Nervous System

Brain is one of the most sophisticated and complex organs in the animal kingdom. It comprises more than 86 billion neurons [1], and several supporting cells which are called glia cells [2]. Neurons in brain organize to form neural circuits enabling to process different kind of sensory information, with the help of glial cells. One type of glial cells, the astrocytes, perform optimization of neuronal environment by maintaining ion and pH balance, clearing waste, and delivering oxygen and glucose to neurons while another type of glial cells, the oligodendrocytes, improve conduction of electrochemical signals by insulating neuronal axons within fatty substance called myelin. On the other hand, another glial cell population with myeloid origin, called microglia, perform immune surveillance and modulate several immune functions in central nervous system (CNS). Thus, brain disorders are caused not only by improper functioning of neurons, but also lack of activity of any of these glial cells.

1.2 Alzheimer's Disease

Alzheimer's disease (AD) is one of the well-known brain disorders affecting more than 46 million people worldwide [3]. AD is difficult to diagnose and there is no treatment available for the disease. Current therapeutics available in market for AD are mostly symptomatic. AD patients require constant care and the cost of AD is increasing day by day. In 2015, the worldwide cost of AD reached USD 818 billion [3]. Since age is the most crucial factor for AD occurence, the rate of getting the disease doubles in every 5 years after age of 65 [4]. The most common form of AD is sporadic (caused by particular genetic changes), it has the late onset, and it does not demonstrate Mendelian pattern of inheritance [5].Thus, complexity of gene function can be attributed to AD progression rather than gene transmission [6]. The pathological hallmarks of AD are accumulation of cerebral plaques of β-amyloid peptide (Aβ), dystrophic neurites and

neurofibrillary tangles in medial-temporal lobe.[7] Furthermore, pathology of AD is characterized by inflammation which is led by brain intrinsic immune cells, the microglia. [8]

AD seems to be multifactorial. The curent and most accepted theory, the 'amyloid hypothesis', suggests that in the context of failing protection and compensation mechanisms in the aging brain, accumulation of the Aβ peptide aggregates induces several pathophysiological changes that ultimately lead to cognitive dysfunction [9]. Aβ is produced from amyloid precusor protein (APP) through sequencially cleaveage by two membrane-bound secretases (β-and γ -secretases) [10].

Although immune system activation is common in neuroinflammatory diseases such as multiple sclerosis (MS) or neurodegenerative diseases, such as AD and Parkinson's Disease (PD), important differences among these disease types are observed. The main difference with respect to immune system alterations in these diseases is the type of adaptive immune cells involved. While adaptive T and B lymphocytes are involved in MS [11]; microglia, perivascular macrophages, and astrocytes are the main effector cells in AD [12]. Moreover, initiating factors also differ among these disease types as protein misfolding triggers AD and PD, while aberrations in T cell autoimmunity is responsible in MS [13].

Recent preclinical, genetic and bioinformatics findings demonstrated that immune activation does not only accompany protein misfolding but also could contribute to disease progression [14]. Some studies even point out much earlier involvement of inflammation [8,15]. In some instances, systemic immune challenges were demonstrated to drive AD-like pathology (Aβ plaques, tau protein aggregation and microglia activation) in wild type mice [16].

1.3 Microglia

1.3.1 Discovery, Localization and Distribution of Microglia

Microglia, the resident immune cells of CNS, were first identified by Rudolf Virchow (1821-1902) owing to its distinct morphology from neurons. He first described them as connective tissue cells which have the functions of repairing injuired tissue and supporting neurons. The discrimination of microglia from other glia cells was performed by Rio-Hortega in early 1900s by silver staining. Rio-Hortega also postulated the mesodermal origin of microglia [17]. However, more recently, it has now been very well established that microglia arise from yolk sac primitive macrophages, which persist in the CNS into adulthood as discussed further [18–20].

Distribution of microglia cells is not homogeneous through the brain and they are encountered less in grey matter than white matter [21]. Microglia population represents 0.5% to 16.6% of the total of cells in the brain in humans, showing similar regional variability as that of rodents [22]. Microglia and macrophages represent important part of innate immune system of brain [23]. Both microglia and macrophages are the resident tissue mononuclear phagocytes and share several functions, including phagocytosis, production of reactive oxygen and nitrogen species, and capability to respond to chemokines and purinergic stimuli [24]. Like macrophages, microglia survey the brain environment for pathogens and provide support CNS homeostasis and plasticity by guarding and remodeling synapses [25]. Even though the origin of microglia has been debated for so long, the present commonly accepted hypothesis supports a first wave of migration from the yolk sac (YS). These microglia precursor cells populate the future CNS around E10 in mice [19,20,26] (Figure 1).

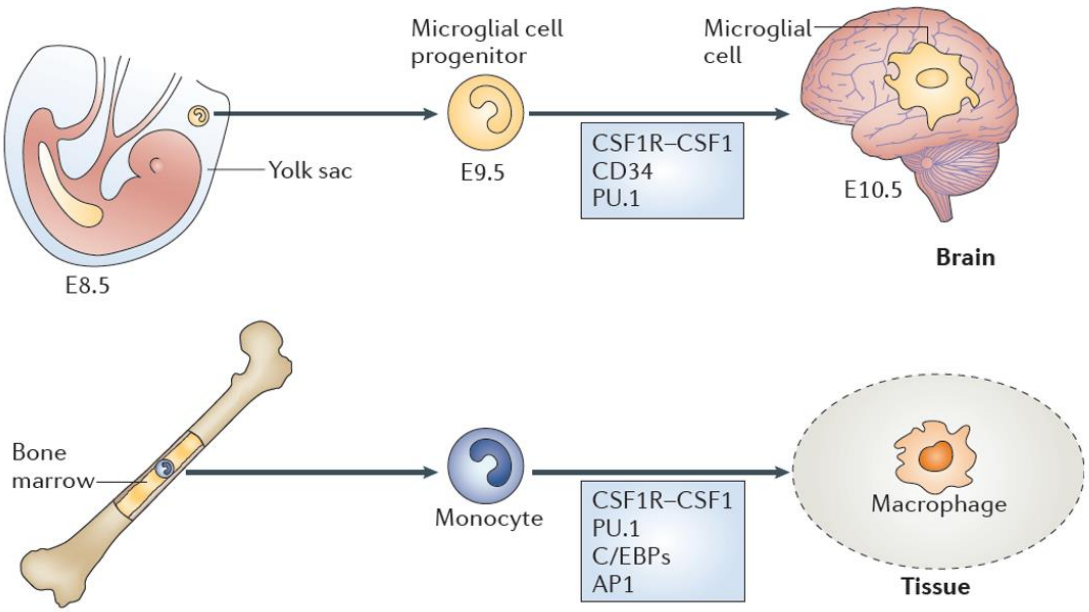

Figure 1 Origin of microglia and macrophages. Despite similar functions, macrophages and microglia cells emerge through different developmental paths and different factors. Colony-stimulating factor 1 (CSF1), the CSF1 receptor (CSF1R), CD34 and the transcription factor PU.1 are needed for differentiation and proliferation of microglia; CSF1, CSF1R and the transcription factors PU.1, CCAAT/enhancer-binding proteins (C/EBPs) and activator protein 1 (AP1) are needed for macrophage differentiation. Moreover, macrophages arise from bone marraw monocytes whenever they are needed. However, microglia arise from yolk microglial cell progenitors at embryonic day 10.5 [27].

1.3.2 Microglia in Alzheimer's Disease

Among the non-neuronal cells, microglia are most closely associated with alterations in AD [28–31]. Aβ is produced from processed APP by membrane bound secretases. Reaching a critical concentration, oligomeric structure are assembled from Aβ peptides and they finally culminate in mature fibrils [32]. Those secondary and tertiary structures of Aβ were found to bind to several receptors of microglia including CD14 [33], CD36 [34,35], CD47 [36], α6β1 integrin [37], class A scavenger receptor [38] , receptor for advanced glycosylation end products (RAGE) [39] and toll-like receptors (TLRs) [34]. Via signaling through these receptors, microglia cells are capable of phagocytosing Aβ particles *in vitro* and *in vivo* [40]. Moreover, Aβ dependent progressive impairment of microglial functions was strongly observed in AD [41]. Impairment of microglia function was also shown by another study conducted with APP-PS1 mice which demonstrated

decreased levels of Aβ binding scavenger proteins and Aβ-degrading enzyme [42]. APP-PS1 mice express human APP and presenilin and it is frequently used in the research of AD [43]. Also, this inefficient Aβ clearance of microglia was observed in AD patients [44]. Those studies demonstrate the important role of microglia in AD [45]. Also, most markers of inflammation such as Interleukin-1 (IL-1) [46], IL-6 [47], granulocyte-macrophage colony stimulating factor (GM-CSF) [47], IL-12 [48], IL-23 [48] and tumor necrosis factor (TNF) [49] were detected in AD models and in the brains of AD patients.

Rare structural variants of Triggering receptor expressed on myeloid cells 2 (TREM2) [50–53], cluster of differentiation 33 (CD33/Siglec3) [54–57] and complement receptor 1 (CR1) [58] were shown to be strongly associated with AD. TREM2 is involved in microglial phagocytosis [59–61] and TREM2 activity ameliorates survival of activated microglia and their myeloid counterparts such as perivascular macrophages in AD [62,63]. TREM2 engages perivascular macrophages or microglia with Aβ plaques by recognizing lipids associated with Aβ plaques [63]. Knock-down studies of TREM2 in APP/PS1 mice showed decreased plaque load in hippocampus [62], proving that ITAM signaling is very important for progression of AD.

1.3.2 Siglecs and CD33

CD33 belongs to the sialic acid-binding immunoglobulun-like lectins (SIGLECS) family [64]. It is expressed on myeloid precursors which give rise to macrophages and microglia cells [65,66]. Depending on sequence similarity and evolutionary conservation, SIGLECS can be categorized into two: evolutionary conserved SIGLECS and CD33-related SIGLECS [67]. SIGLECS recognize sialic acids on the outermost layer of the cell membrane, contributing to adhesion, cell signalling and endocytosis [66,68,69]Extracellular part of SIGLECS comprise V-Set Immunoglobulin and C2 set Immunoglobulin (Ig) domains and the extent of Ig domain vary among SIGLECS [70]. The V set Ig domain is the binding domain of SIGLECS to sialic acids and they can bind sialic acids both cis and trans manner [67]. Most SIGLECS comprise conserved immunoreceptor tyrosine-based inhibitory motifs (ITIMs) and/or ITIM-like motifs in their cytosolic tails and these motifs enable

recruitment of SH2-containing tyrosine phosphatases, SHP1 and SHP2 [71] (figure 2). ITIM signaling inhibits immunoreceptor tyrosine-based activatory motif (ITAM) signaling upon binding its ligand and ensures the regulation of myeloid cell responses [72]. Via phosphatase activity, SHP1 removes the phosphate group from ERK, SYK or other intermediates and ensures that the activation occurs only at the right time [73].

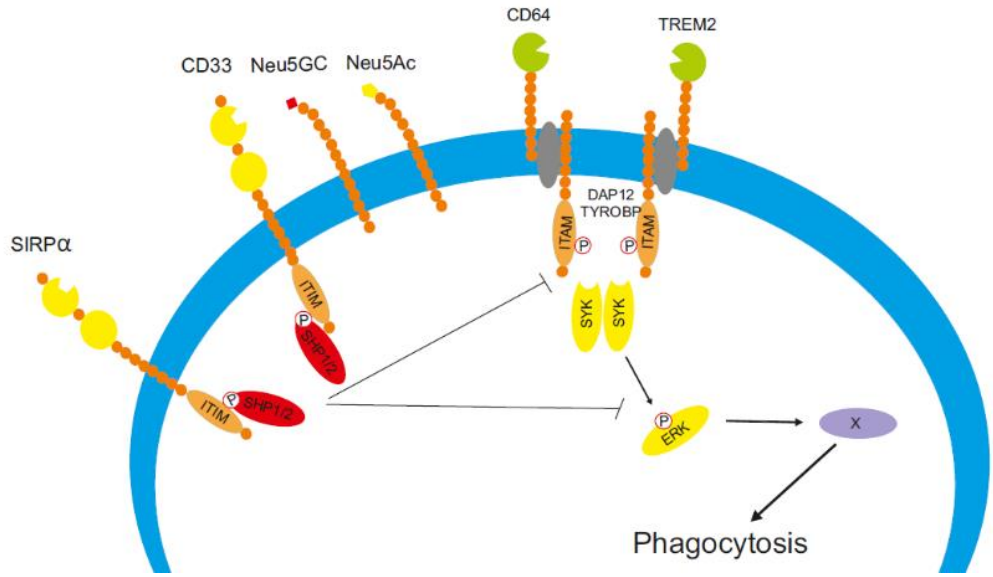

Figure 2 Activatory (ITAM) and inhibitory (ITIM) signaling of microglia. There are two main signaling in microglia and macrophages which control activation. ITAM signaling (through CD64 and TREM2 receptors) is responsible for the activation of microglia when there is activatory ligand is present, whereas ITIM signaling (through CD33 or SIRPα receptors) counter-regulates this activation by phophatase activity of SHP1. SHP1 removes phosphate group from ITAM signaling intermediates SYK and ERK and controls the activation of macrophages/microglia.

1.3.3 CD33 in Alzheimer's Disease

CD33 is mainly expressed on the cells of myeloid origin [74]. Although CD33 is present in both humans and mice, it shows structural differences among these two species (figure 2). Compared to human CD33, mouse analogue has only one ITIM-like domain and has positively charged transmembrane domain which enables to interact with Dap12/Tyrobp adaptor protein [75]. CD33 is known to play roles in peripheral immune activation and proliferation, endocytosis and degradation [66], however, the function of CD33 in brain physiology has not been determined so far. Recent studies point out the involvement of CD33 in Alzheimer's disease [55,76]. Genome-wide association studies (GWAS) showed that single nucleotide

polymorphisms in CD33 gene, which are rs3865444C and rs12459419, are associated with lowered AD risk [77]. On the other hand, another polymorphism, rs3865444A, was found to increase risk of having AD [78]. These findings demonstrate that CD33 is very important for progression of AD and can increase the risk of having AD. Especially, rs3865444C polymorphism, which is causing CD33 to lose its functional binding domain of sialic acids (Exon2), is one of major interest in the research of AD. This polymorphism was also shown to decrease the risk of having AD and underlying mechanism remains to be elucidated [77].

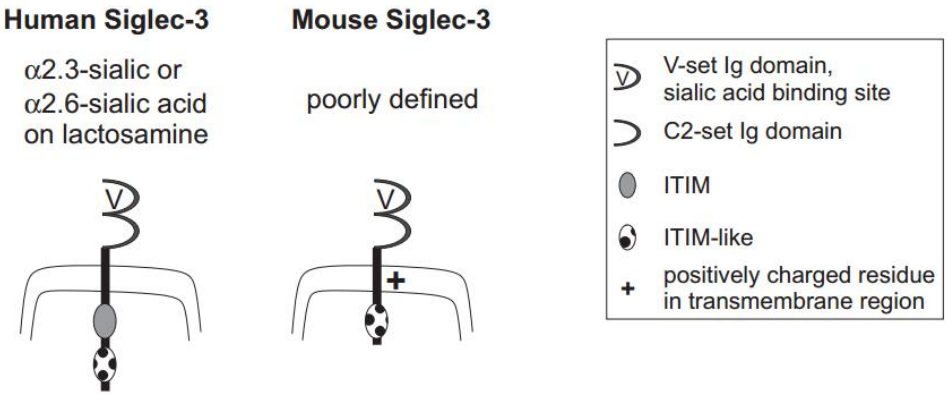

Figure 3 Structure of mouse and human microglia CD33 (Siglec 3). Comparison of human and mouse CD33 shows critical differences in their signaling. In cytosolic domain of mouse CD33, only one ITIM-like domain is found and the binding pattern and activity of mouse siglec-3 is still controversial. However, in cytosolic domain of human CD33, ITIM and ITIM like domain coexist and combination of these motifs lead to inhibition of microglia/macrophage responses [67]

1.4 Sialic Acids and Their Role in Immune Regulation

Sialic acids, major determinants of molecular cell surface phenotype, are 9-Carbon sugar residues found at outermost layer of membrane [79]. Three types of sialic acids are found on mammalian membrane: N-acetlyneuraminic acid (Neu5Ac), N-glycolylneuraminic acid (Neu5Gc) and Ketodeoxynonulosonic acid (Kdn) (Figure 4). Sialic acids were detected for the first time via thiobarbituric acid test in deuterostome lineage and higher vertebrates [80]. As higher species evolved sialic acid utilization, some bacteria species evolved Neu5Ac production pathways to evade host innate immune cell responses [81].

N-Acetylmannosamine (ManNAc) is the precursor for sialic acid biosynthesis pathway to produce Neu5Ac[82]. Once produced, Neu5Ac enters nucleus and forms complex with cytidine-5'-monophosphoric acid (CMP-Neu5Ac) which can be converted to CMP-Neu5Gc by Cytidine monophosphate N-Acetylneuraminic acid hydroxylase (CMAH) [83]. The presence of additional hydroxy group on Neu5Gc might alter its binding properties by changing its pKa, measure of acid strength [84]. Addition of hydroxyl (–OH) group was shown to increase polarity and hydrophilicity of molecules [85]. This effect might be contributing to disease phenotype by making sialic acids more hydrophobic. Effect of this change could cause drastic changes and might impair several functions in brain since sialic acids are found predominantly in brain.

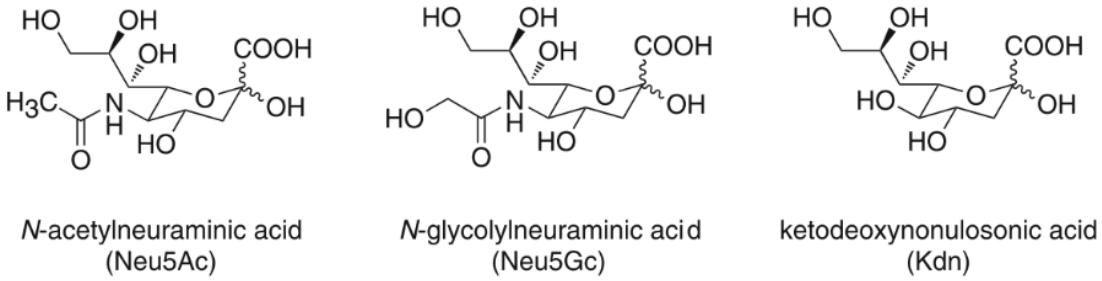

Figure 4 Major types of sialic acids in vertebrates. There are three major types of sialic acids. Neu5GC and Neu5Ac are the most abundant sialic acids. The main difference between these is the presence of –OH group at C5 in Neu5GC [86]

1.4.1 Role of CMAH in Distribution of Sialic Acids

CMAH is the only enzyme specific for Neu5Gc synthesis [87] and expressed variably in different tissues and species [86]. Humans are unable to synthesize Neu5Gc because of a universal 96 bp deletion in CMAH gene [88] (figure 5). This mutation is considered to be a consequence of Alu-mediated recombination resulting in a premature stop codon and highly truncated polypeptide [89]. *Alu* elements are repetitive DNA sequences in genome and through recombination, they can create genomic instability by the deletion of host DNA sequences during their integration into the genome. This integration creates genomic DNA deletions associated with intrachromosomal and interchromosomal recombination events [90,91]. This kind of

recombination event was shown to delete of Reiske iron sulfur binding region *CMAH* gene which is essential for its enzyme activity and eventually, resulted in loss of functional CMAH enzyme [92]. However, despite the lack of CMAH activity, Neu5GC can be metabolically taken from diet in very low levels and utilized in metabolism by humans [93]. Incorporation of Neu5GC occurs via fluid-phase pinocytosis to lysosomes, in which Neu5GC is released from glycoproteins via sialidase activity [94]. Neu5Gc is then delivered to cytosol via sialic acid transporters, where Neu5Gc follows the same path with Neu5Ac [95].

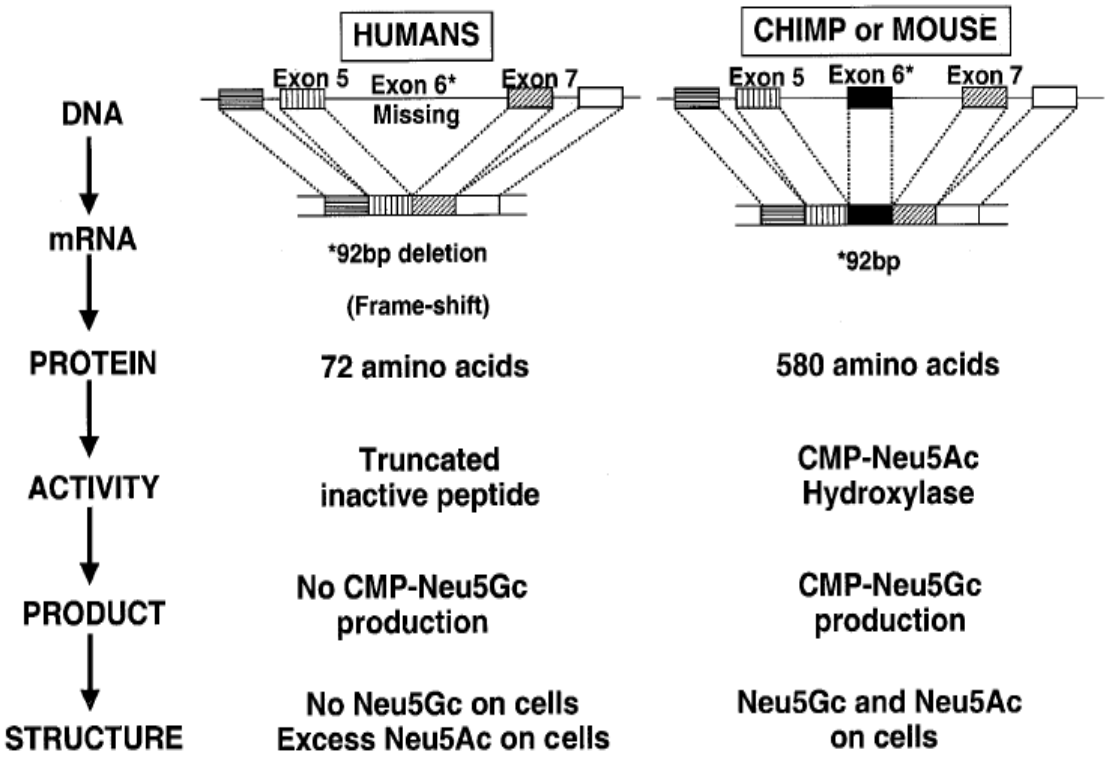

Figure 5 Comparison and expression pattern of CMAH. In humans, because of a 92 bp frameshift deletion in exon 6 of CMAH, a truncated protein of 72 amino acids is produced. However, in other close ancestors of humans (e.g. chimp), as well as in mice, this gene is still active and both Neu5Ac and Neu5Gc are produced [96].

Species	Serum	RBC	Submaxillary gland	Liver	Kidney	Milk	Brain
Human	–	–	nr	nr	–	–	–
Chimpanzee	nr	++	nr	+	+	+[a]	trace[b]
Macaque	+	+	nr	nr	nr	+	–
Mouse	+	+[b]	–	++	nr	nr	trace[b]
Rat	+	+[b]	+	+	+	nr	trace[b]
Rabbit	trace	+	nr	–	+	nr	–
Pig	nr	++	++	+	+	nr	trace[b]
Cow	++	++	+	nr	++	trace	trace[b]
Sheep	+	++	trace	+	+	++	trace
Elephant Afr	nr	nr	nr	++[a]	nr	+	nr
Elephant Asian	nr	nr	nr	++[a]	nr	–	nr
Dolphin	nr	nr	nr	++[a]	++	+[a]	trace[a]
Horse	+	++	trace	–	+	nr	trace
Chicken	–	–	–	–	–	–	–
Xenopus	nr	nr	nr	nr	nr	nr	–

Table 1 Distribution of Neu5Gc in different species and organs. Owing to differential expression of CMAH in different organs and in different species, Neu5Gc presence shows highly diverse expression. Although Neu5Gc is expressed in many species, the common point is either lack or the presence of traces of Neu5Gc in their brain (++: major fraction; +: minor fraction; –: absent; trace: present at 0.8–3%; nr: not reported) [97].

1.4.2 Distribution of Sialic Acids

Sialic acids are most abundant in the brain [98]. Therefore, when they were discovered in 1941 by Ernst Klenk, they were named as neuraminic acids [99]. Despite the high content of sialic acids, Neu5Gc is suppressed in mammal brains and this supression is conserved throughout evolutionary periods [97] (Table 1). Interestingly, the left hemisphere of the human brain showing 30 % more Neu5Ac compared to right hemisphere, which might indicate correlation between neural activity with sialic acid concentration[100]. However, functional outcome of this correlation still remains to be elucidated.

1.4.3 Sialic acids in Diseases

Although Neu5Gc is not present in mammalian brain, it has important roles in other tissues. Adaptation to presence of Neu5Gc was found to important for homeostasis and immune system in mice. $CMAH^{-/-}$ mice exhibited several abnormal phenotype including delayed wound healing and age dependent hearing

loss [87], heightened B cell response [101,102] and tendency for decreased insulin production [103]. However, incorporation of Neu5Gc was found to trigger immune responses is species which are lacking functional *CMAH* gene. Especially in humans, incorporated Neu5Gc caused susceptibility to diseases and it was found to be associated with cancer, atherosclerosis and autoimmune diseases [104,105]. Moreover, several studies demonstrated immune responses against Neu5Gc in humans [93].

Neu5Gc incorporation triggers immune responses in species that adapted to have Neu5Ac solely in their glycocalyx. $CMAH^{-/-}$ mice exhibited several human-like phenotype, including induction of anti-Neu5Gc antibodies [106], increase in cancer-related inflammation and progression of Neu5Gc containing tumors [104,107–109], increased immune clearance of Neu5Gc containing therapeutics [110], delayed wound healing [87], enhanced age-related hearing loss [87,111], altered immune responses [102,112,113], altered sexual selection through Neu5Gc antigenicity [114,115], increased susceptibility towards metabolic disorders [103,116,117], and susceptibility towards muscular dystrophy [118–120]. These studies reveal the importance of Neu5Gc incorporation for the balance of homeostasis in mammals.

2. AIM AND OBJECTIVES

Throughout evolutionary process, organisms gain or lose functions because of emerging mutations. The frameshift mutation emerged in human *CMAH* gene is one of these loss of function mutations and it caused human glycocalyx to have distinct phenotype compared to other mammals. Owing to this loss of function mutation, humans lost the ability to process sialic acids, thus making them incapable of converting N-acetlyneuraminic Acid (Neu5Ac) to N-glycolylneuraminic Acid (Neu5Gc). Despite this loss, humans can still metabolically incorporate Neu5Gc and utilize them as analogue for Neu5Ac and present them on their glycocalyx.

CD33 is one of the sialic acid binding protein found to be involved in progression of Alzheimer's disease. Recent genome-wide association studies revealed that polymorphisms in *CD33* gene are involved in the progression of Alzheimer's disease. Although CD33 is known to be having roles in cellular activation, proliferation, endocytosis and degradation, the function of CD33 in brain physiology has not been clarified so far. CD33 was found to recognize and bind to both Neu5Ac and Neu5Gc and related functional changes were elucidated in celular level in this study. Also, underlying molecular machinery causing these functional changes was assessed.

The effects of Neu5Gc incorporation by immune cells and their impacts on neurodegenerative disorders have not been studied so far. The aim of this study is understand how Neu5Gc incorporation regulates and modifies innate immune cell responses and affects progress of neurodegeneration in vitro. For this reason, murine CMAH gene was expressed in human THP1 macrophages which lack intact CMAH gene. Moreover, CMAH gene has also been overexpressed in human CD33KO THP1 macrophages to investigate whether CD33 signaling is affected by presence of Neu5Gc. These transduced macrophages were characterized in relation to major alterations observed in AD.

3. MATERIALS AND METHODS

3.1 Materials

3.1.1 Cell lines

Cell Line	Origin
ARPE Cells	*Human retinal pigmented epithelial cells* Kindly provided by Mona Mathews, University of Bonn
Stellar™ Competent Cells	*Supercompetent E.coli bacteria* *Clontech® Laboratories, Inc., USA*
THP1 Wild Type Cells	Human monocytes derived from acute myeloid leukemia Kindly provided by AG Hornung, University of Bonn
CD33KOTHP1 monocytes	Human monocytes lacking functional human CD33 derived from acute myeloid leukemia cells Kindly generate d and provided by AG Hornung, University of Bonn
HEK293FT Cells	Human Embryonic Kidney Cells Kindly provided by Jens Kopatz, University of Bonn

3.1.2 Chemicals and reagents

Chemical	Company
100 bp DNA Ladder	Thermo Fisher Scientific Inc., USA
1 kb plus DNA Ladder	Thermo Fisher Scientific Inc., USA
1,4-Diazabicyclo[2.2.2]octane	Sigma Aldrich Chemie GmbH, Germany
2-Mercaptoethanol	Chemicon Europe, Germany
Amphicilin	Sigma Aldrich Chemie GmbH, Germany
Agarose	VWR International GmbH, Germany
Ampuwa ddH2O	Fresenius Kabi Deutschland GmbH, Germany
Aqua-poly/Mount	Polysciences Inc., USA

Biotinylated Amyloid β	Bachem, Germany
Bovine Serum Albumin	Sigma Aldrich Chemie GmbH, Germany
Calcium Chloride ($CaCl_2$)	Sigma Aldrich Chemie GmbH, Germany
ddH2O	Laboratory Made
DEPC-Treated Water	Thermo Fisher Scientific Inc., USA
Dihydroethidium (DHE)	Thermo Fisher Scientific Inc., USA
Dimethyl Sulfoxide (DMSO)	Sigma Aldrich Chemie GmbH, Germany
DiI, cell tracker	Thermo Fisher Scientific Inc., USA
DMEM with L-glutamine and 4.5g/l D-glucose, without sodium pyruvate	Thermo Fisher Scientific Inc., USA
DMEM/F12 [1:1] with L-glutamine and HEPES [15mM]	Thermo Fisher Scientific Inc., USA
Nucleoside triphosphates containing deoxyribose (dNTP) mix	Peqlab, Erlangen, Germany
Ethylenediaminetetraacetic acid (EDTA)	Carl Roth GmbH & Co KG, Germany
Ethanol	Carl Roth GmbH & Co KG, Germany
Ethidium Bromide	Sigma Aldrich Chemie GmbH, Germany
Fetal Calf Serum (FCS)	Thermo Fisher Scientific Inc., USA
First Strand Buffer (5x)	Thermo Fisher Scientific Inc., USA
Fluoresbrite® Polychromatic Red Microspheres 1.0 µm beads	Polysciences Inc., USA
GelStar Nucleic acid gel stain	Lonza Cologne GmbH, Germany
Glacial Acetic acid	Carl Roth GmbH & Co KG, Germany
Glucose	Sigma Aldrich Chemie GmbH, Germany
Glycerol	Sigma Aldrich Chemie GmbH, Germany
HALT™ Protease and Phosphatase Inhibitor Coctail	Thermo Fisher Scientific Inc., USA
Hexanucleotide Mix	Roche Holding GmbH, Germany
Hydrochloric Acid (HCl)	Sigma Aldrich Chemie GmbH, Germany
Isopropanol	Sigma Aldrich Chemie GmbH, Germany
Kanamycin	Sigma Aldrich Chemie GmbH, Germany
L-Glutamine	Thermo Fisher Scientific Inc., USA
Lipofectamine™ Transfection Reagent	Thermo Fisher Scientific Inc., USA
Lipopolysaccharide (LPS)	Invivogen, USA

Lysogeny Broth (LB)	Sigma Aldrich Chemie GmbH, Germany
Lysogeny Broth - Agar	Sigma Aldrich Chemie GmbH, Germany
Magnesium Chloride (MgCl2)	Carl Roth GmbH & Co KG, Germany
Methanol	Carl Roth GmbH & Co KG, Germany
Mowiol	Kremer Pigmente GmbH & Co, Germany
N2 Supplement (100X)	Thermo Fisher Scientific Inc., USA
Non-biotinylated Amyloid β	Peptide speciality laboratories, Germany
Non-Essential Amino acids	Thermo Fisher Scientific Inc., USA
Normal Chicken Serum	Thermo Fisher Scientific Inc., USA
Nuclease Free DNAase	Qiagen GmbH, Germany
Okadaic acid	Sigma Aldrich Chemie GmbH, Germany
Opti-MEM® I Reduced-SerumMedium (1x), liquid	Thermo Fisher Scientific Inc., USA
PageRuler™ Prestained Protein Ladder	Thermo Fisher Scientific Inc., USA
Paraformaldehyde	Sigma Aldrich Chemie GmbH, Germany
Penicilin/Streptomycin (Pen/Strep)	Thermo Fisher Scientific Inc., USA
Phorbol-12-myristate-13-acetate (PMA)	Sigma Aldrich Chemie GmbH, Germany
Phosphate Buffered Saline (PBS)	Thermo Fisher Scientific Inc., USA
Plasmocin	Invivogen, USA
Poly-L-Lysine [PLL]	Sigma Aldrich Chemie GmbH, Germany
Potassium Chloride (KCl)	Sigma Aldrich Chemie GmbH, Germany
QIAzol™ Lysis Reagent	Qiagen GmbH, Germany
Random Hexamer Primer Solution	Roche Holding GmbH, Germany
RPMI Medium	Thermo Fisher Scientific Inc., USA
Sodium Chloride (NaCl)	Carl Roth GmbH & Co KG, Germany
Sodiumhydrogenphosphate (NaH2PO4*H2O)	Carl Roth GmbH & Co KG, Germany
Sodiumhydrogenphosphate (NaH2PO4*7H2O)	Carl Roth GmbH & Co KG, Germany
Sodium Hydroxide (NaOH)	Carl Roth GmbH & Co KG, Germany
Sodium Pyruvate	Thermo Fisher Scientific Inc., USA
Sulfuric Acid (H_2SO_4)	Carl Roth GmbH & Co KG, Germany
SYBR Green	Thermo Fisher Scientific Inc., USA
Trisaminomethane (TRIS)	Carl Roth GmbH & Co KG, Germany

TritonX	Sigma Aldrich Chemie GmbH, Germany
Trolox	Cayman Chemical, USA
Trypan Blue	Sigma Aldrich Chemie GmbH, Germany
Trypsin (0.25%)	Thermo Fisher Scientific Inc., USA

5.1.3 Antibodies

Primary Antibodies For Western Blot

Antibody	Brand	Catalog	IP Conc.	WB Conc
CD33 (WM53)	Abcam	ab30371	1/200	1/1000
P-ERK	Cell Signaling Technologies	9101		1/1000
SHP1	Santa Cruz	SC-7289		1/80
Total ERK	Cell Signaling Technologies	9102	1/100	1/1000

Primary Antibodies and Respective Isotype For Flow Cytometry and Immunocytochemistry

Antibody	Brand	Host	Catalog	Conc.	Isotype	Catalog	Conc.
Catalase							
CD11b	BD Pharmingen	Rat	553307	1/200	Rat IgG2b	555740	1/100
CD206	Acris	Mouse	SM1829P	1/100	Mouse IgG1κ	555746	1/100
CD33 (HIM34)	Exbio	Mouse	11-365-C025	1/400	Mouse IgG1κ	555746	1/200
CD33 (WM53)	Abcam	Mouse	ab30371	1/400	Mouse IgG1κ	555746	1/200
CD64	Santa Cruz	Mouse	SC-1184	2.5/200	Mouse IgG1k	555746	1/200

Secondary Antibodies

Antibody	Brand	Catalog	Conc.
Alexa488-conjugated goat-anti-rat	Invitrogen	A11006	1/200
Anti-Rabbit HRP			
Biotin, anti-mouse	Sigma	B7653	1/200
Cy3-conjugated Streptavidin	Jackson Immuno Research	016-160-084	1/200
Cy5-conjugated goat-anti-mouse IgG	Jackson Immuno Research	115-176-072	1/200
Cy5-conjugated goat-anti-rabbit IgG	Dianova	111-176-144	1/200

Cy5-conjugated goat-anti-rat IgG	Jackson Immuno Research	112-175-167	1/200
Cy5-conjugated Streptavidin	Dianova	016-170-084	1/200

5.1.4 Buffers and solutions

Buffer/Solution	Composition/Company
1% Agarose gel	0.7 g Agarose 70 mL TAE Buffer 5 µL Ethidium Bromide or GelStar Dye
4% Paraformaldehyde	20 g PFA 30 mL NaOH 50 mL PBS (10X) Complete to 500 mL with ddH_2O
10X Bovine Serum Albumin	10 g BSA 100 mL PBS (1X)
Diluent Buffer	Biolegend Inc., USA
KREBS-HEPES Buffer	135 mM NaCl 5 mM KCl 1 mM $MgSO_4$ 0.4 mM K_2HPO_4 5.5 mM Glucose 20 mM HEPES Adjust the pH to 7.4.
Mowiol	4.8 g Mowiol 12 g Glycerol 24 mL 0.2M Tris Buffer 1.32 g DABCO
NuPAGE™ LDS Sample Buffer	Thermo Fisher Scientific Inc., USA
NuPAGE™ MES SDS Running Buffer	Thermo Fisher Scientific Inc., USA
NuPAGE™ Transfer Buffer	Thermo Fisher Scientific Inc., USA
Phosphate Buffered Saline (10X)	5.125 g NaH2PO4*H2O 23.84 g NaH2PO4*7H2O 175.25 g NaCl Complete to 1 L with ddH_2O Adjust pH to 7.3
Restore Plus™ Western Blot Stripping Buffer	Thermo Fisher Scientific Inc., USA
RIPA Buffer	Thermo Fisher Scientific Inc., USA
Tris-Acetate-EDTA (TAE) Buffer	96.8 g Tris Base 22.8 g Glacial Acetic acid 7.4 g EDTA

	Complete to 2 L with ddH_2O
Tris Buffered Saline with Tween® 20 (TBST 10X)	24 g Tris Base 88 g NaCl 10 mL Tween® 20 Complete to 1 L with ddH_2O

5.1.5 Kits

Kit	Company
Anti-Neu5Gc Antibody Kit	Biolegend inc., USA
DynaBeads Protein G Immunoprecipitation Kit	Thermo Fisher Scientific Inc., USA
NucleoBond® Xtra Midi Kit	Macherey Nagel
NucleoBond® Xtra Maxi Kit	Macherey Nagel
SuperScript First-Strand Synthesis System	Thermo Fisher Scientific Inc., USA
Super Signal West Pico Maximum Sensitivity Substrate	Thermo Fisher Scientific Inc., USA
QIAprep Spin Miniprep Kit	Qiagen GmbH, Germany
QIAquick Gel Extraction Kit	Qiagen GmbH, Germany

5.1.6 Media

Media	Components
ARPE Medium	5 mL Pennicilin/Streptavidin (100X) 50 mL FCS (10X) 500 mL DMEM/F12
Freezing Medium	50 % FCS (10X) 10 % DMSO 40 % Culture Medium
LB Media	1 L ddH_2O 25 g LB Powder
MEF Medium	50 mL FCS (10X) 5 mL L-Glutamine (200 mM) 5 mL Non-Essential Amino Acids (100X) 5 mL Sodium Pyruvate (100x) 500 mL DMEM with L-Glutamine, without Sodium Pyruvate, high glucose
THP1 Medium	10 mL Chicken Serum (10X)

	5 mL L-Glutamine (200 mM) 5 mL Pennicilin/Streptavidin (100X) 5 mL Sodium Pyruvate (100x) 500 mL RPMI
THP1 Differentiation Medium	50 µL PMA (1 µg/mL) 1 mL Chicken Serum (10X) 0.5 mL L-Glutamine (200 mM) 0.5 mL Pennicilin/Streptavidin (100X) 0.5 mL Sodium Pyruvate (100x) 50 mL RPMI

5.1.7 Consumable supplies

Consumable	Company
5, 10 and 25 mL plastic pipettes	Sarstedt Inc., USA
6-Well Tissue Culture Plate	Cellstar, Greiner Bio One, Germany
10, 100 and 1000 µL pipette tips	Starlab GmbH, Germany
10 and 50 mL Syringes	Omnifix, Braun Meisungen AG, Germany
Cell strainer	Becton Dickinson GmbH, Heidelberg, Germany
Corning Cell Scraper	Sigma Aldrich Chemie GmbH, Germany
Cryovials (2 ml)	Nunc GmbH & Co KG, Wiesbaden, Germany
Falcon Tubes (15 ml)	Cellstar, Greiner Bio One, Germany
Falcon Tubes (50 ml)	Sarstedt Inc., USA
Filtropur (0.25 µm, 0.4 µm)	Sarstedt Inc., USA
Lab-Tek Chamber Slide w/ Cover Permanox Slide Sterile 4 Well	Labomedic, Germany
Latex Gloves	Ansell Healthcare Europe NV, Belgium
Microscope Cover Glasses	P. Marienfeld GmbH, Germany
Nitrile Gloves	Ansell Healthcare Europe NV, Belgium
Nitrocellulose membrane 0.2 µm	Bio-Rad Laboratories GmbH, Germany
Pasteur Pipettes	Brand GmbH & Co KG, Germany
Petri Dishes	BD Falcon, Germany
QPCR Semi-Skirted 96-Well PCR Plate	VWR International GmbH, Germany
Safe-seal Micro Tubes (0.5 ml, 1.5 ml, 2 ml)	Sarstedt Ag & Co KG, Germany
Tissue Culture Dishes (35 mm, 60 mm, 100 mm)	Sarstedt Inc., USA
Tissue Culture Flask (25 cm^2, 75 cm^2)	Sarstedt Inc., USA
Vacuum driven disposable Bottle Top Filter	Millipore Corporation, MA, USA

5.1.8 Primers and plasmids

Primers For Cloning Purposes (5'-3')	
CMAH forward	GAATTCGCCACCATGATGG
CMAH middle forward	AAGTTCACCGAGGAGTGGAA
CMAH middle reverse	TCTTCCGGATCAGGTTGTTC
CMAH reverse	CGCAGTGCATCAGGAAGCT

Primers for RT-PCR (5'-3')	Forward Primer (5' to 3')	Reverse Primer (5' to 3')
CD33	TGTTCCACAGAACCCAACAA	GGCTGTAACACCAGCTCCTC
CD64	TCGACCCCCAGCTACAGAAT	ACCAGCTTATCCTTCCACGC
GAPDH	CTGCACCACCAACTGCTTAG	TTCAGCTCAGGGATGACCTT
IL-1β	CCAGCTACGAATCTCCGACC	TGGACCAGACATCACCAAGC
SHP-1	GGCACCATCATCCACCTCAA	AGGCTCTCACGCACAAGAAA
SIRPα	GGTCAGCAAAAGCCATGACC	GGCATTCTTCTCGGGCTCAT
TNFα	AACCTCCTCTCTGCCATCAA	CCAAAGTAGACCTGCCCAGA

Name of Plasmid	Source
12ABUUYP_ hCMAH_Opt_pMA	Life Technologies™
pLenti-EF1A	Provided kindly by Gabriel Liviu Bodea, Institute of Reconstructive Neurobiology, University of Bonn, Germany
pMD2.G (Packaging Lentiviral Vector)	Provided kindly by AG Brustle, Institute of Reconstructive Neurobiology, University of Bonn, Germany
psPAX2 (Packaging Lentiviral Vector)	Provided kindly by AG Brustle, Institute of Reconstructive Neurobiology, University of Bonn, Germany

5.1.9 Enzymes and recombinant proteins

Name	Company
Amyloid Beta	Bachem, Germany
AccuPrime™ Pfx SuperMix	Thermo Fisher Scientific Inc., USA
BamHI	Roche Holding GmbH, Germany
Calf Intestinal Alkaline Phosphatase	New England BioLabs GmbH, Germany
DNAase	Qiagen GmbH, Germany
EcorI	Roche Holding GmbH, Germany

InFusion™ HD Enzyme Premix	Clontech® Laboratories, Inc., USA
pHRODO Red Staphylococcus aures bioparticles	Thermo Fisher Scientific Inc., USA
Staphylococcus aureus bioparticles™	Thermo Fisher Scientific Inc., USA
Superoxide Dismutase from bovine erythrocytes (SOD1)	SERVA Electrophoresis GmbH, Germany
T4 DNA Ligase	Roche Holding GmbH, Germany
T4 Polynucleotide Kinase	New England BioLabs GmbH, Germany

5.1.10 Technical equipment

Instrument	Company
- 20 °C freezer	Liebherr, Switzerland
+ 4 °C fridge	Liebherr, Switzerland
Acculab Scale	Sartorius
Axiovert 40 CFL (Microscope)	Carl Zeiss AG
BD FacsCalibur	BD Biosciences
BD FacsDiva	BD Biosciences
Biofuge Fresco (Centrifuge)	Heraeus Holding GmbH, Germany
Cell MateII (Pipette Boy)	Thermo Fisher Scientific Inc., USA
Confocal Olympus IX81	Olympus
DarkReader DR89X Transilluminator	Clare Chemical Research
Eppendorf Mastercycler epgradient S	Eppendorf AG, Germany
EPS 301 - Electrophoresis Power Supply	GE Medical Systems, Germany
Gel Doc 2000 (Gel Imaging System)	Bio-Rad Laboratories GmbH, Germany
Hera Cell 150 (Incubator)	Heraeus Holding GmbH, Germany
Hera Freeze (- 80°C Freezer)	Heraeus Holding GmbH, Germany
Hera Safe (Laminar-air Flow Workbench)	Kendro Laboratory Products GmbH, Germany
KS-15 Control (Shaker)	Edmund Bühler GmbH, Germany
Mastercycler epgradientS realplex4 (qRT-PCR)	Eppendorf AG, Germany
Mefaguge1.0R (Centrifuge)	Heraeus Holding GmbH, Germany
NanoDrop 1000 Spectrophotometer	Thermo Fisher Scientific Inc., USA
PerfectBlue Gelsystem Mini M (Agarose Gel Chamber)	VWR International GmbH, Germany
Pipettes (2 µl,10 µl, 100 µl, 1000 µl)	Eppendorf AG, Germany
Sorvall Discovery 90 SE	HITACHI
Sorvall RC 6+	ThermoScientific
Sorvall 5B Plus	ThermoScientific
Standard Power Pack P25 (Voltage Power Supply)	Biometra GmbH, Germany
Systec D-150 (Autoclave)	Systec GmbH, Germany
Thermomixer Compact	Eppendorf AG, Germany

Water Bath WB/OB7-45	Memmert GmbH & CoKG, Germa
XCell SureLock Electrophoresis Cell	Thermo Fisher Scientific Inc., USA
Severin 800 Microwave Oven	SEVERIN Elektrogeräte
pH Meter CG840	Schott
Pump drive PD 5001 Peristaltic Pump	Heidolph
VacuuHandControl	Vacuumbrand
Vacuu-lan® network for lab	Vacuumbrand
Vortex 2X2	Velp Scientifica
XCell SureLock Electrophoresis Cell	Thermo Fisher Scientific Inc., USA

5.1.11 Softwares

Name	Company
Adobe Reader XI	Adobe Systems, USA
Cellquest Pro	BD Biosciences, USA
Corel Draw ® X5	Corel GmbH, Germany
FlowJo Version 8.7	Tree Star, BD Biosciences, USA
Gene Designer	DNA2.0, USA
Geneious Version 8.1.8	Biomatters, USA
Image J	Open Source, National Institute of Health (NIH), USA
Image Lab	BioRad Laboratories GmbH, Germany
Mendeley Desktop Version 1.17.6	Open Source, Elsevier, Netherlands
Microsoft Office 2016	Microsoft, Germany
Microsoft Windows 8	Microsoft, Germany
Nanodrop Version 3.8.1	Thermo Fisher Scientific Inc., USA
Realplex 2.2	Eppendorf AG, Germany
SPSS Statistics 22 Release	IBM, Germany
WinRar	win.rar GmbH, Germany

3.2 Methods

3.2.1 Cell culture

Cells were thawn quickly in 37^{o}C water bath and added to 15 mL falcon tube containing 4 mL respective medium. The falcon tube is centrifuged for 3 minutes at 1500g and supernatant was discarded. The pellet was resuspended in fresh media and kept in 5% CO_2, 95% humidity and 37^{o}C. When cells reached 80% confluency, depending on the cell type and experimental setup, they are either mechanically scraped or treated with trypsin for 3 minutes. If the cells are in suspension, the cell suspension is transferred to falcon and centrifuged for 3 minutes at 1500g. Cells were frozen down in freezing media (Table 3.1) and kept in -80 ^{o}C fridge for 3 months and then, transferred to -160^{o}C fridge

THP1 cell lines were kindly provided by Dr. Jens Kopatz, Institute of Reconstructive Neurobiology. Depending on the cell culture conditions, cells were either grown in either serum free or 1% inactivated chicken serum. THP1 cells were differentiated with 10 ng/mL PMA for 2 days in 5% CO_2, 95% humidity and 37^{o}C. Afterwards, cells are washed 2 times with fresh medium and they were left for 2 more days in same conditions for cells to recover.

3.2.2 Cellular functional experiments

3.2.2.1 Cell surface marker analysis

Receptor expression was assessed by respective monoclonal primary antibody via FACS. For this procedure, 3x10^{6} monocytic THP1 cells were seeded in 10 cm dishes in the first day in serum free THP1 medium and differentiated with 10 ng/mL PMA. After 48 hours, the medium of the cells were replaced with new media and incubated for two days for differentiation to macrophages. Incubation for 2 days was performed for recovery of macrophages. Cells were deattached mechanicaly by scraping and deattached cells were transferred to 15 cm falcon tubes and centrifuged at 1300 rpm for 3 minutes. The supernatant

was removed and 800 µL THP1 medium was added. The cells were divided into 200 µL aliquots. Respective primary antibody was diluted in PBS. Cells were centrifuged in 7000 rpm in tabletop centrifuge for 3 minutes and each pellet resuspended in 200 µL antibody solution. Next, cells were incubated in ice for 60 minutes. Cells were centrifuged at 7000 rpm for 3 minutes and washed 3 times in this centrifugation condition. Respective secondary antibody is diluted in PBS and the pelleted cells were resuspended with this antibody mixture. Cells were incubated in ice for 30 minutes. Then, cells were centrifuged in 7000 rpm for 3 minutes, washed 3 times with PBS in this centrifugation and eventually, they were resuspended in 200 mL PBS.

FACS analysis was performed in one of Cantos at IMMEI. Voltage values are set depending on morphology of the cells.

3.2.2.2 Neu5Gc staining

10^6 THP1 macrophages were scraped in PBS and centrifuged down at 1300 rpm for 3 minutes to obtain the pellet. Pellets were resuspended in 100 µL diluent buffer and divided into two tubes. The tubes were centrifuged again at 7000 rpm for 3 minutes. Meanwhile, master mix of Neu5Gc antibody, 1/500 concentration of anti-Neu5Gc antibody in 100 µL diluent buffer, is prepared and and used for resuspension of pellet. The antibody pellet mix is incubated at room temperature for 90 minutes. Diluent buffer without antibody was used as control. Master mix of secondary antibody, 1/200 concentration of biotin-anti-chicken antibody in 100 µL diluent buffer was prepared and cells were incubated on ice for 45 minutes. Then, tertiary antibody mix composing 1/200 concentration of Cy5 anti-streptavidin in 100 µL diluent buffer were prepared, the cells were resuspended and incubated on ice for 30 minutes. Washing with diluent buffer were performed for 2 times before each antibody is resuspended. Flow cytometry was performed at 660/20 red channel.

3.2.2.3 Phagocytosis assays

Cells were checked for several phagocytic phenotype. Aβ, neural debris, and *Staphylococcus aureus* coupled pHRODO bioparticles phagocytosis were analyzed in this experimental set.

3.2.2.3.1 pHRODO bioparticle uptake assay

10^5 THP1 monocyte cells per well were seeded in 4-well chamberslide and general differentiation protocol was followed. pHRODO bioparticles were prepared as stock in 200 µL (10X) 1X PBS. The bioparticles were diluted in pre-heated medium and incubated for 2 hours in 37 ^{o}C. Then, slides were washed with PBS three times and fixed in 4% paraformaldehyde (PFA). After 15 minutes, the slides were washed three times with PBS, the walls of chambers were removed and coverslides were placed with 70 µL moviol. The slides were stored at 4°C Fridge and images were taken at confocal microscope. Area and integrated density of images were measured. To remove background of image, mean fluorescent intensity of background was measured. Calculation was performed according to formula below:

Area*Mean Fluorescent Intensity of Background – Integrated density

3.2.2.3.2 Retinal debris production

ARPE cells were thawn according to thawing protocol and cultured in ARPE medium in 15 cm dish and incubated in 5% CO_2, 95% humidity and 37^{o}C until they reached 90 % confluency. When they reached confluency, okadaic acid (1/1000) was added to reach 40 nM working concentration and incubated 24 hours in the incubator. Afterwards, medium was collected and centrifuged at 1500 rpm for 4 minutes and pellet was washed once with PBS. Then, pellets were resuspended in 210 µL RDD buffer containing 30 µL DNAase for 15 minutes at room temperature and transferred to pre-weighted eppendorf tubes. Debris was divided into two depending on whether it will be labeled with Dil dye solution (1/1000, 1 µg/mL). Non-labeled debris is diluted to 100 µg/mL in PBS and stored in -20 ^{o}C. For labeled debris, Dil solution was

added to PBS and the pellet was incubated for 5 minutes at 37 ^{o}C and for 15 minutes at 4^{o}C, respectively. The pellet was washed once with PBS and diluted to 100 µg/mL and stored at -20 ^{o}C until use.

3.2.2.3.3 Aβ and debris phagocytosis

10^5 THP1 monocyte cells per well were seeded in 4-well chamber slide and general differentiation protocol was followed. In the second day of experiment, biotinylated-Aβ was placed in 37°C in incubator for polymerization for 3 days. In the fourth day of experiment, old medium was removed and replaced with 300 µL N2 medium composing 3 µL biotinylated-Aβ (1mg/mL) or 5 µL labeled debris (100 µg/uL) and incubated for 90 minutes. After incubation each chamber was washed with PBS and 4% paraformaldehyde (PFA) was added for fixation. After 15-minute incubation, the chambers were washed 3 times with PBS and blocked with blocking solution containing 10% 1x BSA, 5% normal goat serum and 0.1% Triton-X for 30 minutes. Afterwards, primary antibody for microglia which is rat-anti-CD11b (1:500) in 500 µL PBS was added to each chamber and incubated overnight at 4°C Fridge. Next day, chambers were washed with PBS and secondary antibody mix that contains Alexa 488 Goat-anti-rat(Invitrogen) and CY3-conjugated-streptavidin (only for Aβ uptake) in 1:500 ratio in 500 µL PBS were added and incubated for 90 minutes at room temperature. Finally, the chambers were washed 3 times with PBS. The walls of chambers were removed and with 70 µL moviol, coverslides were placed. The slides were stored at 4°C Fridge and images were taken at confocal microscope. Uptaken Aβ and debris were analyzed via 5 randomly taken images and 3D Reconstruction. Images were analyzed in ImageJ software.

3.2.2.4 Detection of oxidative stress by DHE staining

10^5 THP1 cells were seeded in each chamber of chamber-slides. General differentiation protocol was applied and cells were treated according to scheme (Figure 6). In the day of experiment, macrophages were pre-incubated with SOD1 (60 U/mL- 1/50) and Trolox (40 µM -1/1000) for 1 hour at 37°C. Afterwards, medium of the cells were treated with fresh pre-heated media containing either debris (10

μg/μL), $A\beta_{1-42}$ (10 μM), or Bioparticles (10 μM) for 15 minutes. Meanwhile, DHE (30 μM) was diluted in 1/1000 pre-heated Krebs-HEPES buffer and medium of the cells were replaced with DHE solution and 15-minute incubation at 37 °C was performed. After 15 minutes, chambers were washed 3 times with Krebs-HEPES buffer to avoid absorption of any extracellular oxyethidium formed by autooxydation of DHE. Cells were fixed for 15 minutes in 4% PFA solution containing 0.25% Glutaraldehyde and washed 3 times with PBS. The walls of chambers were removed and with 70 μL moviol, and coverslides were placed. Five images per condition captured and analyzed in ImageJ software. Area and integrated density of images were measured. To remove background of image, mean fluorescent intensity of background was measured. Calculation was performed according to formula below:

Area*Mean Fluorescent Intensity of Background – Integrated density

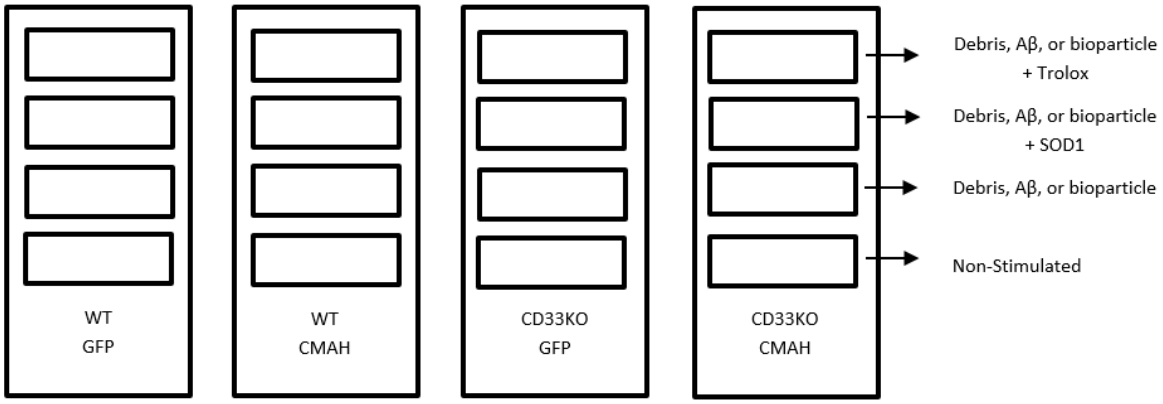

Figure 6 Orientation and layout of the THP1 monocytes in DHE staining

3.2.3 High pressure liquid chromatography (HPLC)

In order or determine the activity of CMAH enzyme in transduced cells, the ratio of Neu5Gc to Neu5Ac should be calculated. xCGE-LIF (Multiplexed Capillary Gel Electrophoresis with Laser Induced Fluorescence Detection) was used to measure the ratio. 10^6 monocytes were seeded on 6-well plate and differentiated to macrophage according to previous protocol. After differentiation and recovery, cells were scraped in

PBS and centrifuged for 3 minutes at 1300 rpm. Following centrifugation, pellet was resuspended in 100 µL RIPA buffer containing 1x HALT proteinase and phosphotase inhibitor. Three time independent repeat of each experiment was performed and the cells were placed and stored at -80 °C until analysis.

xCGE-LIF experiment was performed in cooperation with collaborators in Max Planck Institute for Dynamics of Complex Technical Systems, Magdeburg. Via collaboration, precipitated proteins were concentrated by affinity solid phase extraction and seperated on 2 dimensional (2D) gel electrophoresis system. Then, the bands were excised out with scalpels and N-Glycan structures were extracted from gel. N-Glycan structures were labeled with 9-aminopyrene-1,4,6 trisulfonic acid (APTS) and run a UPLC system to detect Neu5Ac and Neu5Gc amounts.

3.2.4 Molecular biology

3.2.4.1 Molecular cloning

Is (2013) completed murine CMAH cloning in his Masters thesis [121]. Murine CMAH mRNA sequence (NM_001284519.1) was codon optimized according to commonly used codons by Homo sapiens via DNA2.0 software [121]. Mammalian Kosak sequence was added to 3' of gene sequence for translation initiation. While EcorI restriction site was added to 3' region of gene sequence, BamHI restriction site was added to 5' region for cloning into pLenti-EF1A plasmid (figure 7). CMAH gene sequence was commercially synthesized from Life Technologies™: The plasmid map of CMAH was shown in figure 11. The synthesized gene was cloned into pLenti-EF1A (figure 8A) plasmid and cloning was verified by restriction digestion and sequencing analysis. psPAX2 (figure 8B) and pMD2.G (figure 8C) plasmids were kindly obtained from AG Brustle, University of Bonn.

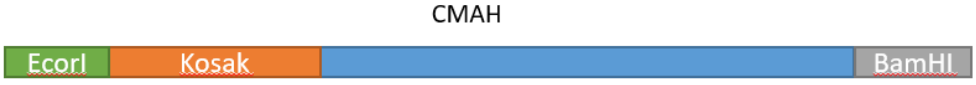

Figure 7 The scheme of synthesized and codon optimized CMAH

3.2.4.2 Bacteria culture

To initiate new bacteria cultures, inoculums or aliquots were taken from -80°C long storage cryovials into 3-5 mL LB medium (for small scale culture) or 200-250 mL LB medium (for large scale cutures) containing appropriate selection antibiotic, placed in 37°C shaking incubators (200-250 rpm) and grown until required bacterial density was reached. For long term storage, bacteria containing LB media was mixed with glycerol in a 1:1 ratio (v/v), placed in cryotubes and stored at -80°C.

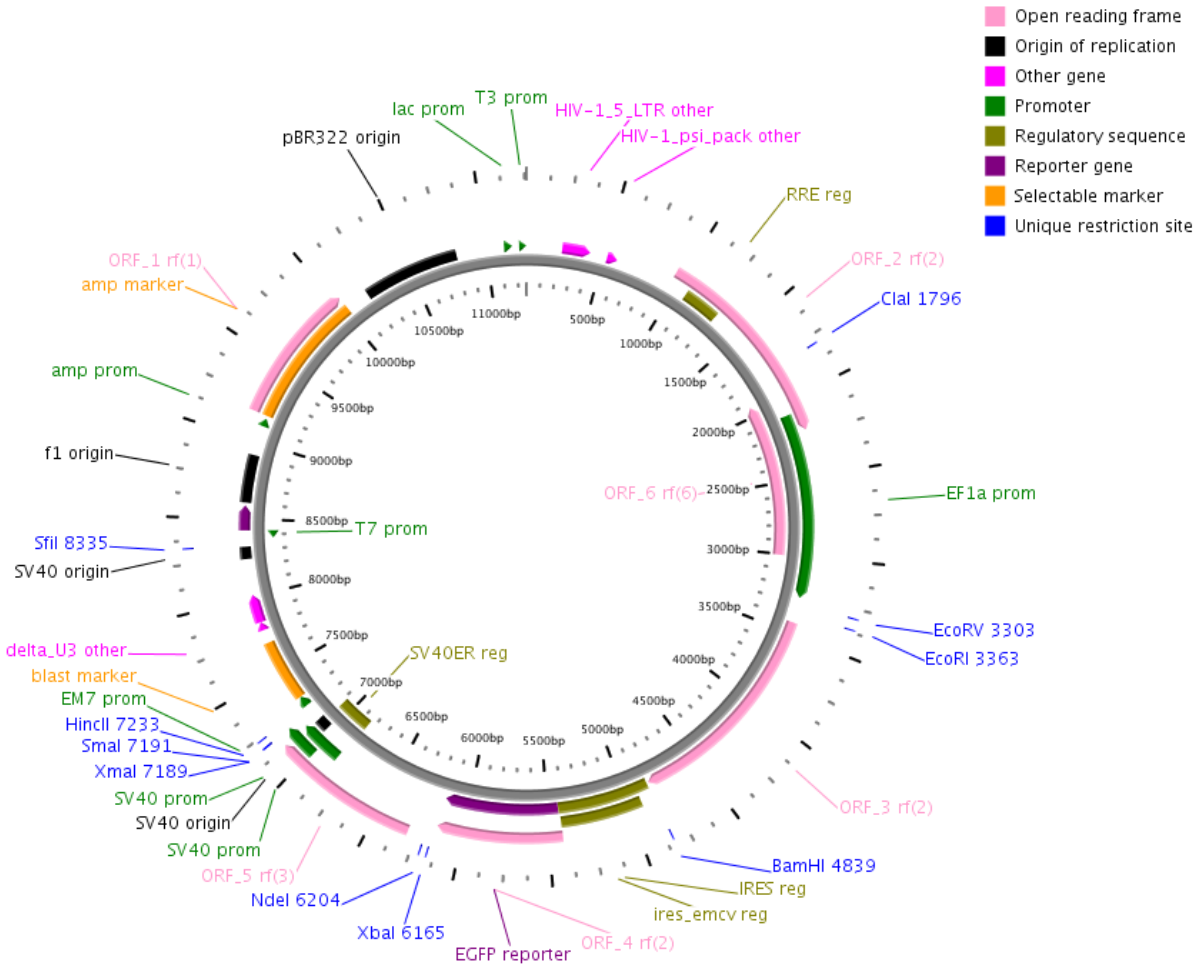

B

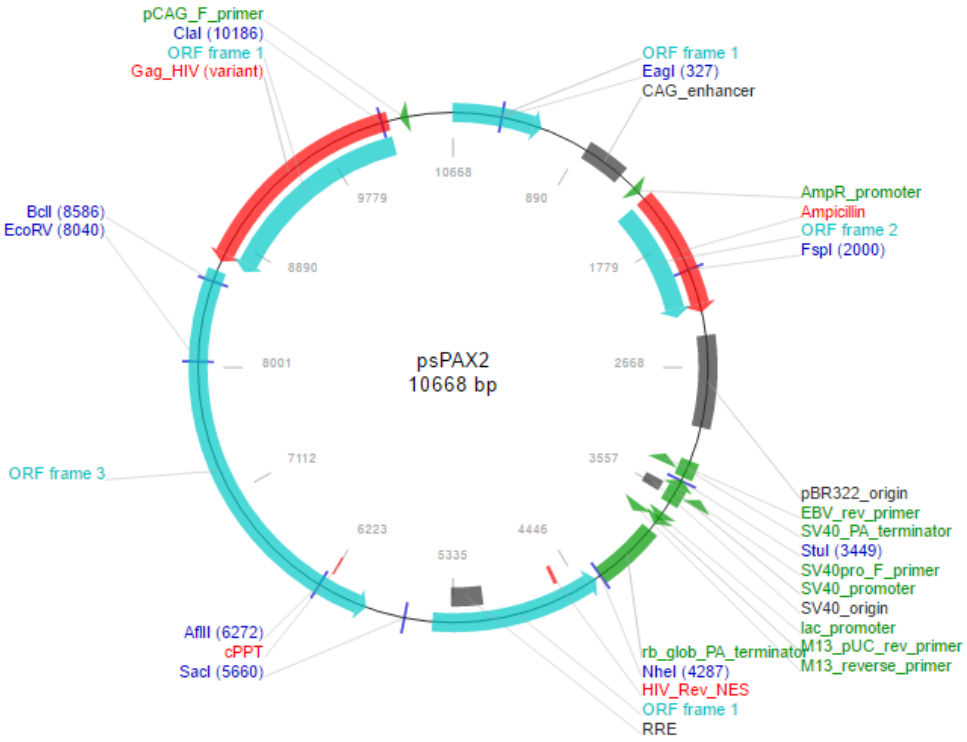

C

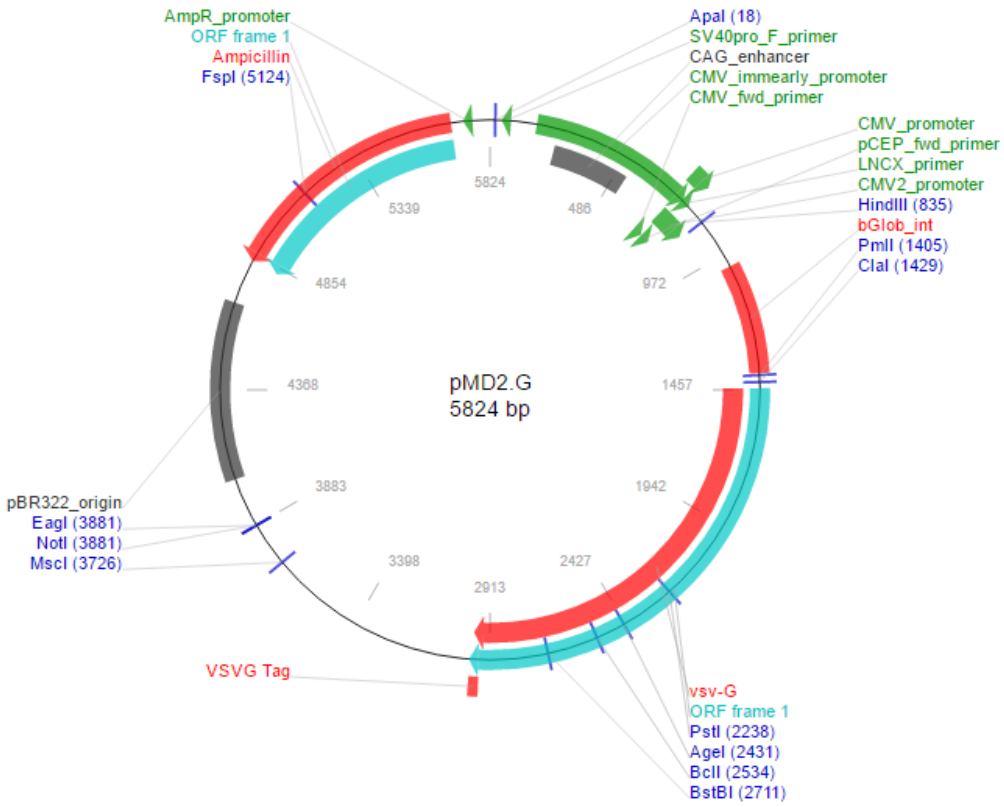

Figure 8 Plasmid maps of (A) Plenti-EF1α Vector, (B) psPAX2 and (C) pMD2.G

3.2.4.3 Plasmid isolation

Depending on the scale of isolation, competent cells were inoculated either to 3 mL culture tubes or 200 mL LB medium in 500 mL Flasks. The bacteria were shaken in 37°C incubator (200-250 rpm) overnight and next day, plasmid isolation for small scale was performed using QIAprep Spin Miniprep Kit and for large scale Macherey Nagel Maxi Prep Kit. The supplied protocol of company was followed during the isolations.

3.2.4.4 Plasmid digestion and ligation

Plasmids (3 µg) were digested using EcoRI and BamHI restriction enzymes in appropriate buffer for 1.5 hour at 37°C. The resulted bands were visualized by gel electrophoresis (1% agarose), using GelStar® Nucleic Stain or ethidium bromide on a Dark Reader Transilluminator, in the presence of 100 bp and 1 kb plus DNA ladder. The correct bands were excised and purified via QIAquick Gel Extraction Kit, followed by MiniElute PCR Purification Kit for improved purity.

Mix Type	Component	Quantity	Condition
Restriction Digestion Mix	BamHI	1 µL (10 U)	
	EcorI	1 µL	
	Buffer A	2 µL	
	DNA	3 µg	
	H_2O	Up to 20 µL	
			Incubated for 2 hours at 37°C
Ligation Mix	Insert	~ 10 ng	
	Vector	~ 50 ng	
	T4 DNA Ligase Buffer	0.5 µL	
	T4 DNA Ligase	1 µL (5 U)	
	H_2O	Up to 5 µL	
			Incubated for 16 hours at 16°C

Table 2 Restriction digestion and ligation mix and components

3.2.4.5 Bacterial transformation and ligation confirmation

Competent bacteria were transformed using all of the ligation mix via the heat-shock method, then plated on agar containing proper antibiotic (ampicillin 100 µg/mL) and incubated overnight at 37°C.

No	Step	Quantity	Temperature	Time
1	Bacteria Thawing	100 µL	On Ice	15 minutes
2	Incubation of Ligation Mix with bacteria	+ 5 µL	On Ice	30 minutes
3	Heat Shock		42°C (water bath)	45 seconds
4	Bacterial wall restabilisation		On Ice	5 minutes
5	Liquid preculturing	+ 900 µL SOC	37°C. (incubator)	60 minutes
6	Bacteria harvesting – centrifugation 7000xg,			3 minutes
7	Concentrating bacteria	- 900 µL medium		
8	Resuspending pellet with remaining medium			
9	Plating on agar	100 µL		
10	Incubation			Overnight

Table 3 Bacterial transformation protocol

Inoculums of resulted colonies were selected and transferred to small culture volume and verified by restriction enzyme digestion and/or sequencing of the isolated plasmids.

3.2.4.6 Polymerase chain reaction (PCR)

In some instances, in order to check ligation products, polymerase chain reaction was used.

Mix Type	Component	Quantity	Condition
Accuprime Pfx DNA polymerase	Enzyme mix	12.5 µL (10 U)	
	Primer Forward	1 µL	
	Primer Reverse	1 µL	
	DNA	10-100 ng	
	H_2O	Up to 25 µL	
			Proceed to PCR Reaction

Table 4 Polymerase Chain Reaction Mixture

No	Step	Temperature	Time
1	Initial Denaturation	94°C	120 seconds
2	Denaturation	94°C	15 seconds
3	Annealing	58-63°C	15 seconds
4	Extension	68°C	1 minute per kb
5	Cycle		30 cycles (Step 2>4)
6	Initial Storage	4°C	overnight
7	Long Term Storage	-20°C	

Table 5 Polymerase chain reaction conditions

3.2.4.7 Real time polymerase chain reaction

Differentiated macrophages were used to assess gene transcription profile of cytokines or some markers.

Modified Phenol Chloroform Extraction Method was used to isolate RNA from cells.

3.2.4.7.1 mRNA isolation via phenol chloroform extraction

No	Step	Quantity	Temperature	Time
1	Washing the cells in 6-well plate in PBS twice			
2	Adding QIAzol to tissue/cells	+ 1 mL		5 minutes
3	Incubation with chloroform with mixing	+ 200 µL	Room temperature	3 minutes
4	Centrifugation 13,000xg,		4°C	15 minutes
5	Collection of the aqueous phase	- 400 µL		
6	Mixing with isopropanol 1:1 (vol)	+ 400 µL	On ice	
7	Centrifugation 13,000xg,		4°C	20 minutes
8	Washing 3 times with 70 % Ethanol	300 µL	On ice	5 minutes
9	Airdrying		Room temperature	Until ethanol evaporates
10	Resuspension of RNA Samples RNAase Free Water	11 µL	On ice	
11	Long Term Storage		- 80°C	2-3 months

Table 6 Protocol of phenol chloroform extraction

3.2.4.7.2 Reverse transcription

Mix Type	Component	Quantity	Condition
Reverse Transcription Mix I	RNA	8 µL	
	Hexanucleotids (mM)	1 µL	
	dNTPs (mM each)	1 µL	
>>> Start RT Program			
	Temperature	**Time**	
	65°C	5 minutes	
	4°C	1 minute	
	4°C	Pause	
Reverse Transcription Mix II	**Component**	**Quantity**	**Condition**
	Forwards Strand Buffer 5x	4 µL	
	DTT (0.1 M)	2 µL	
	SuperScript III	1 µL	
			Completed to 20 µL
>>> Continue RT Program			
	Temperature	**Time**	
	25°C	5 minutes	
	55°C	1 hour	
	70°C	15 minues	
	4°C	Overnight	
	- 20°C		Long Term Storage

Table 7 Protocol of reverse transcription from isolated mRNA

3.2.7.4.3 sqRT-PCR

Mix Type	Component	Quantity	Condition
RT-PCR Mix per well	SybrGreen mix	12.5 µL	
	Primer Forward	1 µL	
	Primer Reverse	1 µL	
	DNA	1 µL	(100 ng/µL)
	H_2O	8.5 µL	
			Proceed to PCR Reaction

Table 8 RT-PCR mix and its components

No	Step	Temperature	Time	Cycle
1	Initial Denaturation	95°C	10 minutes	
2	Denaturation	95°C	15 seconds	40 cycles
3	Annealing	60°C	30 seconds	
4	Elongation	72°C	30 seconds	
5	Inactivation	95°C	10 minutes	
6	Melting Curve	60 - 95°C	20 minutes	
7	Final	95°C	15 seconds	
8	Storage	4°C		

Table 9 RT-PCR reaction condtions

For amplifications, a Mastercycler epgradient S® was used and the results were evaluated with the manufacturer's software. Amplification specificity was confirmed by melting curve analysis and the quantification was carried out using the ΔΔCt method.

$$\Delta Ct = Ct_{TargetGen} - Ct_{ReferenceGene} \quad (1)$$

$$\Delta\Delta Ct = \Delta Ct_{Stimulation} - \Delta Ct_{Control} \quad (2)$$

$$\text{Fold change} = 2^{-\Delta\Delta Ct}$$

3.2.4.8 Plasmid transfection to HEK293FT cells

For the overexpression of proteins, lentiviral particles were generated. In this regard, the lentiviral plasmid containing the gene of interest was mixed with packaging plasmids psPAX2 and pMD2.G and added on HEK293FT cells pre-seeded on poly-L-lysine, in 15cm2 dishes (6.5 x10^6 cells/dish seeded in MEF media 24h.

No	Step	Component	Quantity	Condition
1	Preparation of Lipofectamine Mix	Lipofectamine 2000	72 µL per well	
		Opti-MEM	Complete to 3 mL	Incubation for 5 minutes at RT
2	Preparation of Plasmid Mix	pLENTI-EF1α-Gene	19 µg	
		psPAX2	6 µg	
		pMD2.G	6 µg	

		Opti-MEM	Complete to 3 mL	
3	Final Mix	Lipofectamine Mix + Plasmid Mix	6 mL in total	Incubation for 20 minutes at RT
4	Adding drop-wise on new OPTI-MEM media			
5	Replace medium	MEF Medium	20 mL	After 24 hours
6	Confirm particle production with Lenti-X Stix Test			After 24-48 hours
7	Harvest Particles			After positive band appears in Stix Test
8	Filter the medium with 0.4 µm filters			
9	Storage for later use			- 80 °C

Table 10 Protocol for plasmid transfection to HEK293FT cells to produce viral particles

3.2.4.9 Viral transduction

Viral particles stored in -80 °C fridge were thawn on ice and Lenti-X concentrator was added in 1/3 ratio of previous media volume and kept in 4°C fridge overnight. Centrifugation for 45 minutes at 1500g was performed and the pellet was resuspended in fresh THP1 medium. $3x10^6$ THP1 monocytes were added to the concentrated lentiviral mix and after 2 days, the medium of the cells were changed. After 3 sequential medium change, the cells were transferred to S1 incubator and they were analyzed at FACS for GFP fluorescence. If the cells are GFP positive, half of the cells were frozen and the rest was continued for FACS Sorting.

3.2.4.9.1 Fluorescence activated cell sorting (FACS) isolation of transduced THP1 cells

$20x10^6$ THP1 monocytes were obtained, centrifuged down at 1300 rpm for 3 minutes and they were resuspended in 3 mL PBS. The cells were transferred to Flow Cytometry Core Facility (FCCS), University of Bonn to sort according to GFP fluorescence and GFP^+ monocytes were seperated and transferred to fresh medium. Monocytes were incubated until they reach 90 % confluency. When the cells reached

confluency, GFP fluorescence was measured again and if they reached above 80 % GFP^+ population, experiments were started and the rest of the cells were frozen down in freezing media -80°C and stored for further use.

3.2.5 Immunochemistry

3.2.5.1 Immunocytochemistry (ICC)

For Immunocytochemistry, 10^5 THP1 monocyte cells were seeded on each chamber of chamber slide. Normal differentiation protocol was applied and in the experiment day, table 11 was followed.

No	Step	Quantity	Temperature	Time
1	Washing 3 times	500 µL PBS	RT	
2	Fixing the cells	4 % PFA	RT	15 minutes
3	Washing 3 times	500 µL PBS	RT	
4	Blocking	300 µL Blocking Solution (10 % BSA, 5 % Normal Goat Serum, 0.1 % Triton X-100)	RT	1 hour
	First Antibody	Respective concentration in 500 mL PBS	4°C	Overnight
	Washing 3 times	500 µL PBS	RT	
3	Secondary antibody	Respective concentration in 500 mL PBS	RT	2 hours
4	Washing 3 times	500 µL PBS	RT	
5	Covering slides with cover strips	70 µL Mowiol	RT	
6	Storage			4°C
7	Analysis			

Table 11 Protocol of immunocytochemistry

3.2.5.2 Immunoprecipitation (IP)

10^6 THP1 cells were seeded on 6-well plate and differentiated as previously described. Then, macrophages were detached by scraping in PBS and centrifuged down at 1300 rpm for 3 minutes. Cells were lysed by vortexing in 100 µL RIPA buffer that contains phosphatase and protease inhibitors (HaltTM Protease

Inhibitor) on ice. After 1 hour, the lysate was centrifuged down(13,000xg) at 4°C and the supernatant was used for further determinations.

For antigen precipitation, the lysate supernatant was incubated with magnetic Dynabeads® that were pre-coated with antibodies according to manufacturer's specifications. The immunoprecipitation of the target antigen was performed according to table 12.

No	Step	Quantity	Temperature	Time
1	Beads binding to antibody	100 µL DynaBeads+ Antibody	4°C	2 hours
2	Lysis of the cells	100 µL RIPA Buffer + 1/100 HALT™ Proteinase Coctail	On ice	1 hour
3	Centrifugation 13,000xg,		4°C	15 minutes
4	Antigen (lysate) binding to beads	+ 100 µL DynaBeads	4°C	1 hours
5	Magnetic Seperation of Beads		Room Temperature	
6	Washing 3 times with PBS	200 µL		
7	Elution	10 µL NuPage® LDS Sample Buffer + 20 µL Elution Buffer	70 °C	10 minutes
8	Magnetic Seperation of Beads			-20 °C

Table 12 Protocol of immunoprecipitation which is followed by western blot

3.2.6 Western blot

The antigens isolated by immnoprecipitation were loaded onto 10% NuPAGE® Bis-Tris Gels and run in NuPAGE® MES SDS running buffer, under constant 130 V for 90 minutes. PageRuler Plus prestained protein ladder was used as marker. The protocol presented in Table 13 was used. For transfer of proteins, the gel sandwich structure in figure 9 was established.

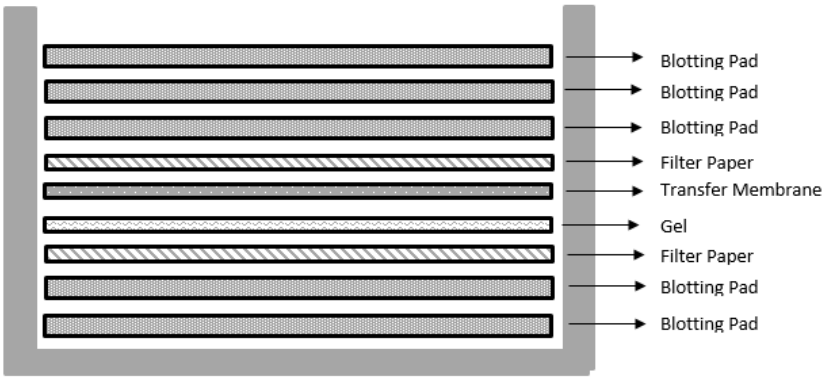

Figure 9 Structure of gel sandwich in western blot

No	Step	Quantity	Temperature	Time
1	Loading Samples	20 µL sample - 5 mL PageRuler prestained protein ladder	On ice	
2	Electrophoresis, 130 V	NuPAGE MES SDS Running Buffer	On ice	90 minutes
3	Blot (See Figure 13), 380 mA	NuPAGE® Transfer Buffer	On ice	1 hour
4	Blocking, rotation	1xTBST Buffer	Room temperature	1 hour
5	Primary antibody, rotation	Respective antibody in 1x 10 mLTBST Buffer	4°C	Overnight
6	Washing	1X TBST		3 times in 15 minutes
7	Secondary antibody, rotation	Respective phospho antibody in 1x 10 mL TBST Buffer	4°C	1 hour
8	Washing	1X TBST		3 times in 15 minutes
9	Peroxidase Labeling	300 µL SuperSignal® West Pico Luminol/Enhancer Solution + 300 µL SuperSignal® West Pico Stable Peroxide Solution	Room temperature	
10	Stripping	Restore Plus WB Stripping Buffer	Room temperature	20 minutes
11	Washing	1X TBST		3 times in 15 minutes
12	Primary antibody, rotation	Respective antibody in 1x 10 mLTBST Buffer	4°C	Overnight
13	Washing	1X TBST		3 times in 15 minutes

14	Secondary antibody, rotation	Respective antibody in 1x 10 mLTBST Buffer	4°C	1 hour
15	Washing	1X TBST		3 times in 15 minutes
16	Peroxidase Labeling	300 µL SuperSignal® West Pico Luminol/Enhancer Solution + 300 µL SuperSignal® West Pico Stable Peroxide Solution	Room temperature	

Table 13 Protocol of Western Blot

4. RESULTS

4.1 Cloning and Expression of CMAH

4.1.1 Cloning of CMAH was completed

Murine *CMAH* gene was synthesized and cloned into pLenti lentiviral vector as previously described (section 3.2.4.1) [121]. Successful cloning was confirmed by digestion of pLenti_CMAH with EcorI and BamHI restriction enzymes that resulted in two DNA fragments (Figure 10). Sanger sequencing further validated the proper insertion of the genes into construct.

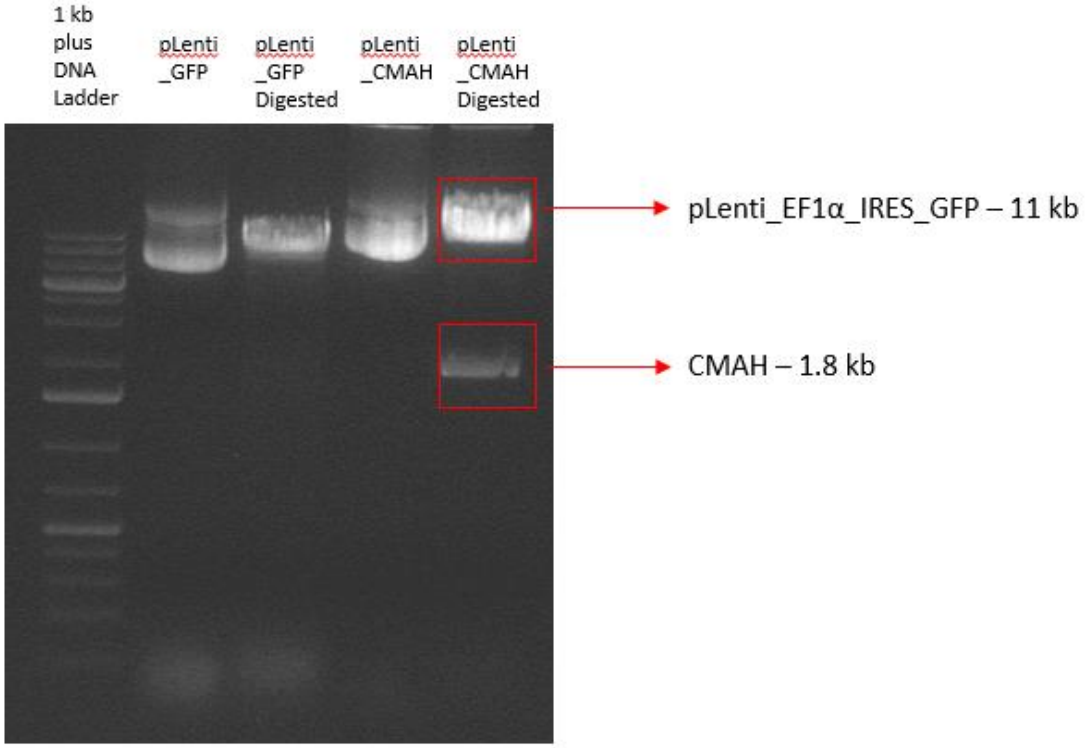

Figure 10 CMAH gene was cloned into the pLenti_EF1α lentiviral vector. Digestion of pLenti_CMAH with EcorI and BamHI restriction enzymes that resulted in two fragments. The 11 kb and 1.8 kb DNA fragments correspond to pLenti_ EF1α and CMAH, respectively.

4.1.2 CMAH expression was detected in wild type and CD33KO macrophages

Empty pLenti vector (GFP) and pLenti_CMAH (CMAH) were transfected with packaging vectors to HEK293FT cells as described in section 3.2.4.8. Afterwards, viral particles were produced and used for

transduction as described according to section 3.2.4.1 [121]. Efficiency of viral particle production was assessed via Lenti-X™ GO-StiX Test from Clontech Laboraties.

THP1 monocytes were transduced with produced lentiviral particles as decribed in section 3.2.4.9. IRES-GFP in pLenti vector enabled constitutive production of green fluorescent protein (GFP). Transduced THP1 monocytes were sorted for GFP$^+$ fluorescence. The GFP$^+$ sorting was performed for both THP1 wild type (figure 11A) and CD33KO (figure 11B) monocytes. The monocytes were first gated in forward and side scatter to distinguish healthy population. Then, at width channel of forward and side scatter, most healthy population were selected for the second time. At the final channel, THP1 monocytes were gated and sorted according to GFP$^+$ fluorescence. Viral transduction efficiency was ranging from 2-5 % in all cell lines.

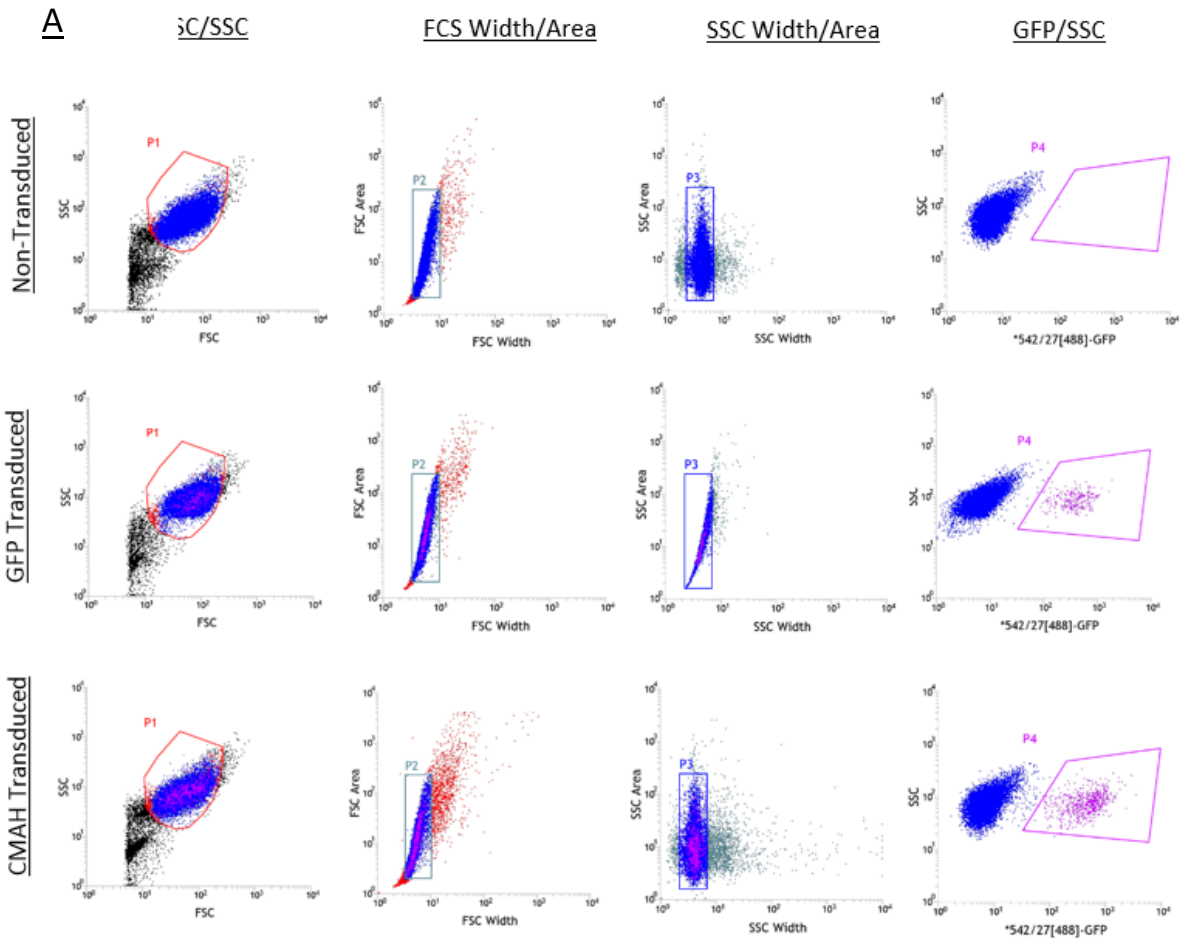

B

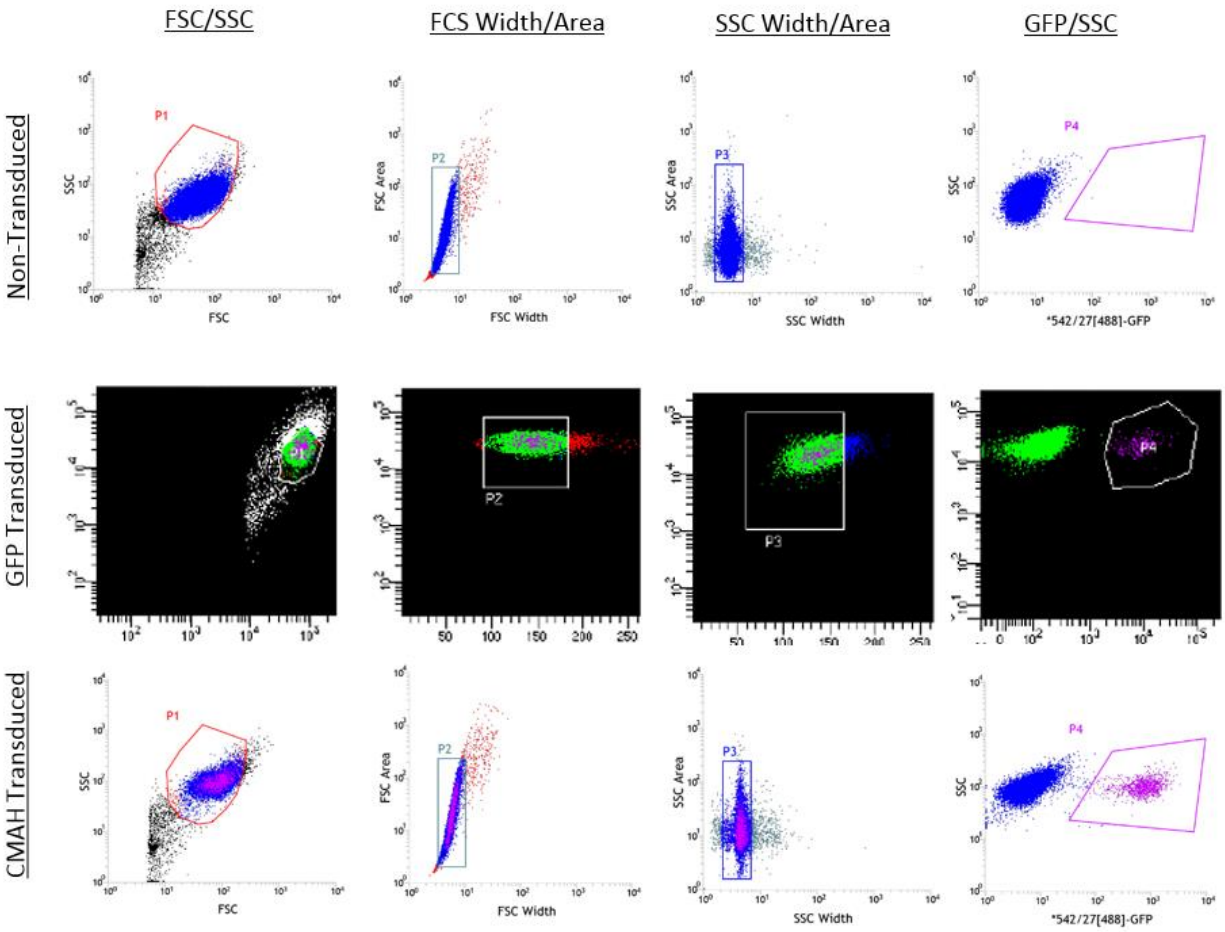

Figure 11 Viral transduced GFP⁺ monocytes were sorted in FACS. Both (A) wild type and (B) CD33KO THP1 monocytes were sorted using 3 different gates. First, the monocytes were gated according to their health in Forward (FCS) and Side scatter (SSC) channels. Then, Clustered monocytes were gated in width and area of FCS and SSC. Finally, the monocytes were gated according to GFP fluorescence. Non-transduced control cells showed no GFP⁺ population.

4.1.3 CMAH expression in THP1 macrophages led to incorporation of Neu5Gc in the glycocalyx

CMAH is the enzyme converting Neu5Ac to Neu5Gc in mammals. Because of frameshift mutation in *CMAH* gene, human cells are not able to synthesize Neu5Gc sugar in their glycocalyx. However, with dietary intake, Neu5Gc can still be incorporated into glycocalyx. To check whether transduced *CMAH* gene is functional in human THP1 macrophages, CMAH expressing THP1 monocytes were differentiated to macrophages (protocol in section 3.2.1) and stained with anti-Neu5Gc antibodies to detect presence of Neu5Gc (protocol in section 3.2.2.2). Initially, the macrophages were grown in both chicken (1%) and human serum (1%). Preliminary results showed that CMAH expressing macrophages were highly positive for Neu5Gc staining in both conditions (data not shown). Chicken serum was selected for further experiments owing to its easier accessibility (Figure 12A). Three independent experiments in chicken serum conditions showed that CMAH expression in THP1 macrophages successfully altered the glycocalyx and led to conversion of Neu5GC from Neu5Ac. After CMAH expression, Neu5Gc staining increased significantly in CMAH expressing wild type macrophages (WT CMAH) compared to empty vector transduced wild type macrophages (WT GFP). WT CMAH showed 91.2 ± 0.67 % Neu5Gc staining while WT GFP showed 0.5 ± 0.3 %, $p < 0.001$ (figure 12B).

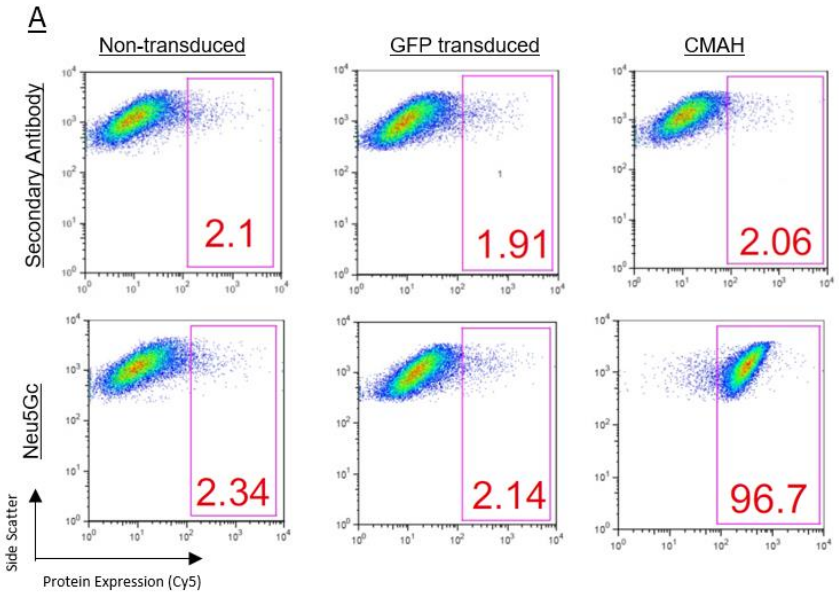

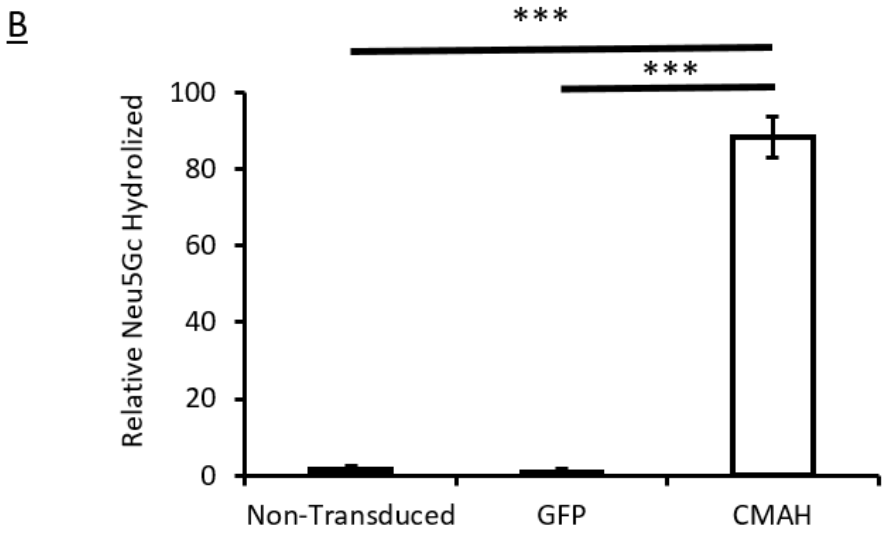

Figure 12 Activity of CMAH in transduced macrophages was demonstrated using anti-Neu5Gc antibodies in FACS. (A) The expression of murine CMAH in THP1 macrophages led to conversion of Neu5Ac to Neu5Gc. (B) While the non-transduced and control plasmid transduced macrophages (GFP) showed minimal Neu5Gc expression, CMAH expression significantly increased Neu5Gc staining in CMAH expressing THP1 macrophages (WT CMAH) (Mean±SEM, n = 3, Analyzed with One Way ANOVA followed by Bonferroni post hoc test p ≤ 0.001, data normalized to WT GFP)

Although CMAH activity was demonstrated by FACS on THP1 macrophages, how much Neu5Ac is converted to Neu5Gc could only be detected by biochemical methods. In collaboration with the group of Dr. Erdmann Rapp (Max Planck Institute for Dynamics of Complex Technical Systems, Magdeburg), advanced high performance multiplexed capillary gel electrophoresis with laser-induced fluorescence detection (xCGE-LIF) technology demonstrated the ratio of Neu5Ac/Neu5Gc in THP1 macrophages (figure 13). While WT GFP did not show any Neu5GC presence, WT CMAH showed 91.73 ± 0.38 % significant conversion of Neu5Ac to Neu5Gc ($p<0.001$, Figure 13C). However, WT CMAH cells was still expressing 8.26 ± 0.38 % Neu5Ac (which could not be converted by CMAH enzyme). Similarly, this pattern was also observed in transduced CD33KO macrophages. Empty vector transduced CD33KO macrophages (CD33KO GFP) showed 100 % Neu5Ac and no Neu5Gc presence. On the other hand, CMAH expressing CD33KO macrophages (CD33KO CMAH) showed 90.02 ± 0.30 % Neu5Gc and 9.98 ± 0.30 Neu5Ac ($p < 0.001$, figure 13C).

A

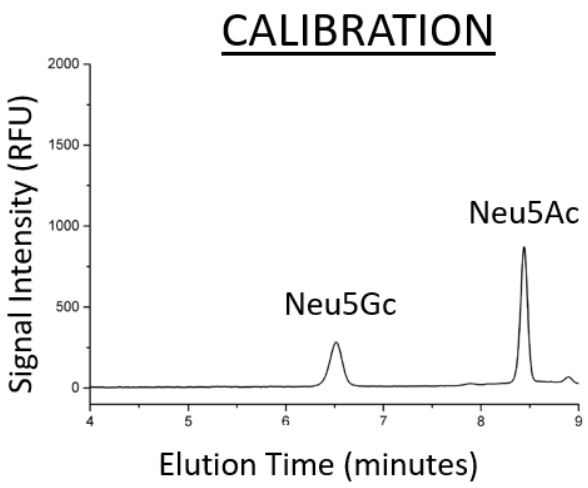
CALIBRATION
Signal Intensity (RFU)
Neu5Gc
Neu5Ac
Elution Time (minutes)

B

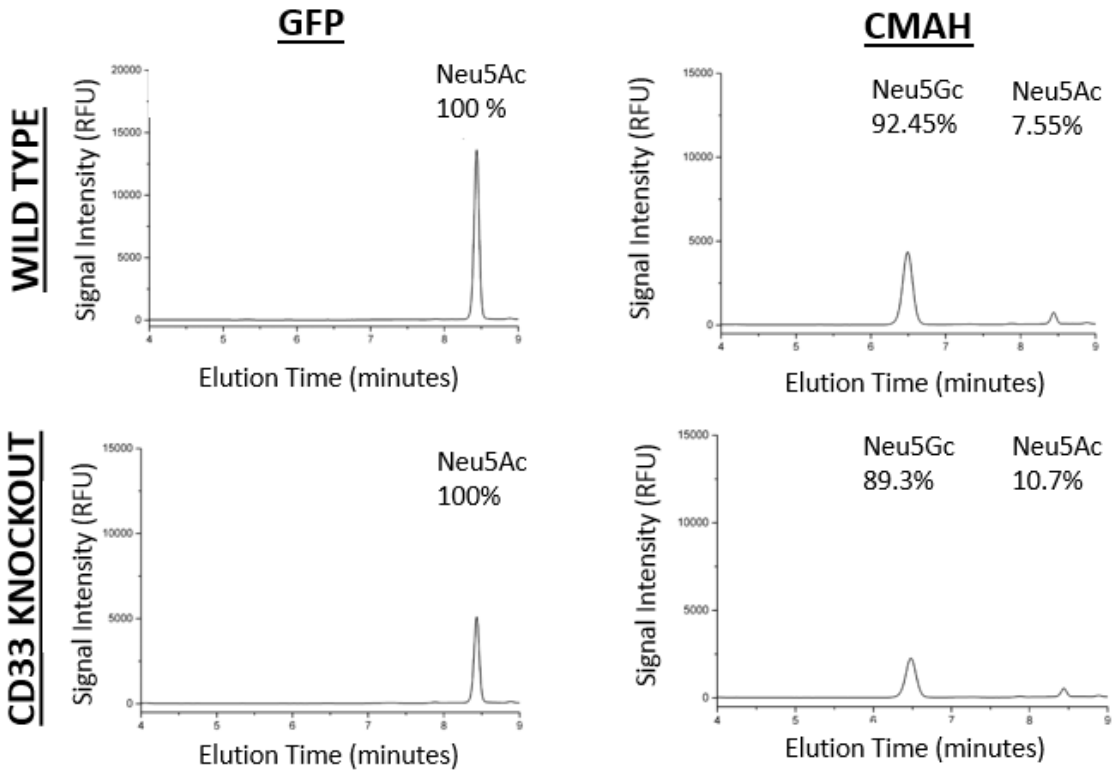
GFP
CMAH
WILD TYPE
CD33 KNOCKOUT
Signal Intensity (RFU)
Neu5Ac
100 %
Neu5Gc
92.45%
Neu5Ac
7.55%
Neu5Ac
100%
Neu5Gc
89.3%
Neu5Ac
10.7%
Elution Time (minutes)

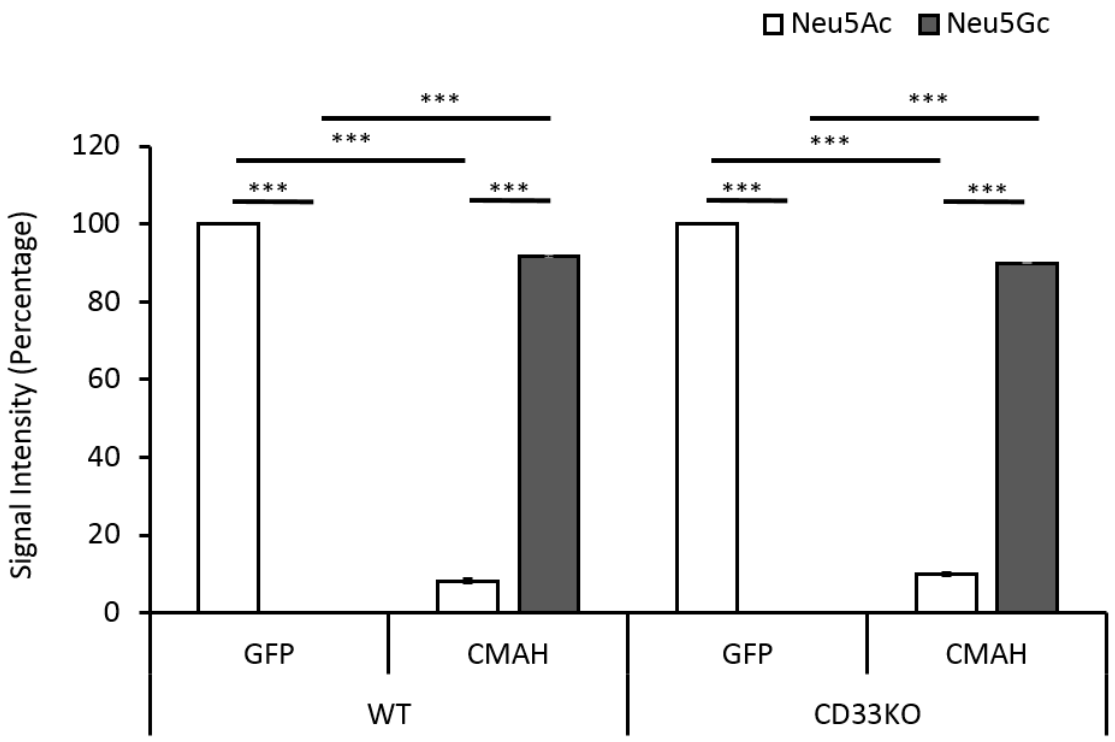

Figure 13 Relative Neu5Gc and Neu5GC presence in transduced macrophages was revealed by Advanced xCGE-LIF technique and CMAH expresing macrophages predominantly expressed Neu5Gc. (A) Elution time of Neu5Ac and Neu5Gc peaks were optimized in HPLC. (B) Transduced macrophages were analyzed for the percentage of Neu5Ac and Neu5Gc. (C) Neu5Gc is predominantly found in CMAH overexpressing macrophages (WT CMAH and CD33KO CMAH), whereas Neu5Ac in control samples (WT GFP and CD33KO GFP). Both Neu5Ac and Neu5Gc were present on CMAH expressing macrophages. (Mean±SEM, n = 3, Analyzed with one way ANOVA followed by Bonferroni post hoc test $p \leq 0.001$, data normalized to WT GFP)

4.2 Phagocytosis and Oxidative Stress

4.2.1 CMAH expressing in THP1 cells show decreased apoptotic debris internalisation and Aβ Phagocytosis

After assessing the significant alterations in the glycocalyx after CMAH expression, functional changes related to AD phenotype were assessed. Since Aβ and apoptotic debris internalisation are highly altered and deteriorated in AD phenotype, uptake of Aβ and debris were analyzed for non-transduced wild type macrophages (NT), WT GFP, and WT CMAH. Aβ particles were incubated for 3 days in 37^{o} C for polymerization and macrophages were treated with particles as described in section 3.2.2.3.3. Retinal

debris was produced from ARPE cells and stained with DiI solution according to section 3.2.2.3.2. Uptake of Aβ and debris were confirmed with 3-dimensional reconstruction of confocal images (figure 14A and 14C, respectively). Aβ phagocytosis decreased significantly in WT CMAH compared to WT GFP (0.69 ± 0.05 FC, $p < 0.001$, figure 14B). Debris phagocytosis also significantly decreased in WT CMAH compared to WT GFP (0.57 ± 0.06 FC, $p < 0.05$, figure 14D). These results led to conclusion that Neu5Gc incorporation in high levels caused by CMAH expression has inhibiting effect on phagocytosis.

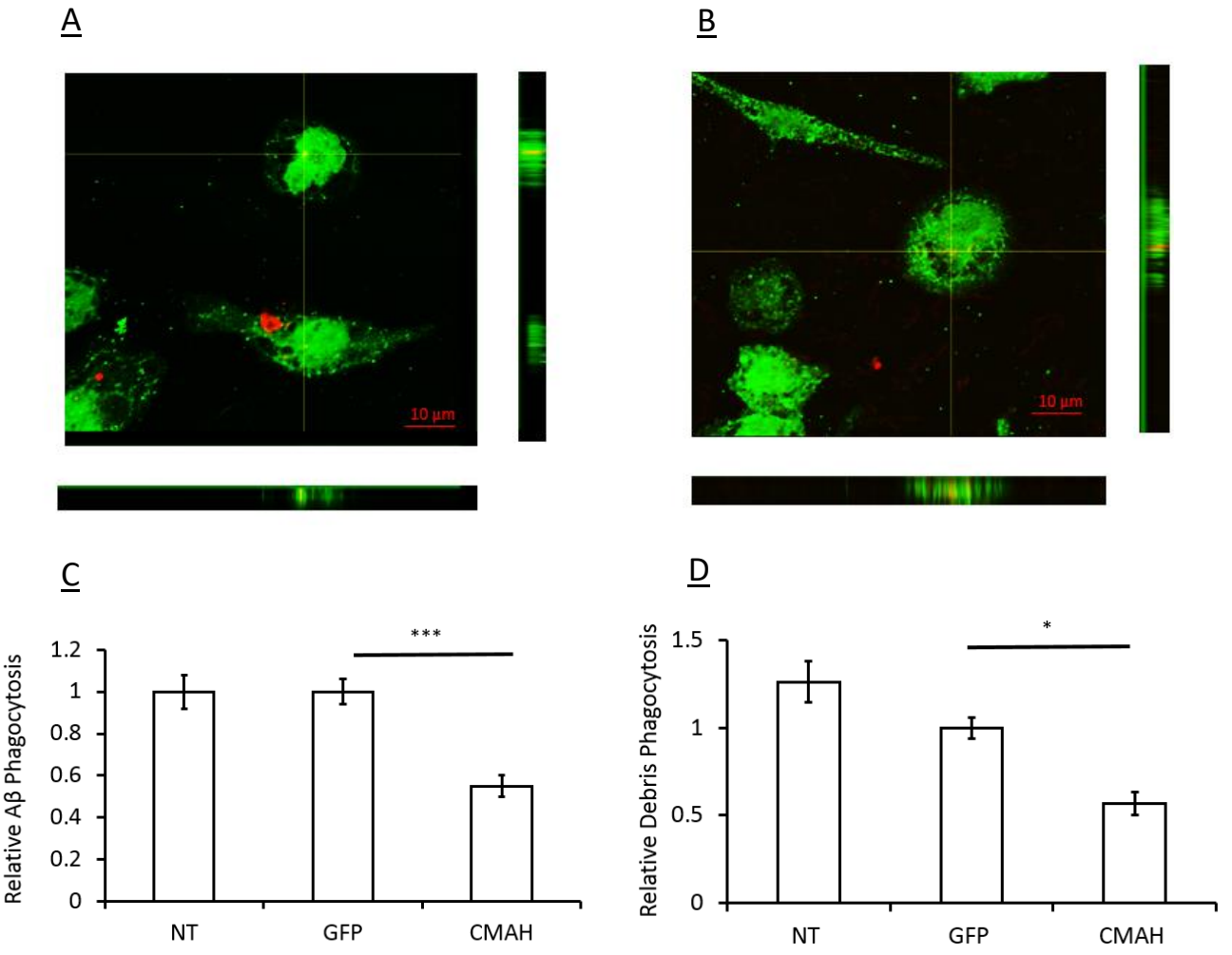

*Figure 14 WT CMAH expressing cells showed decrease in both Aβ and Debris phagocytosis. (A-C) WT CMAH showed significant decrease in Aβ phagocytosis compared to WT GFP. (B-D) WT CMAH demonstrated significant decrease in debris phagocytosis compared to WT GFP (Mean±SEM, n > 3, Analyzed with one way ANOVA followed by Bonferroni post hoc test *** p ≤ 0.001, * p ≤ 0.05, data normalized to WT GFP, Red- Aβ or debris Green-CD11b, scale bar 10 µm)*

4.2.2 CMAH-mediated decrease in debris, Aβ and *Staphylococcus aureus* bioparticle phagocytosis is independent from CD33

Debris uptake is one of the important function of immune cells to regulate homeostasis. After observing decrease in phagocytosis caused by CMAH expression, I investigated the possible role of CD33 in this decline as it is one of markers of AD and it can recognize sialic acids. The effect of CMAH expression in debris phagocytosis was independent from CD33. In CD33KO CMAH, debris phagocytosis was decreased compared to CD33KO GFP (CD33KO CMAH showed 0.39 ± 0.09 FC, $p < 0.001$, figure 15). Previous decrease in wild type conditions was also confirmed in this setting (WT CMAH showed 0.45 ± 0.03 FC, $p < 0.001$). Moreover, there was also no effect of CD33 in debris phagocytosis. No significant change in CD33KO GFP was observed compared to WT GFP (CD33KO GFP showed 0.92 ± 0.13 FC, figure 15B in debris phagocytosis).

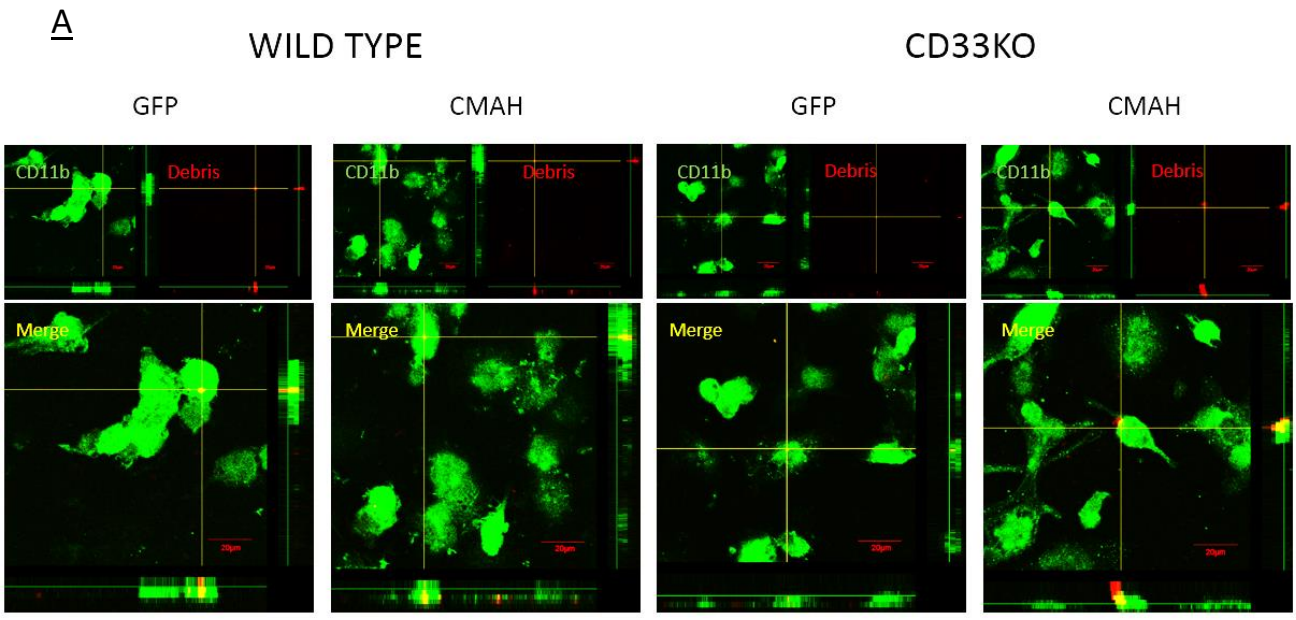

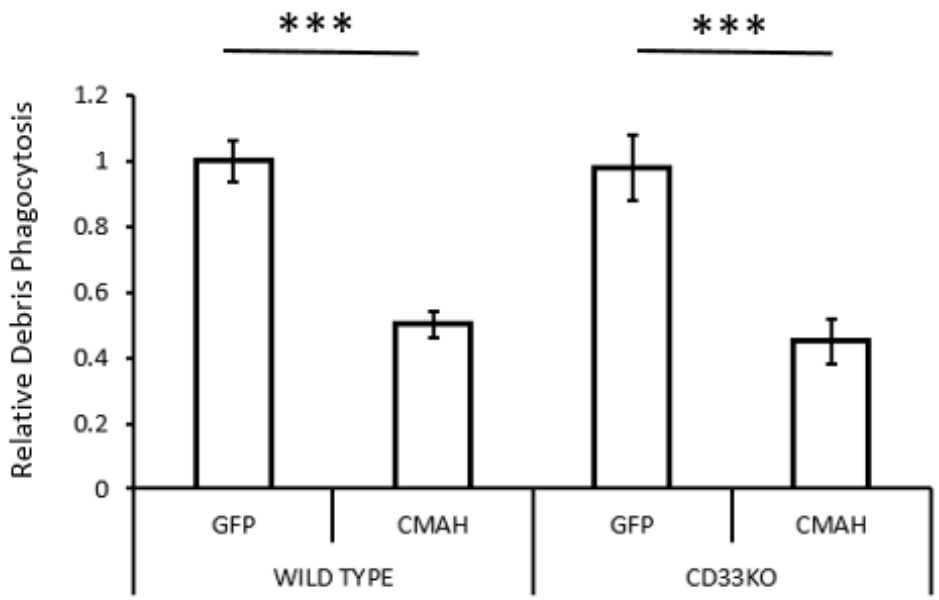

Figure 15 CMAH expression caused decrease in debris phagocytosis independent from CD33. (A) Uptaken debris in transduced macrophages can be observed in 3D constructed images. All the macrophages intenalized debris successfully (Green:CD11b, Red: neural debris), (B) CMAH expression caused significant decrease in both wild type and CD33KO macrophages. There was no difference between WT GFP and CD33KO GFP (Mean±SEM, n = 3, Analyzed with one way ANOVA followed by Bonferroni post hoc test p ≤ 0.001 data was normalized to WT GFP)

Previously, CD33 was found to be associated with AD and Aβ uptake [54,122] . Since I have revealed that CMAH expresssion decreases Aβ uptake (figure 14), I next investigated whether CD33 might be involved in this decrease (Figure 16A). Again, WT CMAH showed significantly decreased Aβ uptake compared to WT GFP (0.49 ± 0.02 FC, $p < 0.01$, figure 16B). Knocking-out CD33 increased the levels of Aβ uptake and CD33KO GFP showed significant increase in Aβ uptake compared to WT GFP (CD33KO GFP showed 1.88 ± 0.13 FC, $p < 0.001$, figure 16B), whereas CD33KO CMAH also showed significant decrease in Aβ phagocytosis compared to CD33KO GFP (1.12 ± 0.13 FC, $p < 0.001$, figure 16B). Thus, CMAH expression in CD33KO macrophages diminished the elevated levels of Aβ phagocytosis in CD33KO GFP to WT GFP levels.

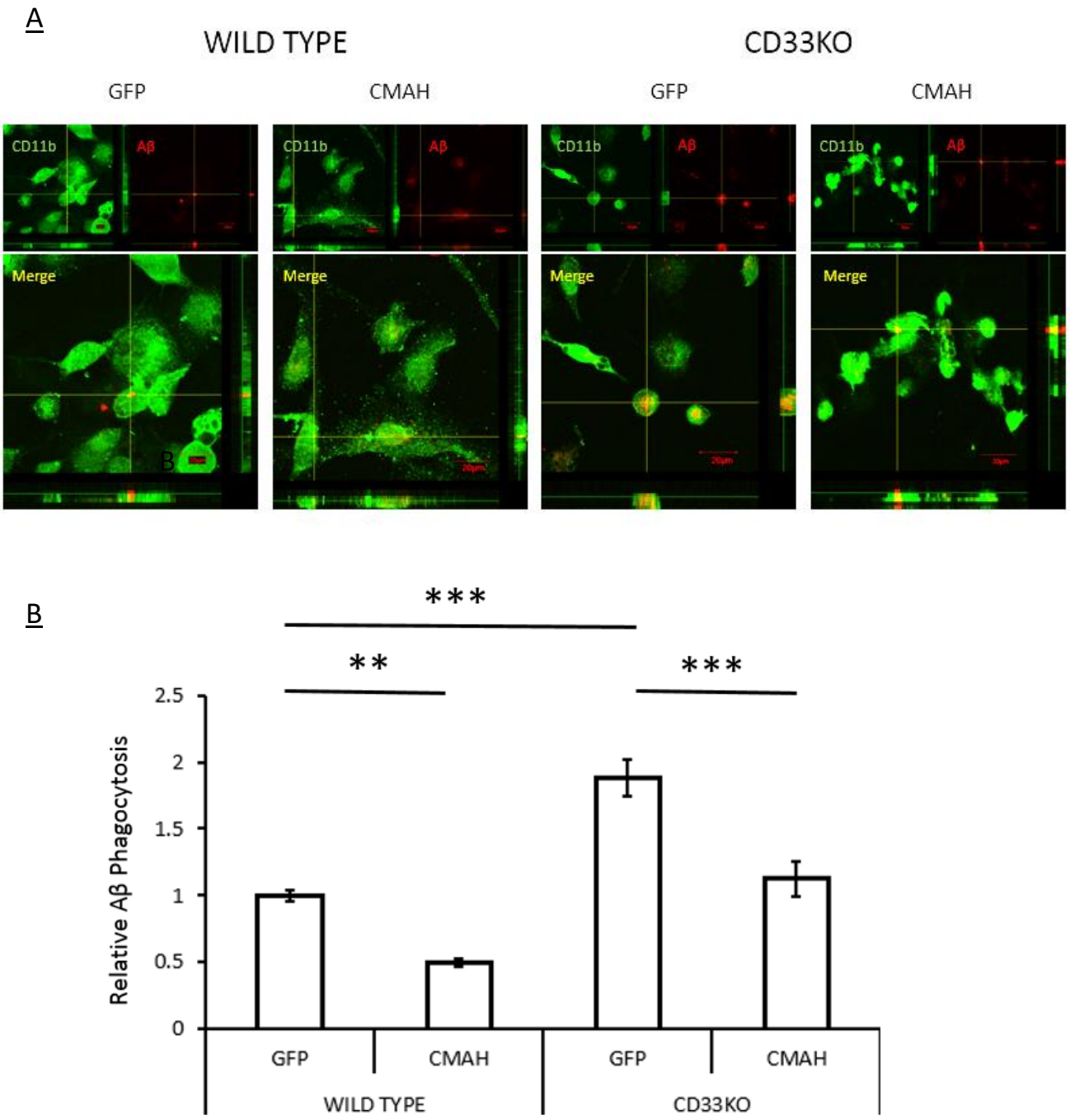

*Figure 16 CMAH expression decreased Aβ uptake independent from CD33 and it decreased elevated phagocytic phenotype of CD33KO macrophages to normal levels. (A) 3D constructed images of uptaken Aβ in transduced macrophages can be observed. All the macrophages have succesfully taken Aβ particles (Green:CD11b, Red: Aβ) (B) CMAH transduction caused significant decrease in both wild type and CD33KO background. There was significant increase in CD33KO GFP compared to WT GFP. Combination of lack of CD33 with CMAH overexpression decreased the uptake to normal level (Mean±SEM, n = 4, Analyzed with one way ANOVA followed by Bonferroni post hoc test ***p ≤ 0.001, ** p ≤ 0.01, data normalized to WT GFP)*

Bacterial bioparticle uptake is an important function of macrophage cells. Bacterial particles which were coupled to phRODO dye was used to assess internalization by macrophages (figure 17A). phRODO is pH sensitive dye which is fluorescencent when internalized by macrophages within lysosomes [123,124]. The experiment was completed according to section 3.2.2.3.1. WT CMAH showed significant decrease in bioparticle uptake compared to WT GFP (0.68 ± 0.06 FC, $p < 0.001$, Figure 17B). The uptake of bioparticles was also analyzed in CD33KO background to detect CD33-dependent effects. No significant difference was observed between WT GFP and CD33KO GFP (CD33KO GFP showed 0.75 ± 0.27 FC in bioparticle uptake). Increased uptake in WT GFP that is significantly decreased by CMAH expression; CD33KO leads to trend of decreased uptake (not reaching significance) that is further accentuated by CMAH expression (CD33KO CMAH showed 0.69 ± 0.30 FC in bioparticle uptake and the difference was not significant).

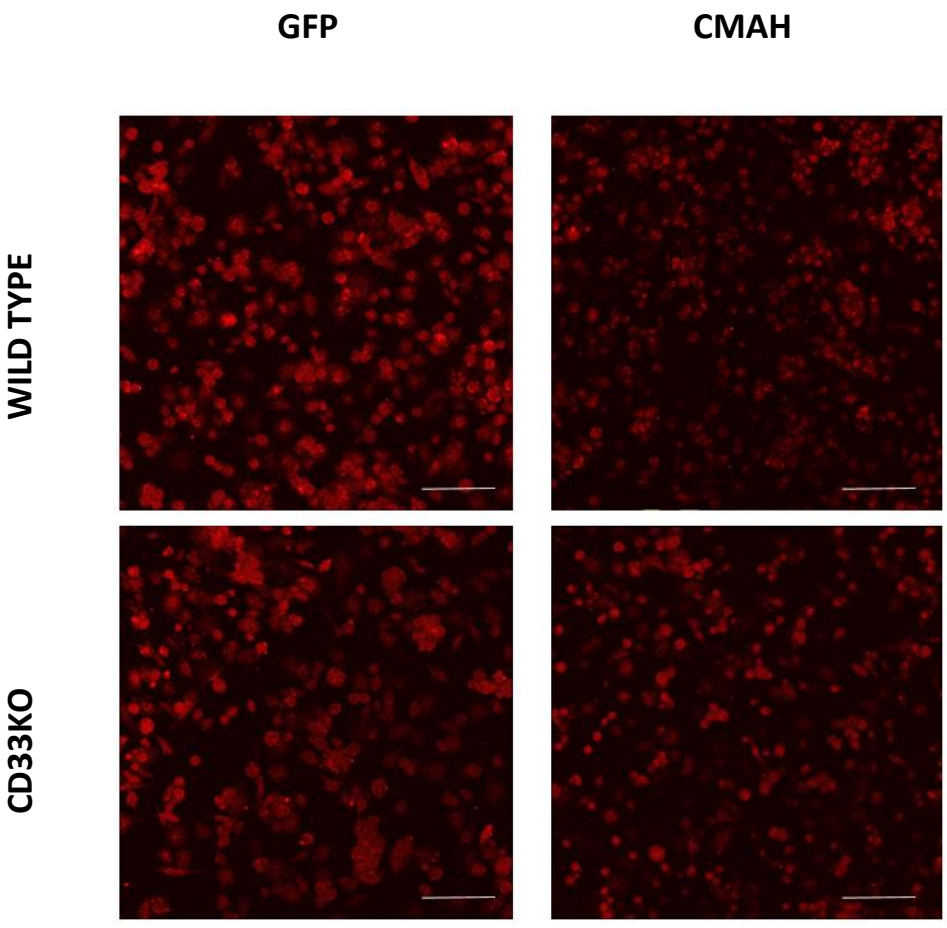

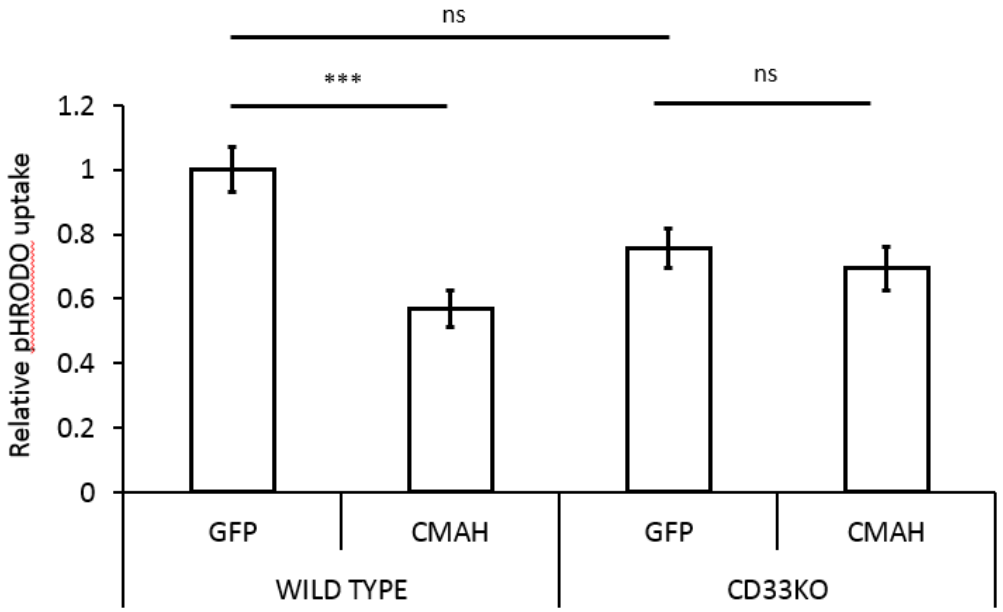

*Figure 17 CMAH expression decreased phRODO coupled bacterial bioparticles in macrophages and the responses were accentuated in CD33KO background. (A) Macrophages taken up phRODO bioparticle appeared as red in the images taken in confocal microscope. (B) WT CMAH showed decreased bioparticle uptake compared to WT GFP. However, this difference was not observed in CD33KO background. Also no significant change was observed between CD33KO GFP and WT GFP (Mean±SEM, n = 5, Analyzed with one way ANOVA followed by Bonferroni post hoc test ***p ≤ 0.001, **, data normalized to WT GFP, scale bar= 40 µm)*

4.2.3 Decreased neuraminidase activity caused impaired phagocytosis

Prior to phagocytosis, macrophages and other phagocytic cells remove sialic acids on their membrane [125]. Although the underlying reason of this clearance has not been clarified completely, it might be to remove the effect of inhibitory signaling of ITIM signaling to initiate complete phagocytosis. Since removal of sialic acids were performed with neuraminidases, I investigated whether neuraminidase activity was altered in CMAH expressing macrophages in pathological conditions. To mimic pathological conditions, macrophages were treated with pre-incubated Aβ particles. *Sambucus nigra* lectin was used to stain the sialic acids on macrophages [126] and decrease in lectin staining after Aβ treatment was measured. WT CMAH showed significant decrease in response to Aβ treatment compared to response of WT GFP (WT CMAH showed 5.03 ± 2.11 % vs while WT GFP showed 19.96 ± 3.88 %, $p < 0.05$, figure 18). CD33KO GFP showed a decrease in response to Aβ treatment, but the difference was not significant compared to

response of WT GFP (CD33KO GFP showed 8.18 ± 3.73 % response to Aβ treatment, figure 18). Moreover, despite that there was decrease in response of CD33KO CMAH compared to WT CMAH, the decrease in response of CD33KO CMAH was not significant (CD33KO CMAH showed 3.96 ± 2.63 % decrease in response to Aβ treatment, figure 18)

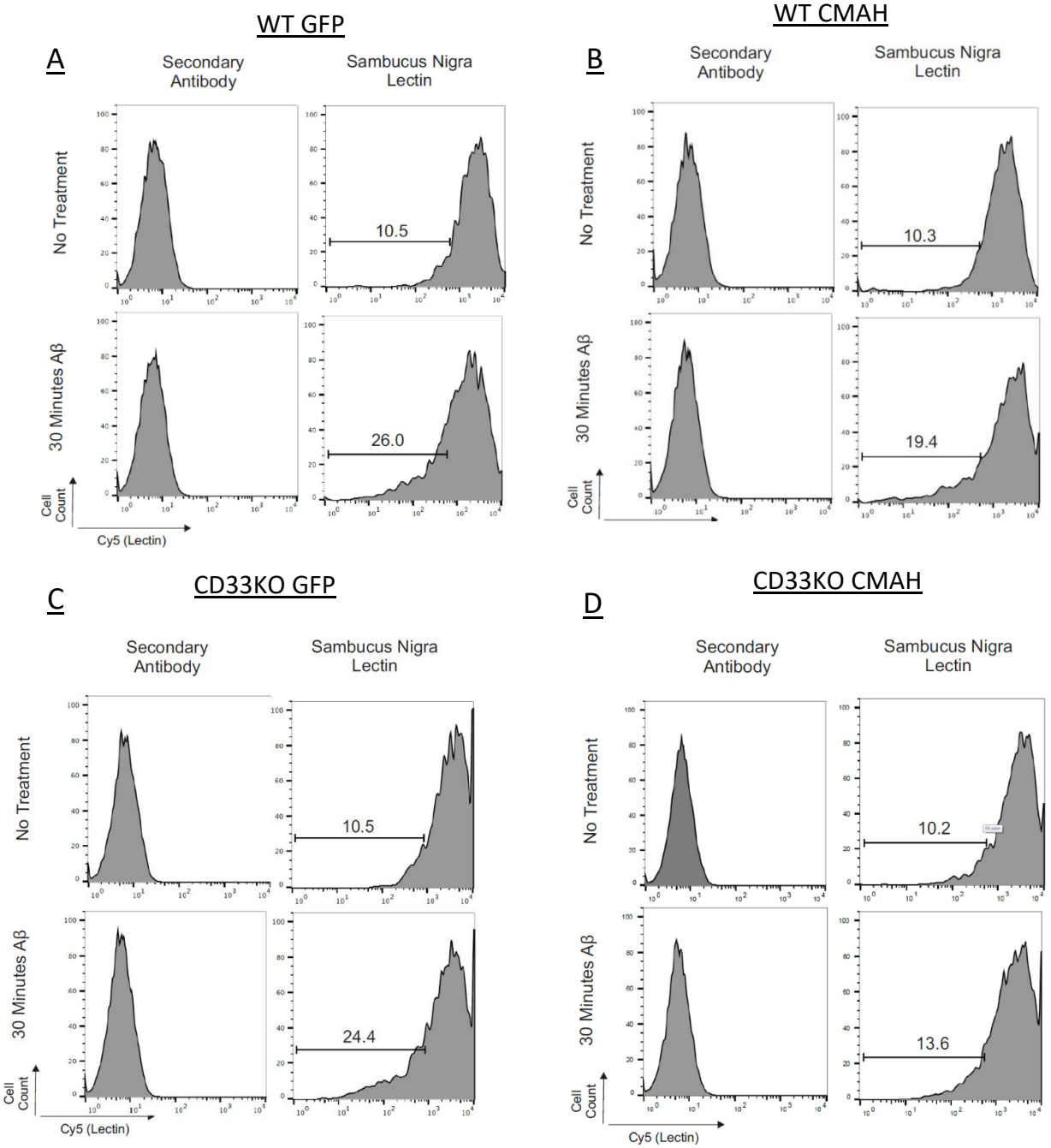

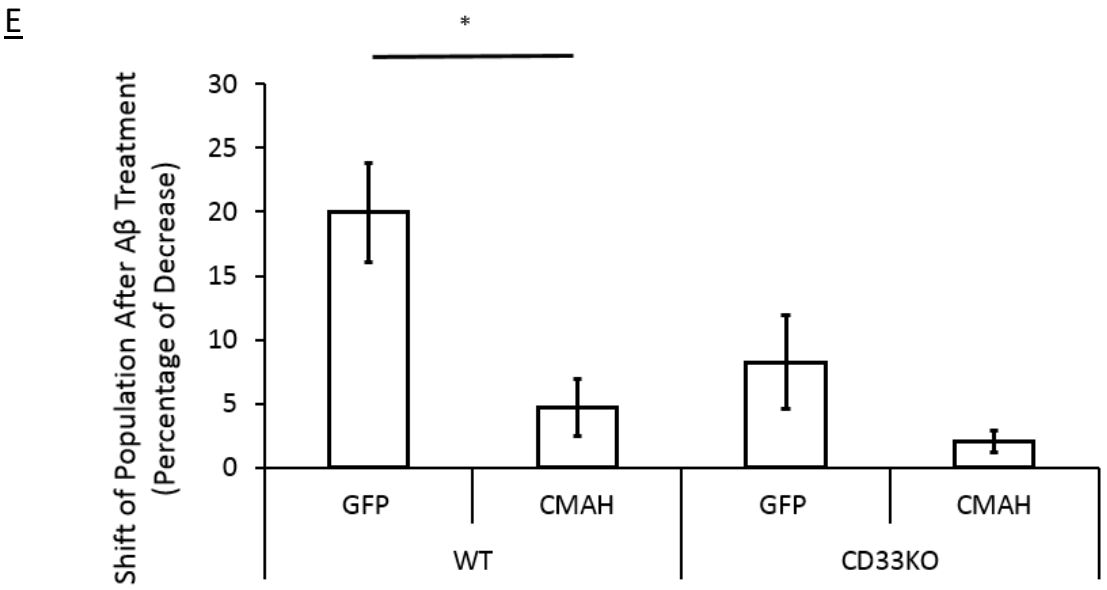

*Figure 18 CMAH expression caused diminished response to Aβ demonstrated by lectin staining. Responses of (A) WT GFP, (B) WT CMAH, (C) CD33KO GFP and (D) CD33KO CMAH to Aβ treatment were analyzed by FACS after lectin staining. Decrease in lectin staining after Aβ stimulation was assessed for each macrophage type (E) WT CMAH showed significant decrease in response to Aβ treatment compared to WT GFP. Despite marked decrease in response of CD33KO GFP compared to WT GFP, the decrease was not significant. Moreover, there was no significant change between CD33KO CMAH and WT CMAH (Mean±SEM, n = 3, Analyzed with one way ANOVA followed by Bonferroni post hoc test * p ≤ 0.05, data normalized to WT GFP).*

4.2.4 Superoxide release was increased in CMAH transduced macrophages

Free radical production is a defense mechanism for macrophages to fight against pathogens. Reactive oxygen species (ROS) such as peroxides, superoxide, hydroxyl radical, and singlet oxygen are released to clear the area of infection [127]. However, improper functioning of ROS production mechanisms can also damage the organisms' residents cells. In this experiment, the effect of CMAH expression on reactive oxygen species (ROS) production was assessed via DHE staining (figure 19A). DHE reacts with superoxide anions and forms a red fluorescent product (ethidium) which intercalates with DNA and by measuring the DHE staining [128,129], ROS production by macrophages can be analyzed. WT CMAH elicited significant

increase in ROS production compared to WT GFP (CMAH transduced cells showed 1.45 ± 0.06 FC, $p < 0.001$, figure 19B).

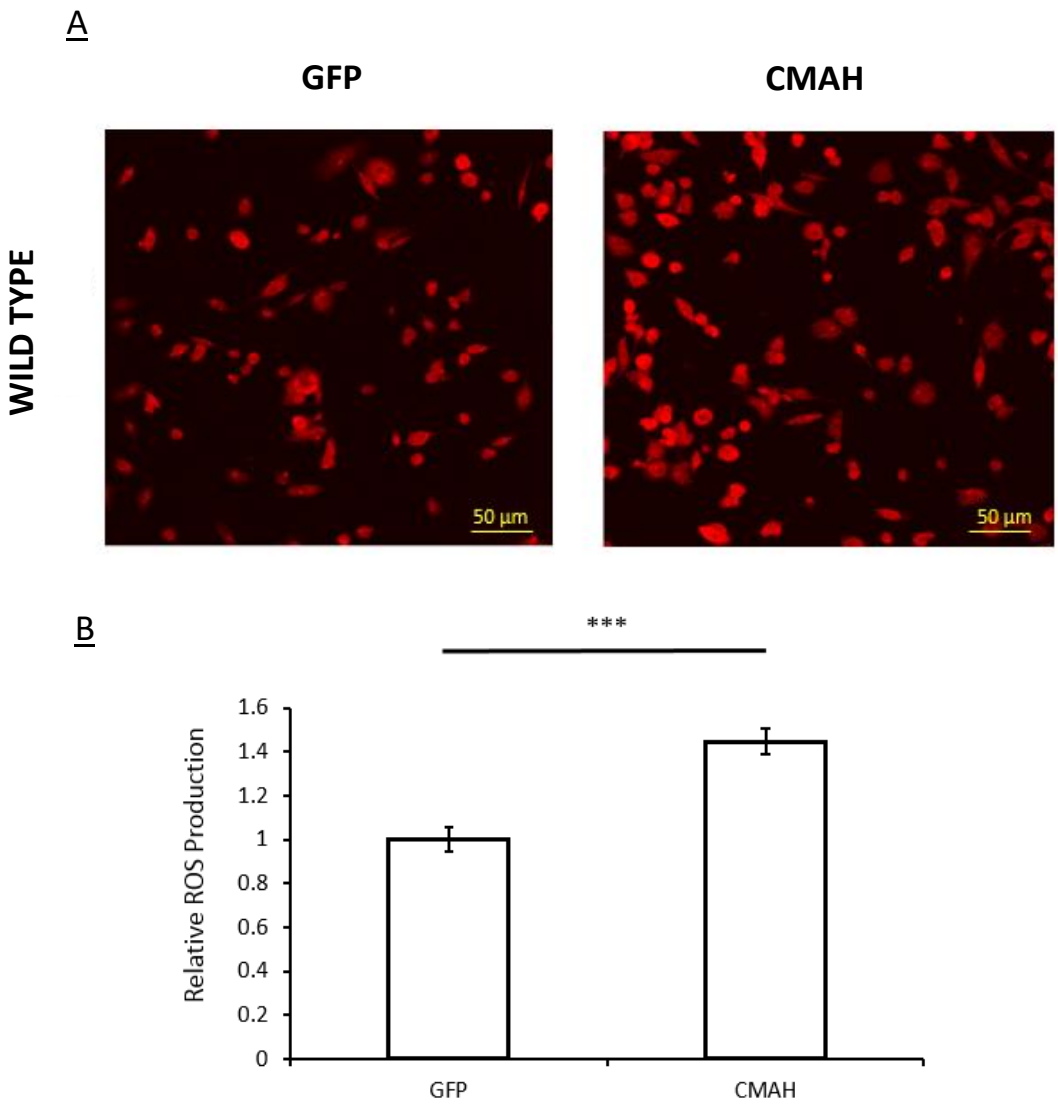

Figure 19 CMAH expression caused increase in ROS production in wild type background. DHE is a dye intenalized by macrophages and it gives red color though reaction with superoxides. (A) Red color was measured using images from confocal microscope. (B) WT CMAH showed significant increase in ROS production compared to WT GFP (Scale Bar – 50 µM, Mean±SEM, n > 3, Analyzed with Student's T-test *** $p \leq 0.001$, data normalized to WT GFP)

To analyze how ROS production is affected by stimulation, macrophages were incubated with debris, Aβ, and *Staphylococcus aureus* bioparticles and analyzed via DHE staining. To confirm stimulus dependent increase, Trolox and SOD1 were used as ROS scavengers. Aβ stimulated WT GFP showed significant increase compared to non-stimulated condition (1.40 ± 0.07 FC, $p < 0.001$, figure 20A). SOD1 and trolox treated WT GFP elicited significant decrease in ROS production compared to Aβ stimulated condition (SOD1 and trolox showed 1.04 ± 0.06 FC, $p < 0.001$ and 0.89 ± 0.05 FC, $p < 0.001$, figure 20A, respectively). WT CMAH showed significant increase in ROS production compared to WT GFP in non-stimulated conditions, similar to previous experiments (CMAH expressing macrophages showed 1.28 ± 0.07 FC, $p < 0.001$, figure 20A). However, after Aβ stimulation, WT CMAH did not elicit any significant change (Aβ stimulated WT CMAH showed 1.38 ± 0.05 FC, figure 20A). Scavengers caused significant decrease in ROS production caused by CMAH expression (SOD1 and trolox treated WT CMAH showed 0.96 ± 0.04 FC and 0.93 ± 0.06 FC, $p < 0.001$, figure 20A).

Neural debris stimulation caused significant increase in WT GFP compared to non-stimulated condition (1.47 ± 0.05 FC, $p < 0.001$, figure 20B). This increase was eliminated by scavenger addition. (SOD1 and trolox treated WT GFP showed 0.96 ± 0.06 FC, $p < 0.001$ and 0.86 ± 0.05 FC, $p < 0.001$, figure 20B, respectively). Similar to previous experiments, WT CMAH showed significant increase in ROS production compared to WT GFP (WT CMAH showed 1.29 ± 0.06 FC, $p < 0.01$, figure 20B). However, after debris stimulation, WT CMAH did not elicit any significant change (debris stimulated WT CMAH demonstrated 1.37 ± 0.06 FC, figure 20B). Moreover, scavengers caused significant decrease in ROS production caused by CMAH expression (SOD1 and trolox treated WT CMAH showed 0.96 ± 0.06 FC and 0.92 ± 0.06 FC, $p < 0.001$, figure 20B).

Finally, treatment of *Staphylococcus aureus* bioparticles to WT GFP in ROS production demonstrated patterns of Aβ and debris stimulatIon experiments. Bioparticle treated WT GFP showed significant increase compared to non-stimulated condition (1.46 ± 0.06 FC, $p < 0.001$, figure 20C). Also, SOD1 and trolox caused significant decrease compared to bioparticle stimulated condition (SOD1 and trolox treated WT GFP showed 0.98 ± 0.06 FC, $p < 0.001$ and 0.86 ± 0.06 FC, $p < 0.001$, figure 20C, respectively). Similar to previous experiments, WT CMAH showed significant increase in ROS production compared to WT GFP (WT CMAH showed 1.38 ± 0.08 FC, $p < 0.001$, figure 20C). After bioparticle stimulation, despite marked increase in ROS production compared to bioparticle stimulated control macrophages, WT CMAH did not elicit any significant change (Bioparticle stimulated WT CMAH showed 1.62 ± 0.08 FC, figure 20C). Scavengers eliminated the increase in ROS production caused by CMAH expression (SOD1 and trolox treated WT CMAH showed 1.08 ± 0.06 FC and 1.07 ± 0.05 FC, $p < 0.001$, figure 20C).

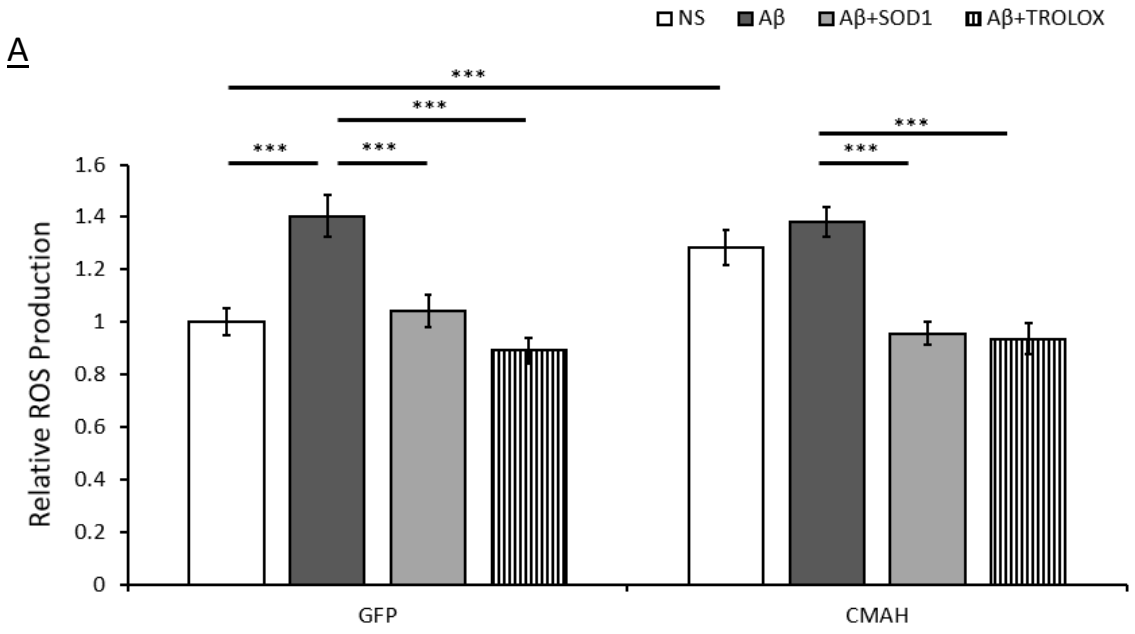

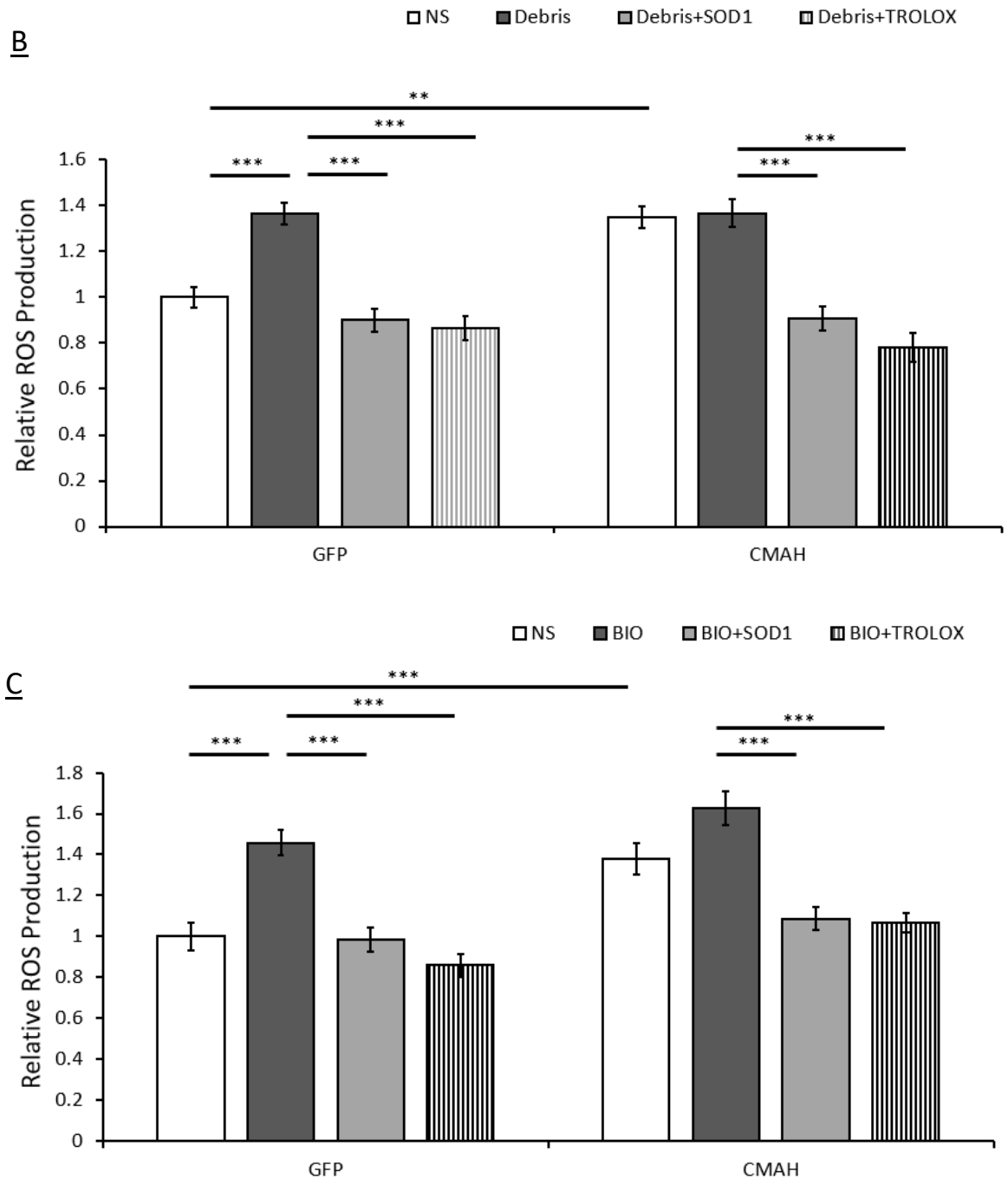

*Figure 20 ROS production did not change after (A) Aβ, (B) debris and (C) Staphylococcus aureus bioparticle stimulation by CMAH expression. After stimulation with particles, WT GFP showed significant increase compared to non-stimulation conditions (NS). Moreover, SOD1 and trolox scavengers significantly decreased ROS production caused by stimulus compared to particle stimulated conditions. Non-stimulated WT CMAH showed significant increase in ROS production compared to non-stimulated WT GFP. Trolox and SOD1 treated macrophages showed significantly decrease in ROS production and reverted the increase caused by CMAH expression. WT CMAH did not show significant increase in particle stimulated condition compared to non-stimulated condition. (Mean±SEM, n > 3, Analyzed with one way ANOVA followed by Bonferroni post hoc test ***p ≤ 0.001, ** p≤ 0.01, data normalized to non-stimulated WT GFP)*

4.2.5 CMAH-mediated superoxide release was dependent on CD33

CD33-related-Siglecs were shown as important regulator of ROS production in macrophages [130]. To assess the role of CD33 in ROS production, CD33KO GFP and CD33KO CMAH were included (Figure 21A). CD33KO CMAH showed significant decrease in ROS production compared to WT CMAH (0.79 ± 0.04 FC, $p < 0.001$, figure 21B). Moreover, no significant change was observed between CD33KO GFP and CD33KO CMAH (CD33KO GFP showed 0.91 ± 0.06 FC, figure 21B) proving that CMAH increases ROS production in CD33 dependent manner.

A

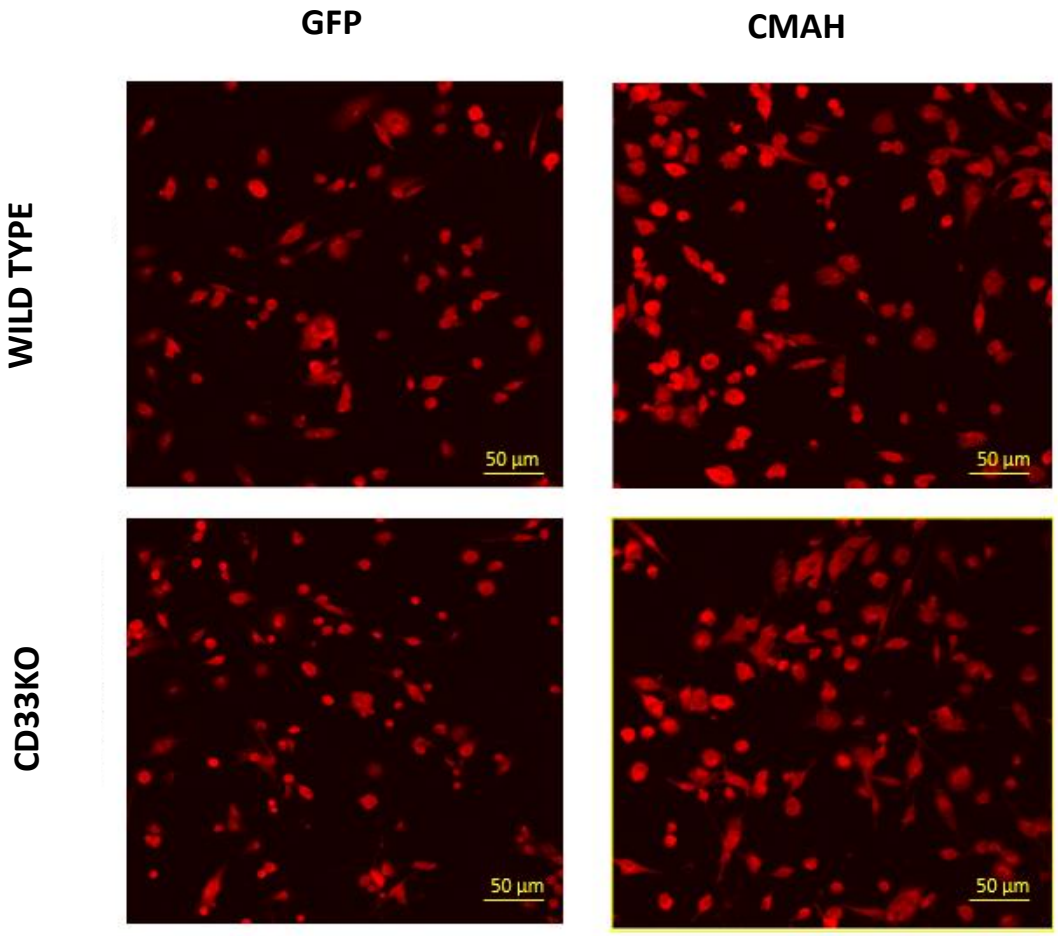

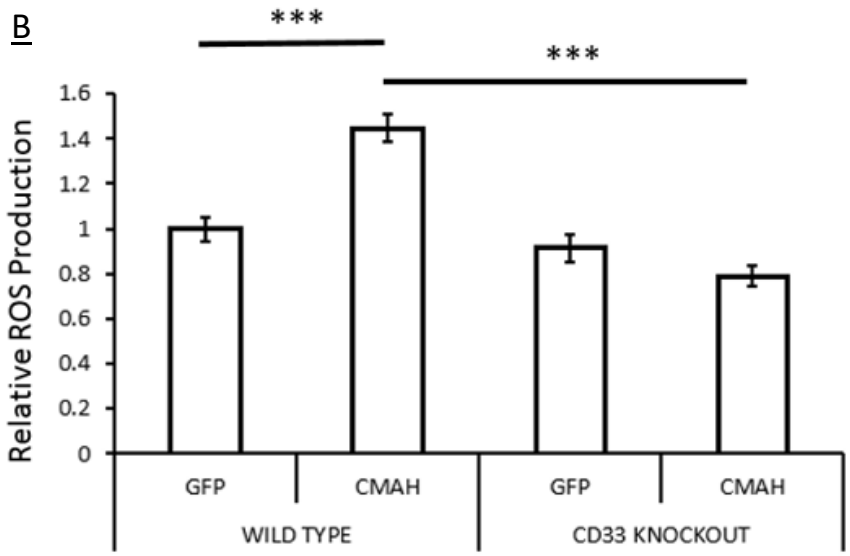

*Figure 21 Increase in ROS production caused by CMAH expression is dependent to CD33. CD33KO CMAH showed significant decrease in ROS production comprared to WT GFP. No significant difference was observed between WT GFP and CD33KO GFP (Scale Bar – 50 µM, Mean±SEM, n > 3, Analyzed with one way ANOVA followed by Bonferroni post hoc test ***p ≤ 0.001, data normalized to WT GFP)*

To investigate the combined effect of CD33 loss and CMAH expression in ROS production, CD33KO GFP and CD33KO CMAH were also stimulated with Aβ, neural debris or *Staphylococcus aureus* bioparticles. Aβ stimulation did not cause any significant change in CD33KO GFP and CD33KO CMAH compared to Aβ stimulated WT GFP (CD33KO GFP and CD33KO CMAH showed 1.33 ± 0.06 FC and 1.24 ± 0.08 FC, figure 22A, respectively). The scavenger controls of CD33KO GFP demonstrated significant decrease compared to Aβ stimulated condition (SOD1 and trolox treated CD33KO GFP showed 0.96 ± 0.04 FC, $p < 0.001$ and 0.95 ± 0.05 FC, $p < 0.001$, figure 22A). Although significant decrease was observed in SOD1 treated CD33KO CMAH (0.84 ± 0.05 FC, $p < 0.01$, figure 22A), trolox control did not elicit any significant change compared to Aβ stimulated in CD33KO CMAH (0.94 ± 0.06 FC, figure 22A). CD33KO CMAH also showed significant decrease compared to WT CMAH (0.97 ± 0.06 FC, $p < 0.001$, figure 22A).

Debris stimulated CD33KO GFP showed significant increase compared to non-stimulated CD33KO GFP (Debris stimulated CD33KO GFP showed 1.72 ± 0.10 FC, $p < 0.001$ while non-stimulated CD33KO GFP showed 0.99 ± 0.08 FC, figure 22B). Scavenger controls of CD33KO GFP showed significant decrease compared to debris stimulated CD33KO GFP (SOD1 and trolox controls elicit 0.95 ± 0.06 FC, $p < 0.001$ and 0.98 ± 0.07 FC, $p < 0.001$, figure 22B). Debris stimulated CD33KO GFP showed increase in ROS production compared to debris stimulated WT GFP. However, this increase was not significant. CD33KO CMAH did not respond to debris like CD33KO GFP. Despite marked increase in ROS production after debris stimulation, there was no significant change (Debris stimulated CD33KO CMAH showed 1.20 ± 0.08 FC, figure 22B). While trolox treatment to CD33KO CMAH caused significant decrease compared to debris stimulated condition (trolox control showed 0.82 ± 0.06 FC, $p < 0.05$, figure 22B), SOD1 treatment did not elicit any significant change (SOD1 treatment showed 0.95 ± 0.06 FC, figure 22B). Most importantly, debris stimulated CD33KO CMAH showed significant decrease compared to debris stimulated CD33KO GFP (CD33KO CMAH showed 1.20 ± 0.08 FC, $p < 0.01$, figure 22B).

Results of ROS production after bioparticle stimulation showed similarity to Aβ stimulation experiments. Bioparticle stimulated CD33KO GFP and CD33KO CMAH did not elicit any significant change compared to bioparticle stimulated WT GFP (CD33KO GFP and CD33KO CMAH showed 1.28 ± 0.07 FC and 1.20 ± 0.05 FC, respectively, figure 22C). Bioparticle stimulation to CD33KO GFP caused increase compared to non-stimulated CD33KO GFP but the difference was not significant (non-stimulated CD33KO GFP showed 1.02 ± 0.08 FC, figure 22C). The scavenger controls of CD33KO GFP caused significant decrease compared to bioparticle stimulated condition (SOD1 and trolox treated CD33KO GFP showed 0.93 ± 0.07 FC, $p < 0.001$ and 0.89 ± 0.05 FC, $p < 0.001$, figure 22C). Likewise Aβ stimulation experiments, SOD1 treated CD33KO CMAH showed significant decrease compared to bioparticle stimulated CD33KO CMAH (SOD1 treated CD33KO CMAH showed 0.90 ± 0.06 FC, $p < 0.05$, figure 22C). On the other hand, trolox treatment to CD33KO CMAH did not elicit any significant change (0.94 ± 0.05 FC, figure 22C).

A

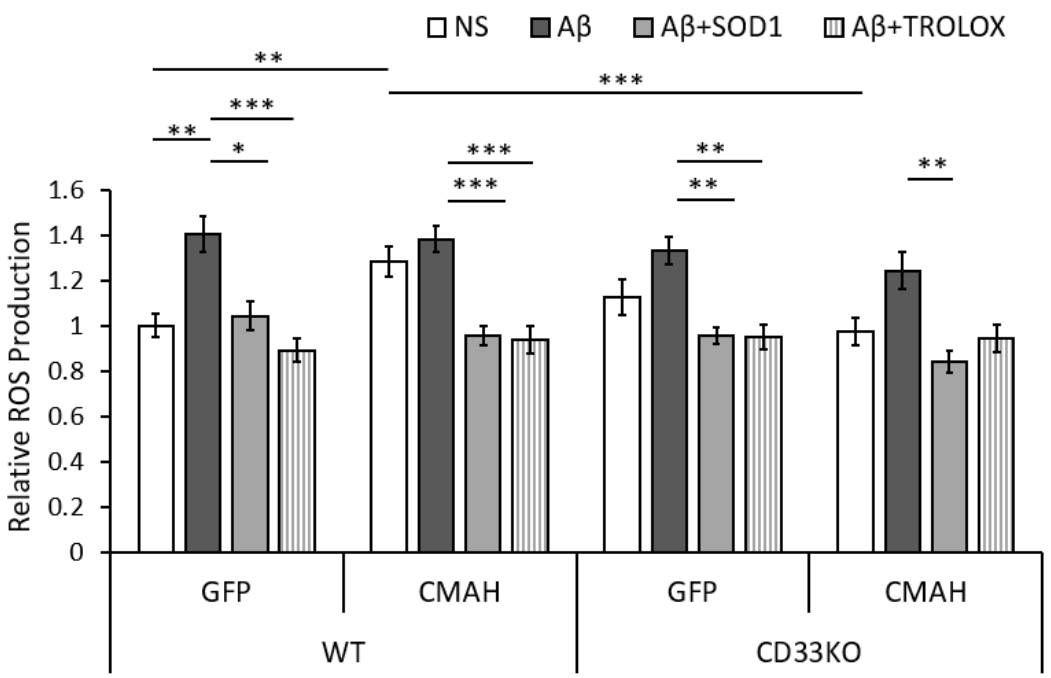
NS
Aβ
Aβ+SOD1
Aβ+TROLOX
Relative ROS Production
1.6
1.4
1.2
1
0.8
0.6
0.4
0.2
0
GFP
CMAH
GFP
CMAH
WT
CD33KO

B

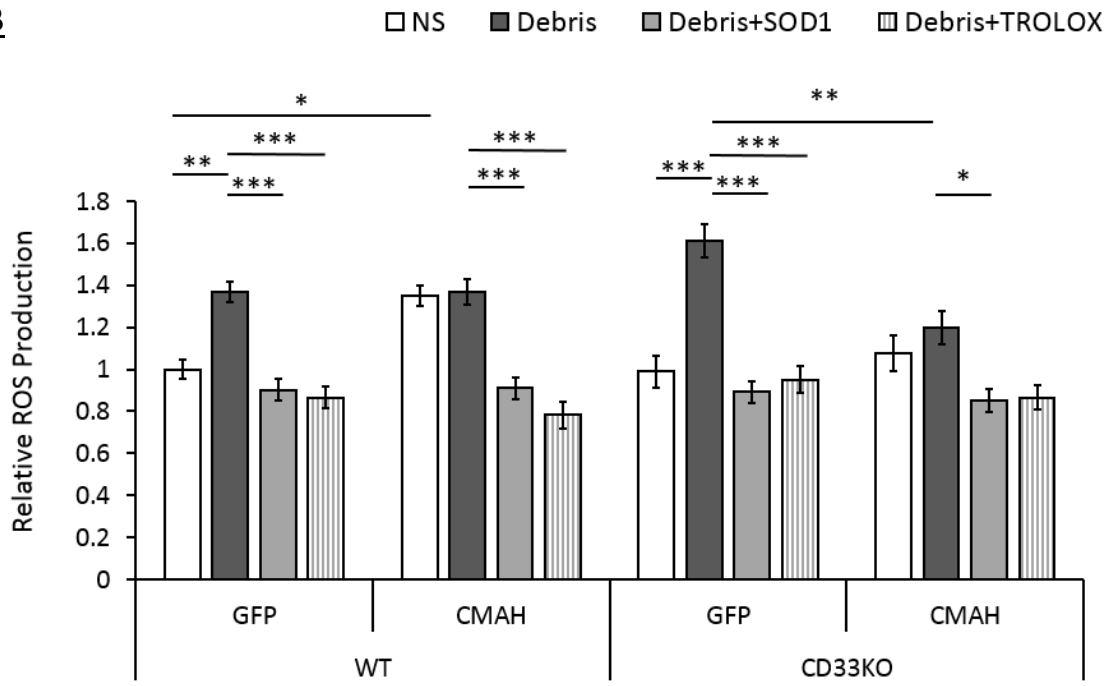
NS
Debris
Debris+SOD1
Debris+TROLOX
Relative ROS Production
1.8
1.6
1.4
1.2
1
0.8
0.6
0.4
0.2
0
GFP
CMAH
GFP
CMAH
WT
CD33KO

C

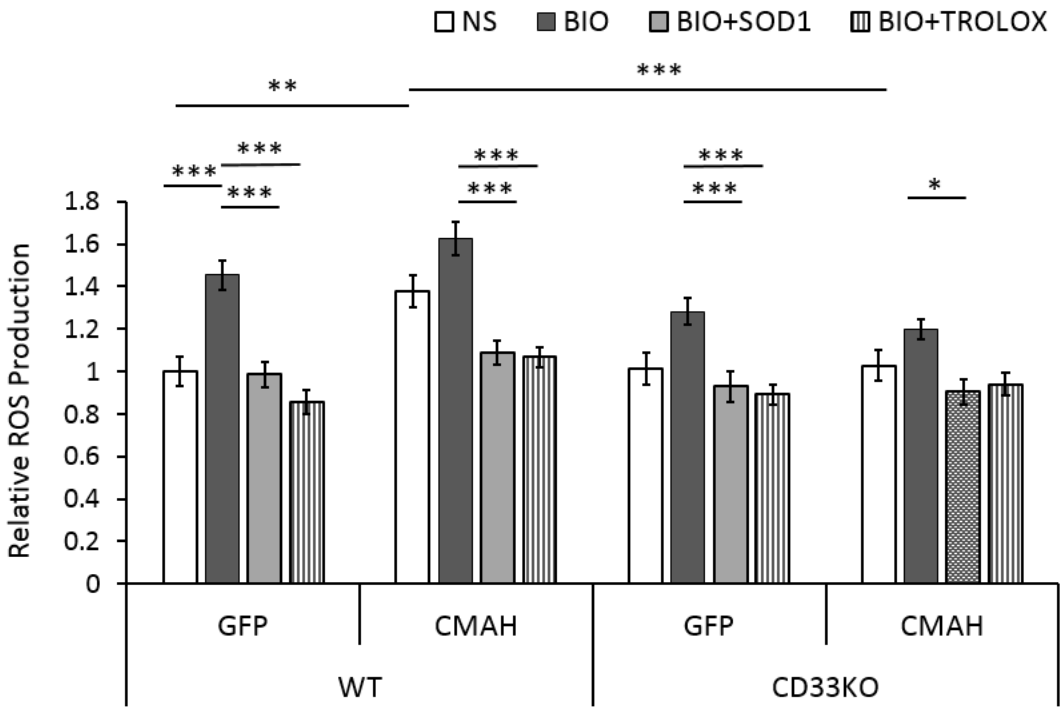

*Figure 22 ROS production in CD33KO cells is limited by CMAH expression after stimulation with (B) neural debris and (C) Staphylococcus aureus bioparticles. In (A) Aϐ and bioparticle stimulated conditions, stimulation did not elicit any significant change between wild type and CD33KO backgrounds. However, CD33KO CMAH showed significant decrease after debris stimulation compared to WT CMAH. Non-stimulated CD33KO CMAH showed significant decrease in all stimulation experiments compared to WT CMAH macrophages (Mean±SEM, n > 3, Analyzed with one way ANOVA followed by Bonferroni post hoc test *** p ≤ 0.001, ** p ≤ 0.01 * p ≤ 0.05, data normalized to non-stimulated WT GFP)*

The results of non-stimulated conditions compared to WT CMAH were also reproduced in stimulation experiments. Non-stimulated CD33KO CMAH showed significant decrease compared to non-stimulated WT CMAH in Aβ stimulation experiments (0.97 ± 0.06 FC, $p < 0.01$, figure 22A), debris stimulation experiments (1.04 ± 0.10 FC, $p < 0.05$, figure 22B) and bioparticle stimulation experiments (1.02 ± 0.07 FC, $p < 0.01$, figure 22C).

4.3 Immune Gene Transcription and Protein Expression

4.3.1 IL1β and TNFα transcription did not change in CMAH expressing macrophages

As pro-inflammatory cytokines, transcription of IL1β and TNFα, were analyzed. All the analysis were performed in non-stimulated conditions. Both cytokines did not show any significant difference between WT GFP and WT CMAH (WT CMAH showed IL1β and TNFα transcription as 0.97 ± 0.18 FC, figure 23A and 1.37 ± 0.17 FC, figure 23B respectively). However, pro-inflammatory cytokines transcription showed significant increase in CD33KO GFP compared to WT GFP (IL1β transcription showed 10.96 ± 0.74 FC, $p < 0.01$, figure 23A, TNFα transcription showed 3.35 ± 0.29 FC, $p < 0.001$, figure 23B). CMAH expression in CD33KO background recovered the increase caused by CD33 loss (IL1β transcription showed significant decrease in CD33KO CMAH compared to CD33KO GFP (IL1β transcription showed 2.88 ± 0.99 FC, $p < 0.05$, figure 23A). Although there is tendency towards decrease in TNFα transcription in CD33KO CMAH, the decrease was not significant (TNFα transcription in CD33KO CMAH showed 2.21 ± 0.55 FC, figure 23B)

A

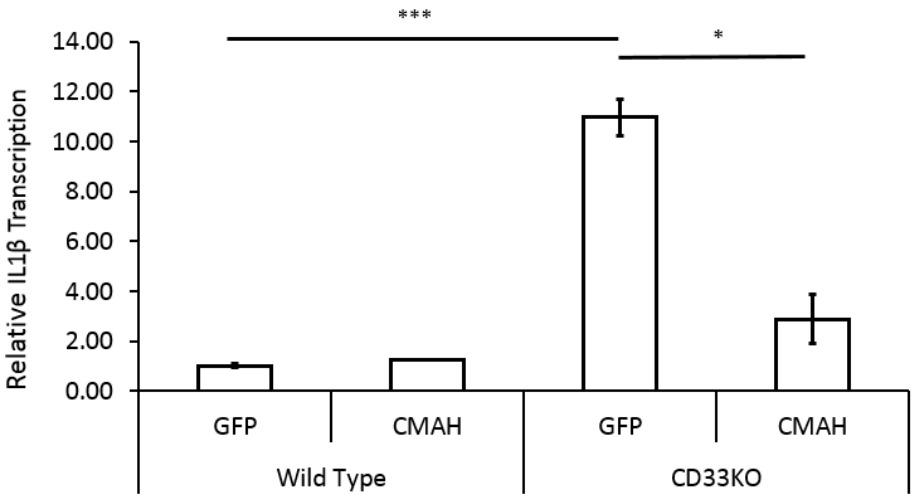

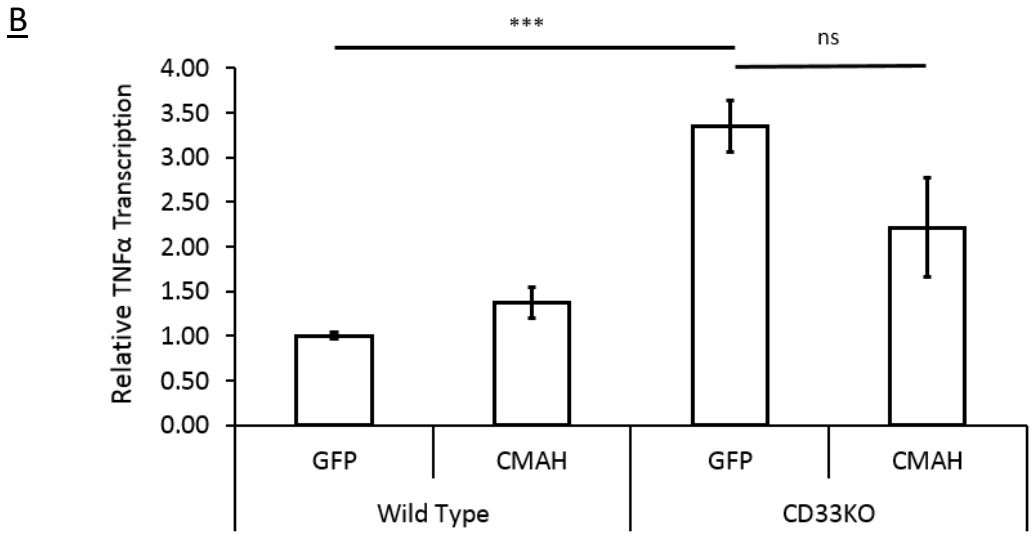

*Figure 23 CMAH expression did not elicit any significant change in proinflammatory cytokines and diminished the reactivity of CD33KO macrophages. All the transduced macrophages were analyzed for (A) IL1β, and (B) TNFα. WT CMAH did not show any significant change in comparison to WT GFP for both cytokines. However, CD33KO GFP showed increased transcription of IL1β, and TNFα compared to WT GFP. On the other hand, this increase diminished significantly in IL1β when CMAH is expressed (Mean±SEM, n > 3, Analyzed with one way ANOVA followed by Bonferroni post hoc test *** p ≤ 0.001, ** p ≤ 0.01 * p ≤ 0.05, data normalized to WT GFP)*

4.3.2 SIRPα, SHP1 and TREM2 gene transcription did not change after CMAH expression

Neu5Gc incorporation can affect the cellular inhibition and activation of macrophages in several ways. Transcription of key markers which might be affected by CMAH expression was analyzed in non-stimulated conditions (figure 24). Upon ligand binding, SHP1 is recruited and controls inhibitory ITIM signaling. SHP1 transcription did not change in WT CMAH compared to WT GFP (WT CMAH showed 0.90 ± 0.15 FC, figure 24A). However, CD33KO GFP showed significant increase in SHP1 transcription, compared to WT GFP (CD33KO GFP showed 1.82 ± 0.13 FC, $p < 0.01$, figure 24A). There was no significant change between CD33KO GFP and CD33KO CMAH. (CD33KO CMAH showed 1.43 ± 0.30 FC, figure 24A).

Like CD33, SIRPα also regulates inhibitory ITIM signaling through SHP1 recruitment [131]. Transcription of SIRPα was analyzed in non-stimulated conditions. Results did not show any significant change in transcription of SIRPα in WT CMAH compared to WT GFP (WT CMAH showed 0.87 ± 0.13 FC, figure 24B).

Expressing CMAH in CD33KO background did not cause any significant change in transcription as well compared to WT GFP (CD33KO GFP and CD33KO CMAH showed 0.87 ± 0.13 FC and 0.87 ± 0.13 FC, figure 24B, respectively). Moreover, there was no significant change in SIRPα transcription between CD33KO GFP and CD33KO CMAH (figure 24B). In addition, transcription of TREM2 was analyzed as activatory ITAM signaling molecule. TREM2, via its adaptor molecule TYROBP, regulates activatory ITAM signaling and changes in CD33 signaling might have caused changes in ITAM signaling. Similar to SIRPα, there was no significant change in between WT CMAH and WT GFP (WT CMAH showed 1.17 ± 0.07 FC, figure 24C). Moreover, transcription of TREM2 did not show any significant change in CD33KO background compared to WT GFP (CD33KO GFP and CD33KO CMAH showed 1.01 ± 0.14 FC and 0.81 ± 0.11 FC, figure 24C, respectively). There was also no significant change between CD33KO GFP and CD33KO CMAH (figure 24C).

A

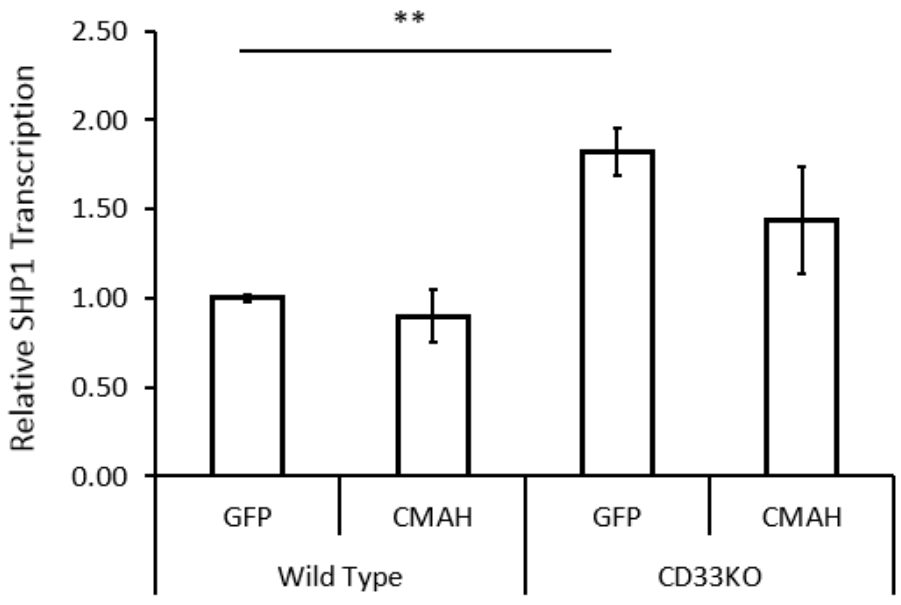

B

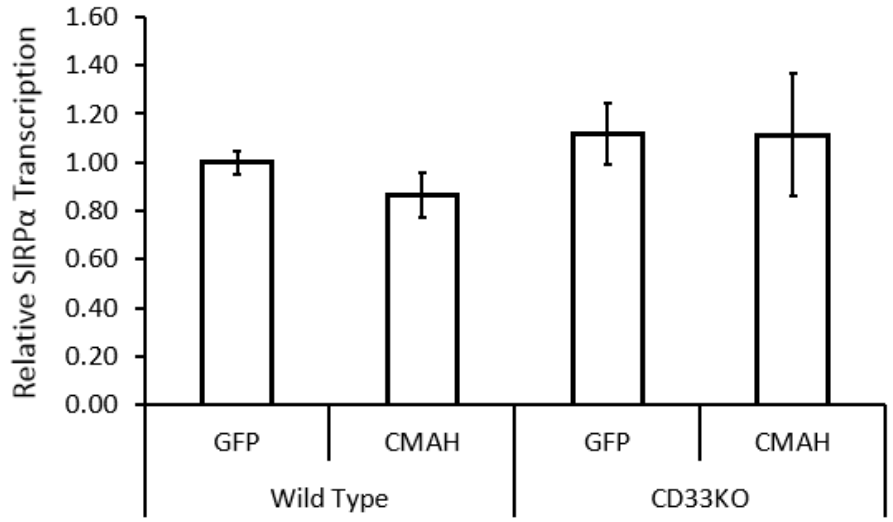

C

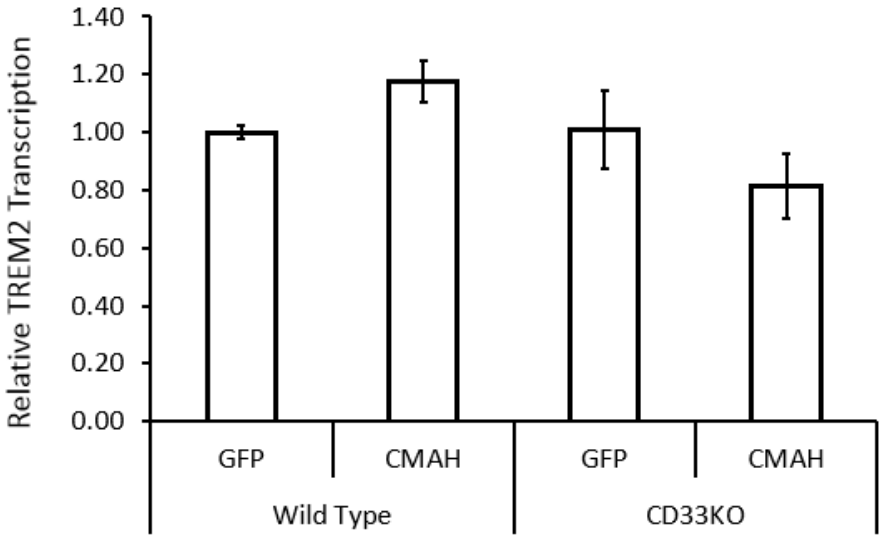

*Figure 24 Transcription of key markers of ITIM and ITAM signaling of macrophages did not change after CMAH expression. Transcription key markers; (A) SHP1 (B) SIRPα and (C) TREM2 were analyzed. Significant increase in SHP1 transcription was observed in CD33KO GFP compared to WT GFP. However, no significant difference was observed in the transcription of SIRPα and TREM2 levels among transduced macrophages. (Mean±SEM, n > 3, Analyzed with one way ANOVA followed by Bonferroni post hoc test ** p ≤ 0.01, data normalized to WT GFP)*

4.3.3 Transcription and protein expression of CD64 were not altered in CMAH expressing macrophages

Fcγ signaling is important for the activatory phenotype of macrophages [132]. To observe whether Neu5Gc incorporation exerts its effect by FcᵞR signaling, transcription and expression of Fcγ receptor I alpha chain (CD64) was checked. To check its expression, anti-CD64 antibody was used in flow cytometry (figure 25A). There was no significant difference in WT CMAH compared to WT GFP at both expression level (WT CMAH showed 1.12 ± 0.02 FC, figure 25B) and transcriptional level (WT CMAH showed 1.22 ± 0.11 FC, figure 25C). However, significant decrease in transcription and expression were observed in CD33KO GFP and in CD33KO CMAH compared to WT GFP (CD33KO GFP showed 0.11 ± 0.01 FC, $P < 0.001$, and CD33KO CMAH showed 0.32 ± 0.12 FC, $p < 0.001$, figure 25B, in expression, respectively). Moreover, this decrease was also significant at transcription levels of CD33KO GFP and CD33KO CMAH (0.11 ± 0.01 FC, $P < 0.001$ and 0.09 ± 0.02 FC, $p < 0.001$, figure 25C). There was no significant change in both transcription and expression of CD64 between CD33KO GFP and CD33KO CMAH.

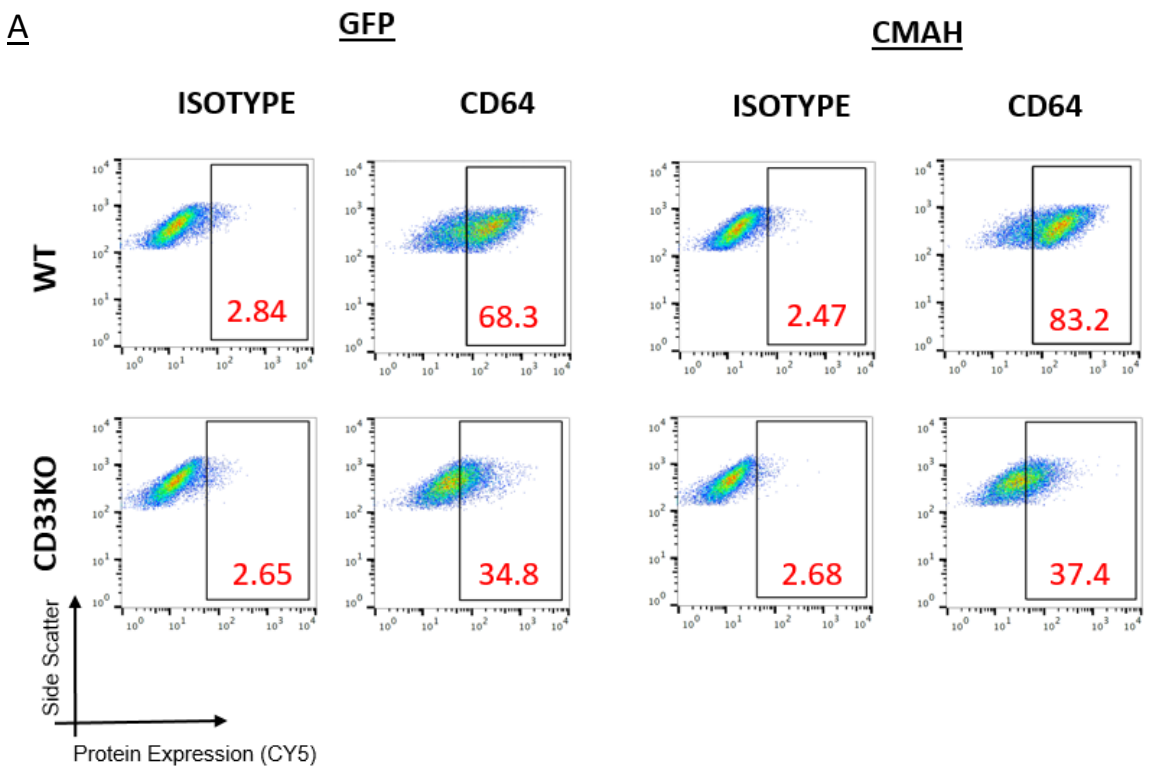

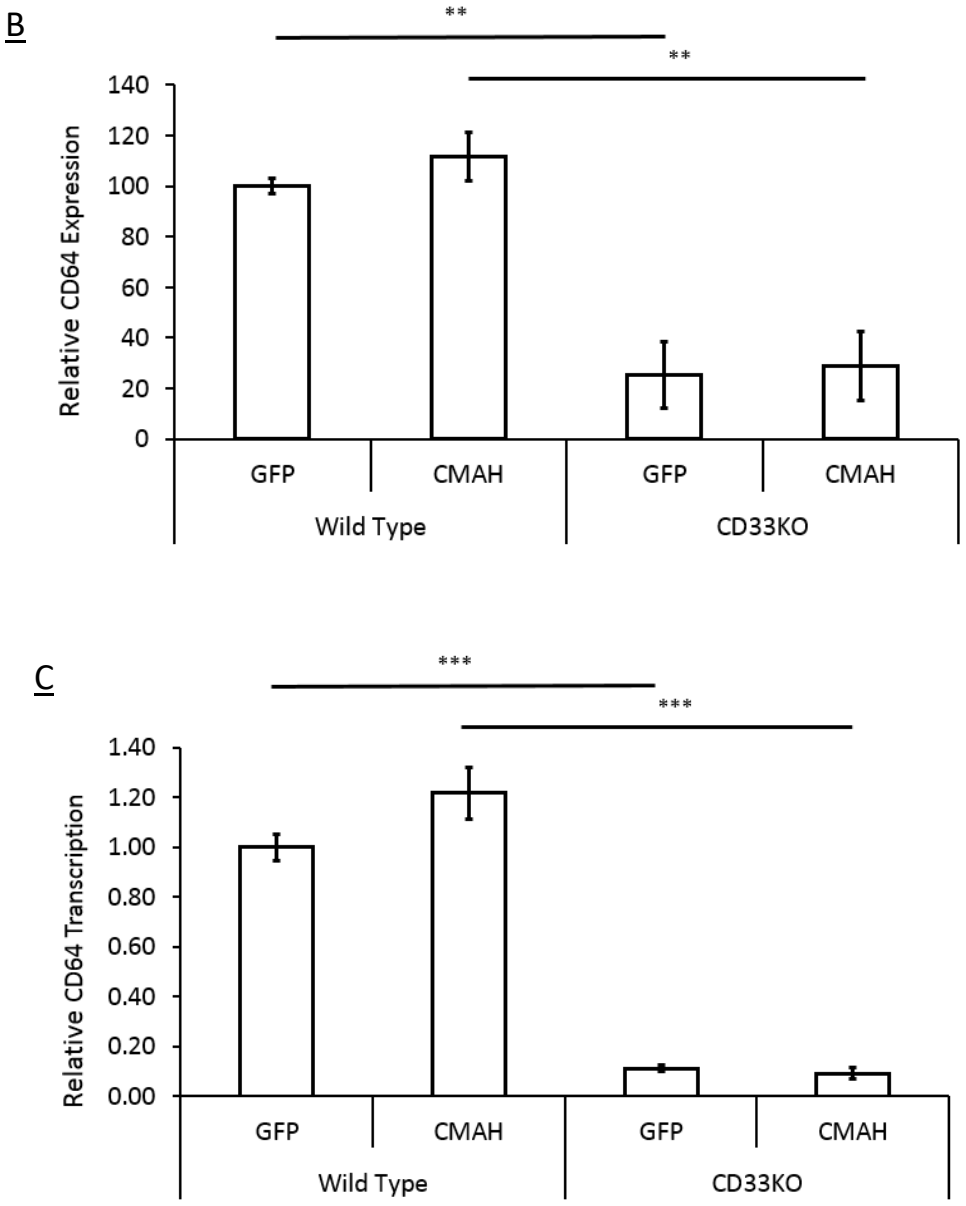

*Figure 25 CMAH expression did not exert its effects through Fcγ signaling. (A) Expression profile of CD64 was assessed with anti-CD64 antibody compared to isotype control. No significant change was observed between WT GFP and WT CMAH in both expression and transcription. On the other hand, (B) CD33KO GFP showed significant decrease in CD64 in expression. (C) This decrease was also observed in transcription levels in transduced macrophages. CD33KO macrophages showed significant decrease in transcription compared to wild type macrophages (Mean±SEM, n > 3, Analyzed with one way ANOVA followed by Bonferroni post hoc test ***p ≤ 0.001, data normalized to WT GFP)*

4.4 Signaling

4.4.1 Cis binding of sialic acid to CD33 did not change in CMAH expressing macrophages

CD33 is able to bind to sialic acids in both trans and cis fashion [67]. In this experiment, cis interaction of CD33 was assesed via utilization of different binding epitopes of CD33 antibodies which are Ig V and C2 set Ig domains. Sialic acid binding domain is located in V-set Ig domain. While WM53 clone binds to V-Ig domain, HIM34 clones bind to C2 domain, which can be blocked by cis binding. In flow cytometry, binding of these two antibody clones were assessed (figure 26A) and cis bound CD33 was calculated by subtracting binding of HIM34 clone from WM53. Then, to calculate cis/total bound CD33, cis value is divided to total CD33 which is detected by binding of WM53 clone. WT CMAH showed 89.73 ± 2.19 % HIM34 and 93.97 ± 1.25 % WM53 binding (figure 26B). CD33KO macrophages, CD33KO GFP and CD33KO CMAH, did not show any binding to CD33 antibodies owing to frameshift mutation in *CD33* gene. While WT GFP showed 85.91 ± 0.89 HIM34 and 91.45 ± 1.24 WM53 binding, CD33KO GFP showed 3.83 ± 1.55 HIM34 and 2.38 ± 1.13 WM53 protein binding. Also, CD33KO CMAH showed 0.47 ± 1.02 % HIM34 and -0.27 ± 0.18 %, figure 26B. This decrease was significant for both antibodies ($p < 0.001$, figure 26D). Afterwards, relative ratio of cis/total bound CD33 was calculated and there was no change between WT GFP and WT CMAH (WT CMAH showed 0.76 ± 0.25 FC, figure 26C)

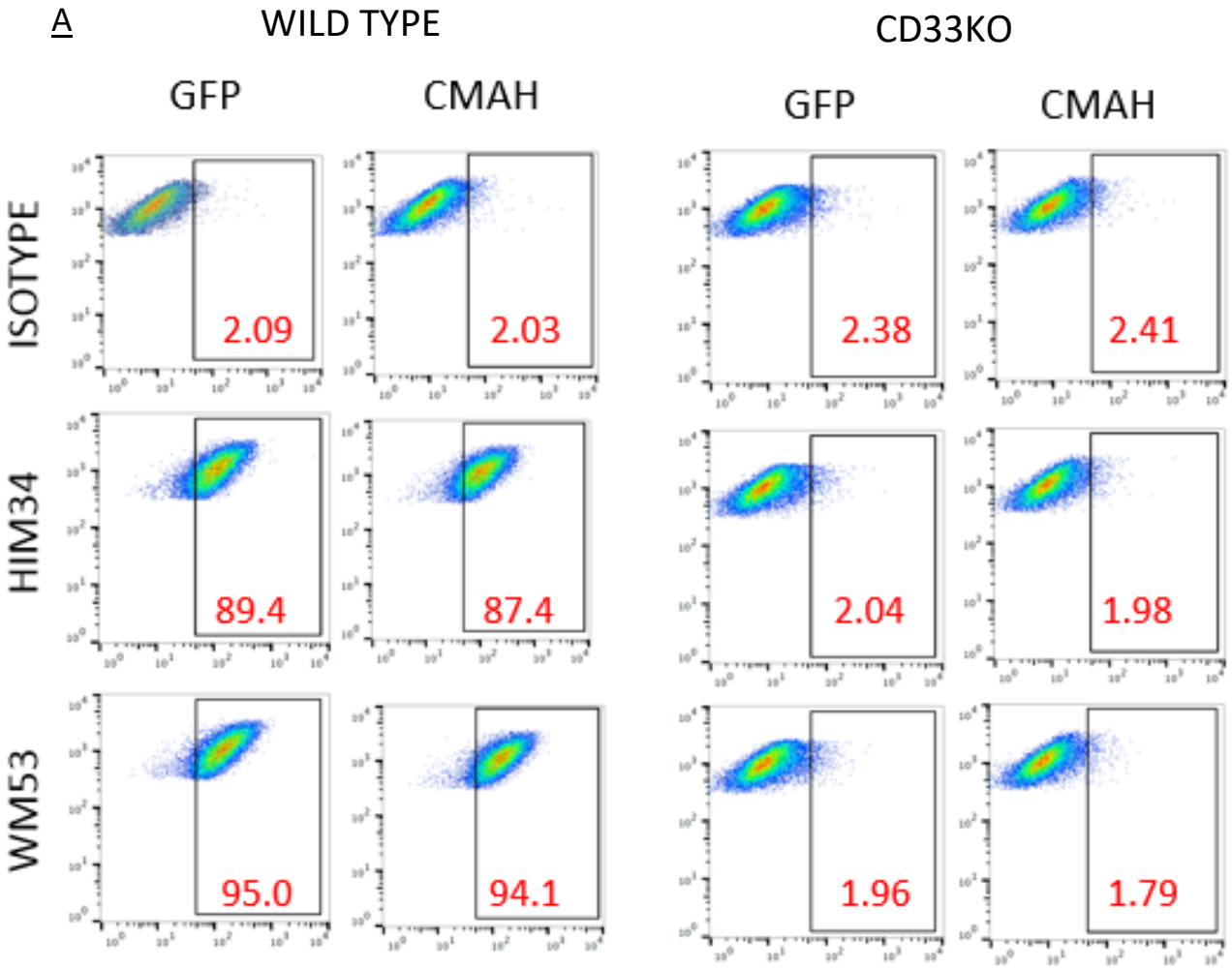
A
WILD TYPE
CD33KO
GFP
CMAH
GFP
CMAH
ISOTYPE
HIM34
WM53
2.09
2.03
2.38
2.41
89.4
87.4
2.04
1.98
95.0
94.1
1.96
1.79

B

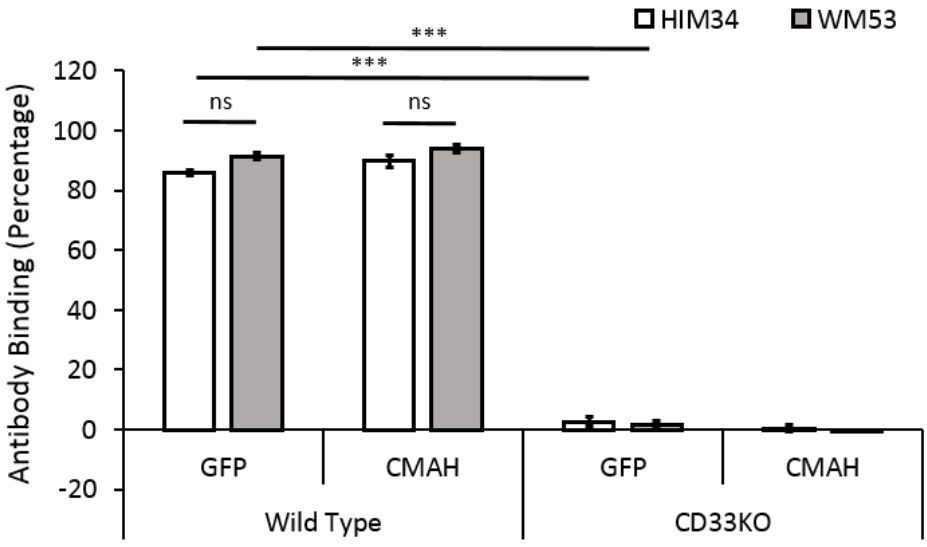
HIM34
WM53
***
***
ns
ns
120
100
80
60
40
20
0
-20
Antibody Binding (Percentage)
GFP
CMAH
GFP
CMAH
Wild Type
CD33KO

C

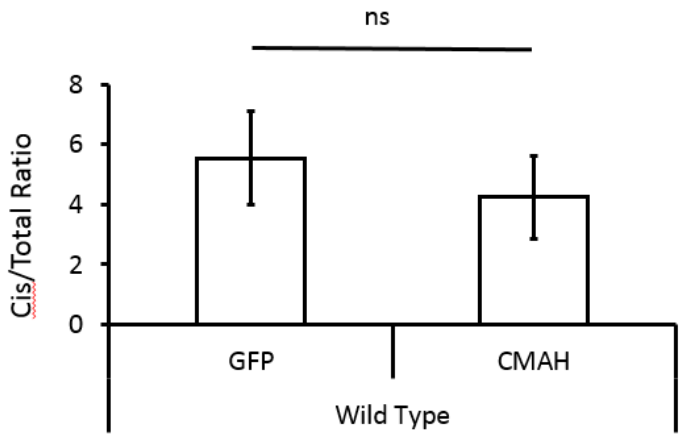

*Figure 26 Cis/Total binding of CD33 did not change after CMAH expression. CD33 can bind to sialic acids in both cis and trans manner. While HIM34 clone of anti-CD33 can bind to C2 Ig domain and be blocked by cis binding, WM53 can bind to variable region (V-set Ig) and gives total binding. (A) Binding of HIM34 and WM53 clone were assessed with flow cytometry. (B) There was significant decrease in all antibody binding in CD33 knockout macrophages compared to wild type macrophages (Mean±SEM, n = 3, Analyzed with one way ANOVA followed by Bonferroni post hoc test ***p ≤ 0.001) (C) No significant difference was observed between WT GFP and WT CMAH (Mean±SEM, n = 3, Analyzed with Student's T-test p ≤ 0.05, data normalized to WT GFP)*

4.4.2 Slight increase in phosphorylation of activatory signaling intermediate molecule, ERK in CMAH expressing macrophages

ITAM signaling is generally directed through phosphorylation of intermediate molecule ERK. Phosphorylated form of ERK is the activated form of this molecule and it shows that the cells are more phagocytic [133]. In this experiment, Phospho/Total ERK was measured via Western blot. Although there is marked increase in WT CMAH compared to WT GFP, the difference was not significant (WT CMAH showed 1.22 ± 0.07 FC, figure 27). On the the other hand, CD33KO GFP showed significant increase in p-ERK/t-ERK ratio compared to WT GFP (CD33KO GFP showed 1.40 ± 0.14 FC, $p < 0.01$, figure 27). Despite marked increase, CD33KO CMAH didn't show significant difference compared to WT CMAH (1.68 ± 0.14 FC, $p < 0.01$, figure 27). There was also no significant difference between CD33KO GFP and CD33KO CMAH (figure 27).

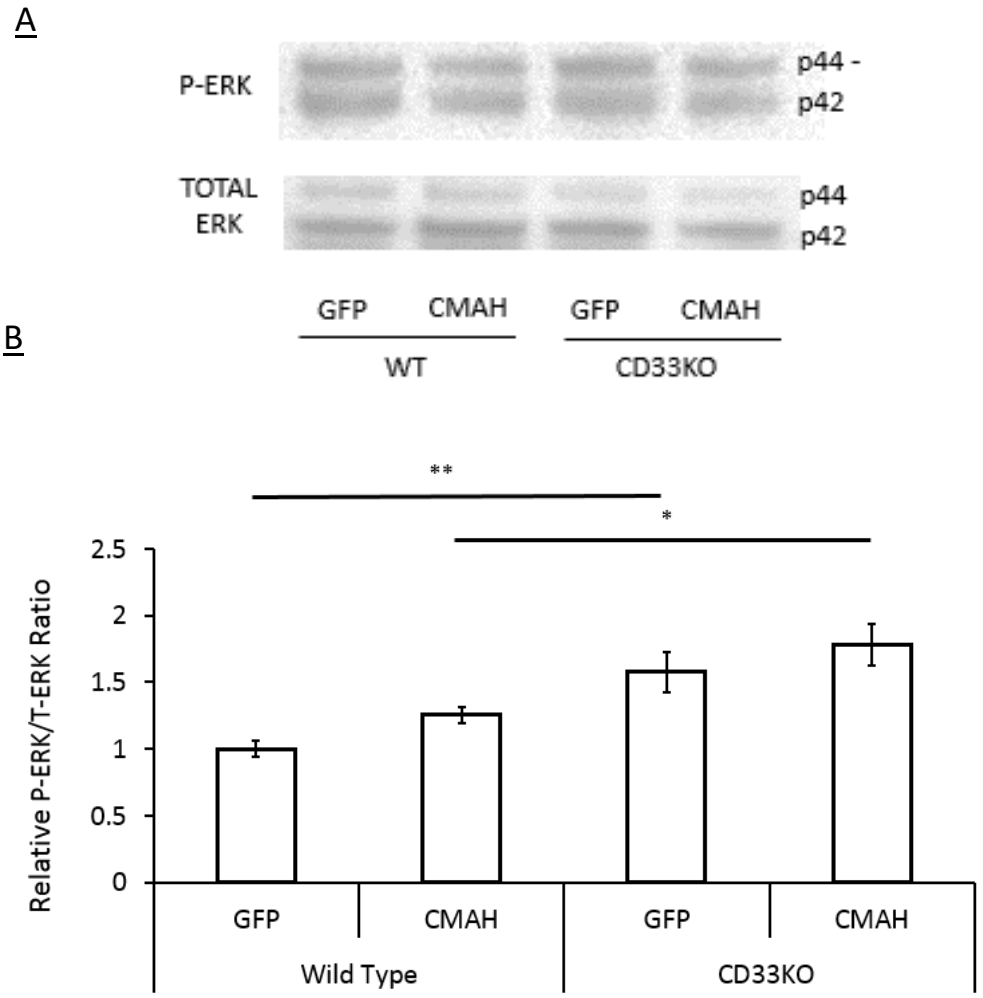

*Figure 27 Phosphorylation of ERK was increased after CMAH expression but the difference was not significant. (A) From transduced macrophages, protein samples were isolated and stained for phospho and total ERK. The bands in western blot were in correct sizes and detected for both phospho and total ERK. (B) There was significant increase in CD33KO GFP compared to WT GFP. However, despite there was increase in WT CMAH and WT GFP, this difference was not significant. Also, CD33KO CMAH showed significant increase compared to WT CMAH (Mean±SEM, n > 3, Analyzed with one way ANOVA followed by Bonferroni post hoc test ** p ≤ 0.01, data normalized to WT GFP)*

4.4.3 SHP1 recruitment to CD33 was decreased in CMAH overexpressing macrophages

SHP1 is an important regulatory molecule for ITIM signaling and inhibition of macrophage responses. In normal conditions, CD33 binds to sialic acids which is leading to recruitment of SHP1 [73]. However, binding of Neu5Gc instead of Neu5Ac might have caused aberrations in SHP1 recruitment. To check SHP1

recruitment to CD33, protein samples from differentiated macrophages were immunoprecipitated against CD33 and stained for SHP1 and CD33 in western blot. Immunoprecipitated SHP1 and CD33 were in right sizes in the blot (figure 28A). The results showed that there was significant decrease in SHP1 recruitment to CD33 after CMAH expression compared to WT GFP (WT CMAH showed 0.54 ± 0.03 FC, $p < 0.001$, figure 28B)

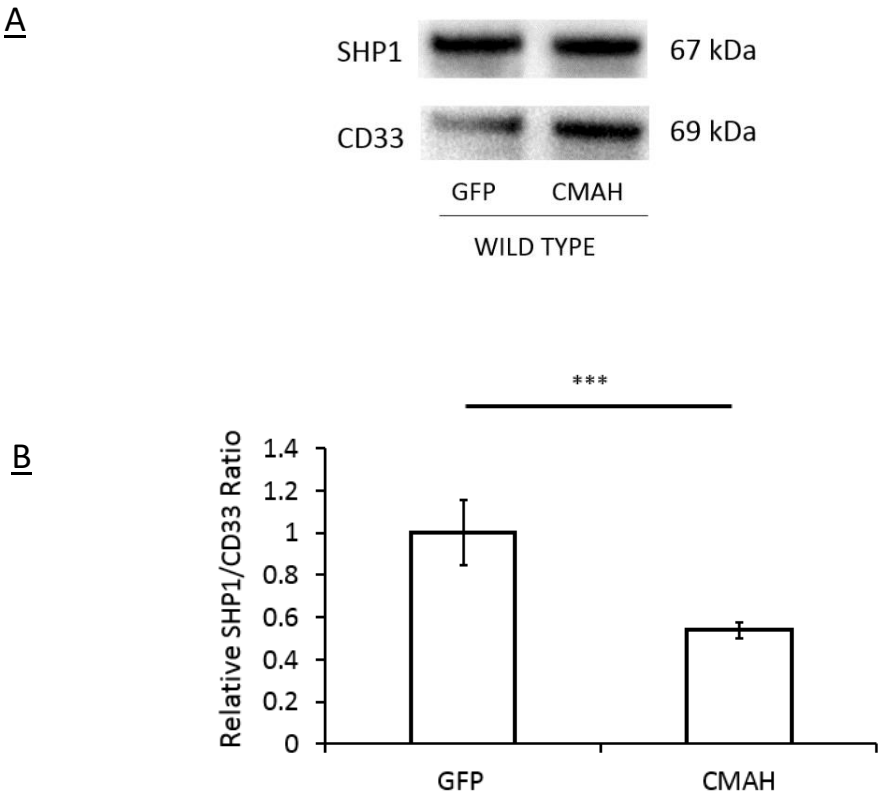

*Figure 28 CMAH expression caused decrease in SHP1 recruitment to CD33 (A) Total proteins were isolated with anti-CD33 antibody and CD33 bound proteins were isolated via immunoprecipitation. Then, immunoprecipitated proteins were stained for SHP1 and total CD33. The bands in western blot were in correct sizes and detected for both SHP1 and CD33. (B) There was significant decrease in SHP1 recruitment in WT CMAH compared to WT GFP (Mean±SEM, n > 3, Analyzed with Student's T-test *** p ≤ 0.001, data normalized to WT GFP)*

4.4.4 Peroxisomal catalase activity was increased in CMAH expressing macrophages

Macrophages and microglia respond to oxidative stress by increasing peroxisomal catalase activity [134] and catalase activity is mostly observed in peroxisomes [134]. In previous experiments, CMAH expressing macrophages displayed increased oxidative stress in CD33 dependent manner. Macrophages were differentiated as previously described and immunostained according to section 3.2.5.1. Transduced macrophages were stained with anti-catalase antibody to investigate whether ROS production caused complementary increase in catalase activity. Anti-CD11b antibody was used to stain the macrophages (figure 29A). The staining results showed increased peroxisomal catalase activity in WT CMAH compared to WT GFP (WT CMAH showed 1.89 ± 0.22 FC, $p < 0.01$, figure 29B). CD33KO GFP did not present any significant difference compared to WT GFP (1.09 ± 0.09 FC, figure 29B). Moreover, CD33KO CMAH demonstrated significant increase in catalase activity compared to CD33KO GFP (CMAH expressing macrophages showed 1.83 ± 0.17 FC, $p < 0.001$, figure 29B, compared to CD33KO GFP). CD33KO CMAH also did not show any significant difference compared to WT CMAH.

4.4.5 CMAH expressing macrophages showed increased lysosomal activation in CD33 dependent manner

Neuraminidases were shown to have decreased activity towards Neu5Gc [93]. To observe whether the number of lysosomes or lysosomal activation was altered through CMAH expression, transduced macrophages were stained against CD68 as activated macrophages were known to increase CD68 expression[135]. WT CMAH showed significant increase in CD68 staining compared to WT GFP (WT CMAH showed 1.50 ± 0.14 FC, $p < 0.01$, figure 30B). No significant change was observed between CD33KO GFP and WT GFP (CD33KO GFP showed 0.66 ± 0.09 FC, figure 30B, in CD68 staining). On the other hand, CD33KO CMAH showed significant decrease in CD68 staining compared to WT CMAH (CD33KO CMAH showed 0.70 ± 0.08 FC, $p < 0.001$, figure 30B). There was no significant change between CD33KO GFP and CD33KO CMAH.

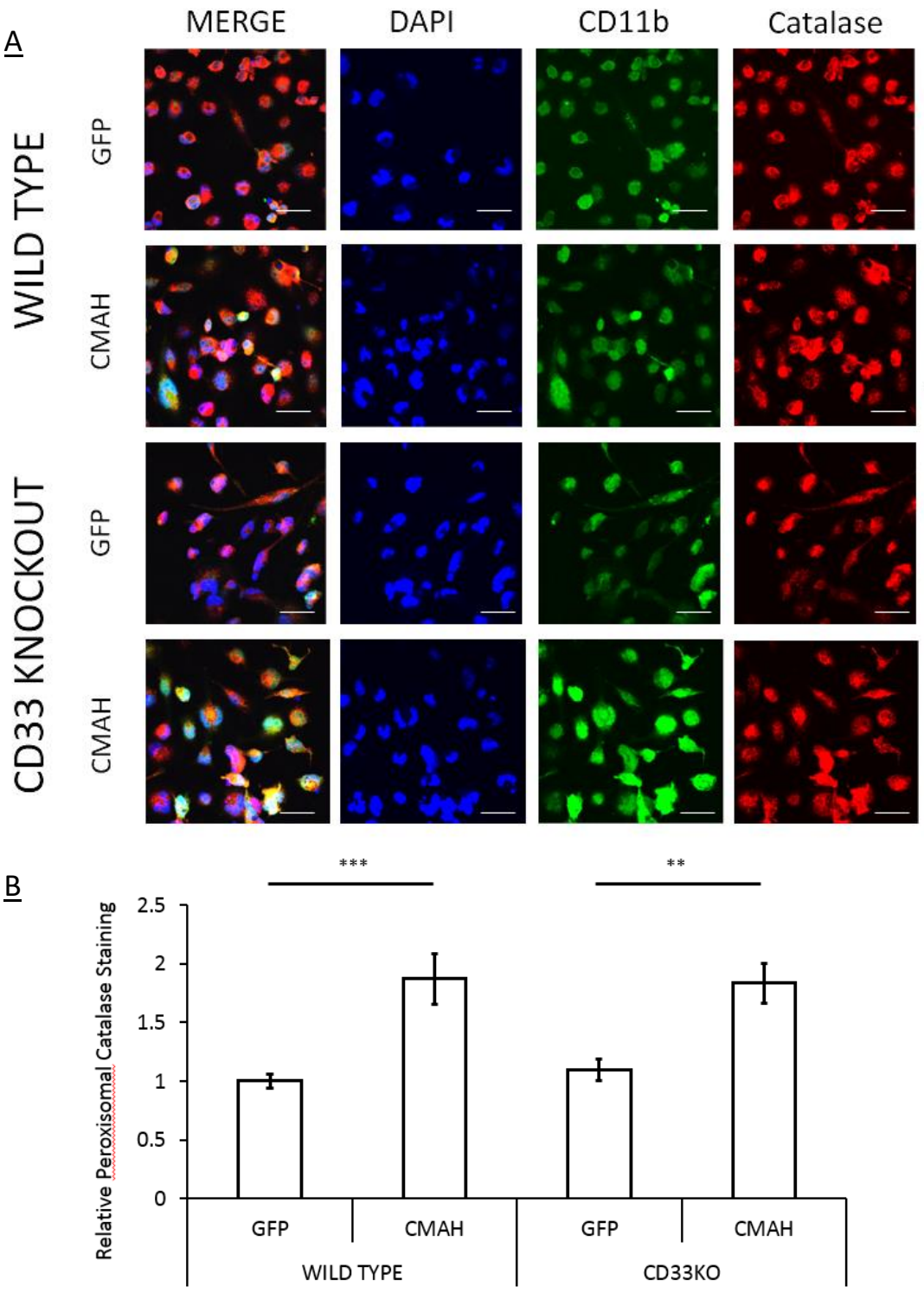

*Figure 29 CMAH expression caused increase in peroxisomal catalase activity in CD33 independent manner. WT CMAH showed significant increase compared to WT GFP in catalase staining. Also, CD33KO CMAH showed significant increase in catalase staining, However, lack of CD33 did not cause any significant change in catalase activity and there was no significant difference between CD33KO GFP and WT GFP (Mean±SEM, n > 3, Analyzed with one way ANOVA followed by Bonferroni post hoc test *** p ≤ 0.001 ** p ≤ 0.01, data normalized to WT GFP, scale bar 50 µm, blue-DAPI, green-CD11b, red-catalase)*

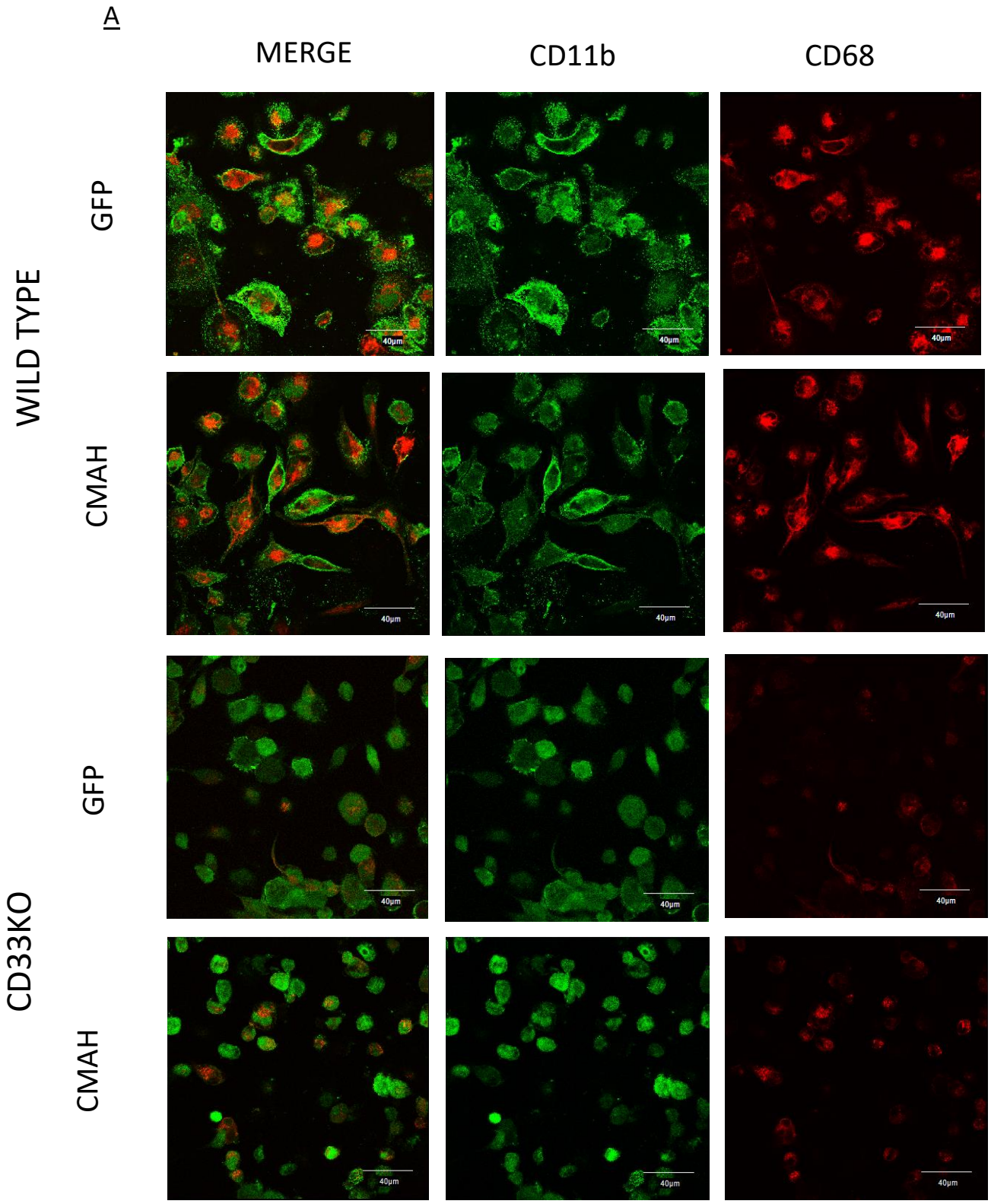
A
MERGE
CD11b
CD68
WILD TYPE
GFP
CMAH
CD33KO
GFP
CMAH
40µm

B

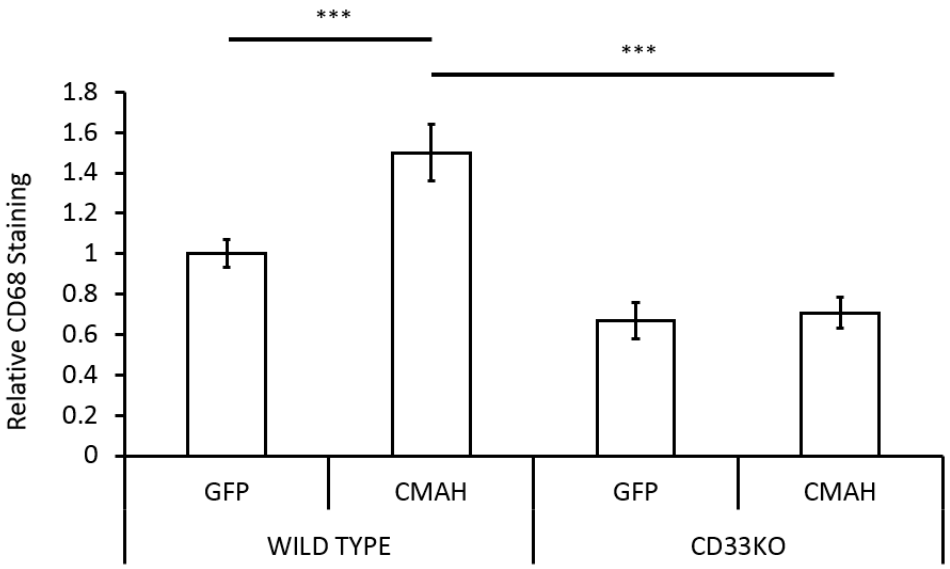

*Figure 30 CMAH expression caused increase in lysosomal activation in CD33 dependent manner. WT CMAH showed significant increase in CD68 staining compared to WT GFP. There was no significant change between CD33KO GFP and WT GFP. CD33KO CMAH significant decrease in CD68 staining compared to WT CMAH. No significant change was observed between CD33KO GFP and CD33KO CMAH (Mean±SEM, n > 3, Analyzed with one way ANOVA followed by Bonferroni post hoc test *** p ≤ 0.001 **, data normalized to WT GFP, scale bar 40 µm, green-CD11b, red-CD68)*

5. DISCUSSION

5.1 Sialic acids in brain

Brain is different from many organs in several ways, one of the most important aspects being the unproportional amount of sialic acids. Although the functional relevance of sialic acids in brain have been studied extensively, effect of sialic acids in respect to neurodegeneration has not been clarified completely. In this study, I tried to characterize responses of macrophages when foreign type sialic acid is present on its glycocalyx. Since macrophages and microglia cells are functionally similar [24], I tried to understand how immune cells in general respond to presence of different sialic acid (Neu5Gc). Main functional alterations related to neurodegeneration such as ROS production, phagocytosis, cytokine production, and ITIM/ITAM signaling related molecules were analyzed in this study. I incorporated Neu5Gc via expressing CMAH gene in macrophages.

Sialic acids are encountered as bound to glycan (sialoglycans) [136]. Sialoglycans in brain possess unique structure and composition. Most of brain sialic acids are found in lipid-bound form as gangliosides [136]. Gangliosides take part in signal transduction as part of lipid rafts, mediate axon-myelin interactions and can serve as receptors for neurotrophic bacterial toxins [136]. Sialic acids can also be found in protein-bound form as homopolymer of >90 sialic acid residues. This structure of sialic acids are named polysialic acid (PSA). PSA is involved in the modulation of cell-cell interactions and play crucial role in neuronal development and regeneration [137–139]. Moreover, PSA has been recently shown as reservoir for growth factors [140,141]. All of these sialic acid dependent processes might cause aberrations when there is foreign sialic acid present.

In the brains of mammals, Neu5Gc is found only in traceable amounts. The reason lying behind this distinction has not been clarified so far. But there are several hypothesis about the lack of Neu5Gc in brain. One of the hypothesis state that sialic acid-binding lectins, whether pathogenic or endogenous, might have different preference over different sialic acid types, and these may affect the balance of Neu5Ac and Neu5Gc presence. Since this balance is controlled by CMAH gene, selective down-regulation of CMAH gene is the most plausible explanation till now [86]. This is why, expressing CMAH gene in immune cells is one of the most plausible ways to analyze wrong sialic acid incorporation. However, since this enzyme is expressed under Elongation factor 1 α (EF1α) promoter, the results which were shown in this study could represent only over-feeding, extreme, or pathological conditions. EF1α promoter is very strong promoter and drives gene expression to very high levels.

5.2 Role of CMAH in sialic acid metabolism

Neu5Gc can be called as a marker of the deuterostome lineage of animals (vertebrates and so-called "higher" invertebrates), and and it represents a unique evolutionary step that occurred at or just before the Cambrian expansion, ~500 million years ago [142]. Approximately 2–3 million years ago, our ancestors inactivated the gene *CMAH*, and since then, Neu5Gc could not be produced from Neu5Ac [143]. This mutation could be traced till Neandertals. Like humans, neandertals were known to not express Neu5Gc, [144]. Neu5Gc could not be produced in human and their very close ancestors because of 92 bp deletion in exon 6 that caused the frameshift in CMAH enzyme's catalytic domain, leading to a truncated inactive peptide. This evolutionary change seem to be specific *Homo sapiens* and causes several different outcomes.

5.3 Consequences of Neu5Gc incorporation from dietary sources

Despite the inability of humans to produce Neu5Gc endogenously, it can still be detected in small amounts in human epithelial and endothelial cells [93], and also in human carcinomas [95,145]. Mice engineered to have

a human-like mutation in the *Cmah* gene, shows no evidence of any alternate pathway for Neu5Gc biosynthesis [87]. Thus, metabolic incorporation via dietary consumption is the only possible source of the Neu5Gc that is found in human tissues.

Uptaken Neu5Gc has been shown to drive several pathologies in humans. Humans who consumed Neu5Gc were found to express circulating anti-Neu5Gc antibodies in variable proportion. Chronic inflammation induced in this way was shown to drive carcinoma formation in $CMAH^{-/-}$ mice [109]. Moreover, Neu5Gc causes vulnerability against several infectious disases, such as malaria [146], viral infections [147] and bacterial infections [148]. Also, Neu5Gc incorporation contributes to progression of muscular dystrophy [120]. For this reason, the results of this study could shed light upon functional alterations caused by Neu5Gc incorporation.

5.4 Consequences of Neu5GC incorporation from CMAH expression

5.4.1 Validation of CMAH activity in human macrophages

CMAH is the only enzyme to produce Neu5Gc from Neu5Ac. In literature, $Cmah^{-/-}$ mice was shown to be incapable of producing Neu5Gc [87]. The aim of this thesis was to study the effects of wrong sialic acid incorporation in cellular system. To investigate Neu5Gc effects, CMAH expressing macrophages were used as model and CMAH gene was virally transduced to THP1 monocytes. To confirm the model is functional, transduced and differentiated macrophages were stained with anti-Neu5Gc antibody. Transduced macrophages were stained against anti-Neu5Gc and WT CMAH was able to synthesize Neu5Gc. This result demonstrated that cloning strategy of CMAH gene into pLenti lentiviral vector was sufficient to drive production of Neu5Gc from Neu5Ac in macrophages.

The focus of this study was to analyze the effects of CMAH in human macrophage cells. Despite proven conversion of Neu5Ac to Neu5Gc, the percentage of each sialic acid was still needed to be elucidated. In collaboration with the group of Dr. Erdmann Rapp, advanced xCGE-LIF technique showed that around

10 % of Neu5Ac and 90 % Neu5Gc remained in CMAH transduced macrophages. Previous attempts of feeding experiments with 3 mM Neu5Gc led to incorporation 28% in fibroblast cells, and 61% in neuroblastoma cells [94]. In our experimental setup, Neu5Gc could reach up to 90 % in CMAH expressing macrophages, WT CMAH and CD33KO CMAH. This Neu5Gc percentage is very high compared to normal levels and results obtained could demonstrate long term adaptation of Neu5Gc accumulation or extreme feeding conditions with Neu5Gc.

5.4.2 Toxicity of Neu5Gc accumulation

Neu5Gc accumulation can be toxic not only by disrupting activatory and inhibitory signaling of macrophages, but also through its metabolites, such as glycolate which can cause long term adaptations. These adaptations can limit the innate immune responses of macrophages, such as phagocytosis or reactive oxygen species production. These two innate immune responses are critical for proper functioning of macrophages, thus, these innate responses were analyzed in this study for both wild type and CD33KO macrophages.

5.4.2.1 Decreased phagocytosis via diminished neuraminidase activity

Macrophages are the first line of defense in response to tissue injuiry [149]. Several studies demonstrated that CMAH expression decreases phagocytic capacity of macrophages [113]. In this study, uptake of Aβ, retinal debris and bioparticle uptake were assessed. CMAH expressing macrophages showed decreased uptake compared to control macrophages. However, there was no effect of CD33, an important regulator of phagocytosis, on uptake. These result showed that decrease in uptake might be a consequence of other factors rather than changes in signaling of macrophages. In literature, neuraminidases were shown to have decreased affinity towards Neu5Gc [112,113,150]. Prior to phagocytosis, sialic acids are removed by host neuraminidases and especially, NEU1 is critical for proper functioning of phagocytosis [125]. I hypothesized that Neu5Gc could not be cleaved as easy as Neu5Ac by host neuraminidases and this could lead to

decreased phagocytosis in immune cells. To test this hypothesis, transduced macrophages were treated with fibrillary Aβ and amount of sialic acids which could not be cleaved by host neuraminidases were measured with lectin staining. CMAH expressing macrophages showed more staining after lectin staining, indicating that neuraminidases in CMAH expressing macrophages could not indeed cleave sialic acids. Having –OH group might have decreased the affinity of neuraminidases in Neu5Gc in contrast to Neu5Ac. Thus, CMAH expressing macrophages could not enter phagocytic stage and Aβ could not be uptaken. Since priming of phagocytosis is disrupted in CMAH expressing macrophages, this mechanism can also explain the decrease in other uptake experiments (figure 31). But these experiments can only demonstrate changes in cellular level and there might be other factors which can only be revealed *in vivo* setting.

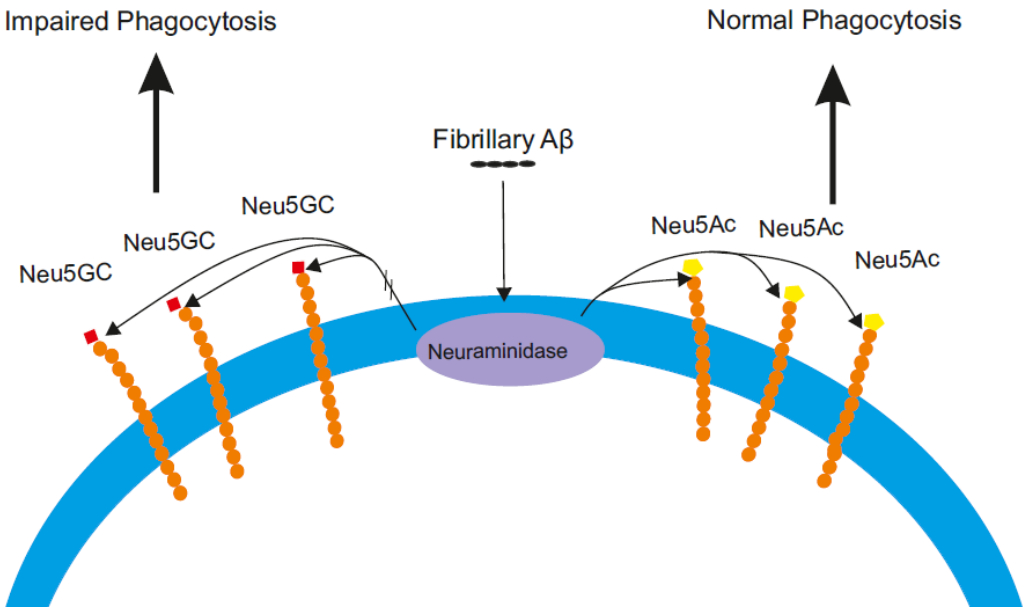

Figure 31 Proposed mechanism for decrease in phagocytosis caused by CMAH expression. When there is a stimulus (Aβ) in the surrounding environment, macrophages prime to phagocytosis by cleaving sialic acids in glycocalyx. Since Neu5Gc could not be cleaved by neuraminases, macrophages could not enter complete phagocytic state.

5.4.2.2 Metabolites of Neu5Gc increases oxidative stress and depletes scavenger reservoir of macrophages

Uptaken Neu5Gc was shown to give rise to glycolate and glucosamine 6-phosphate end products [151]. However, Neu5Ac was metabolized to acetate and glucosamine 6-phosphate [152]. The main catalytic different product of Neu5Gc compared to Neu5Ac is having glycolate instead of acetate. Glycolate was shown to increase oxidative stress in hepatocytes via oxalate cycle [153]. In oxalate cycle, glycolate is first converted to glyoxlate and then to oxalate. As side product of these conversions, H_2O_2 is produced (figure 32). Produced H_2O_2 is neutralized by peroxisomal catalase.

In our study, CMAH expressing macrophages showed increased peroxisomal catalase activity. The most plausible explanation to this phenoma is that CMAH expression causes more production of Neu5Gc which in turn leads to more metabolic turnover of Neu5Gc and thereby, more production of metabolite, glycolate. In order to cope with this kind of oxidative stress, macrophages increased their peroxisomal catalase activity. However, this mechanism could have possibly depleted oxidative stress scavenging mechanisms of macrophages.

5.4.2.3 Accumulated Neu5Gc limits the responsiveness of macrophages and reverts the activated phenotype of macrophages

Recent findings showed that $CMAH^{-/-}$ mice demonstrated increased sensitivity to endotoxic shock [113]. Thus, it is reasonable to assume that CMAH expressing macrophages would display decreased sensitivity to external stimuli. I observed that under non-treated conditions, transcription of proinflammatory cytokines was similar in WT CMAH compared to WT GFP. This finding is also supported by previous literature findings.

CD33KO macrophages were known to display increased Aβ phagocytosis [122], increased ROS production after stimulation [154] and increased proinflammatory cytokine production [155]. These results were reproduced in our experimental setup. However, when CMAH is expressed on CD33KO background

(CD33KO CMAH), the increased responses of macrophages reverted to normal conditions. Neu5Gc accumulation inhibited the elevated cellular responses of CD33KO macrophages. Also CD33KO CMAH could not respond to SOD1 and trolox scavengers after stimulation. This phenomena could be explained by internal toxicity of Neu5GC rather than aberrations in internal signaling. Owing to increased ROS scavenging and decreased neuraminidase activities, macrophages could not respond properly. I concluded that Neu5Gc pushed the macrophages into an irreversible activated phenotype.

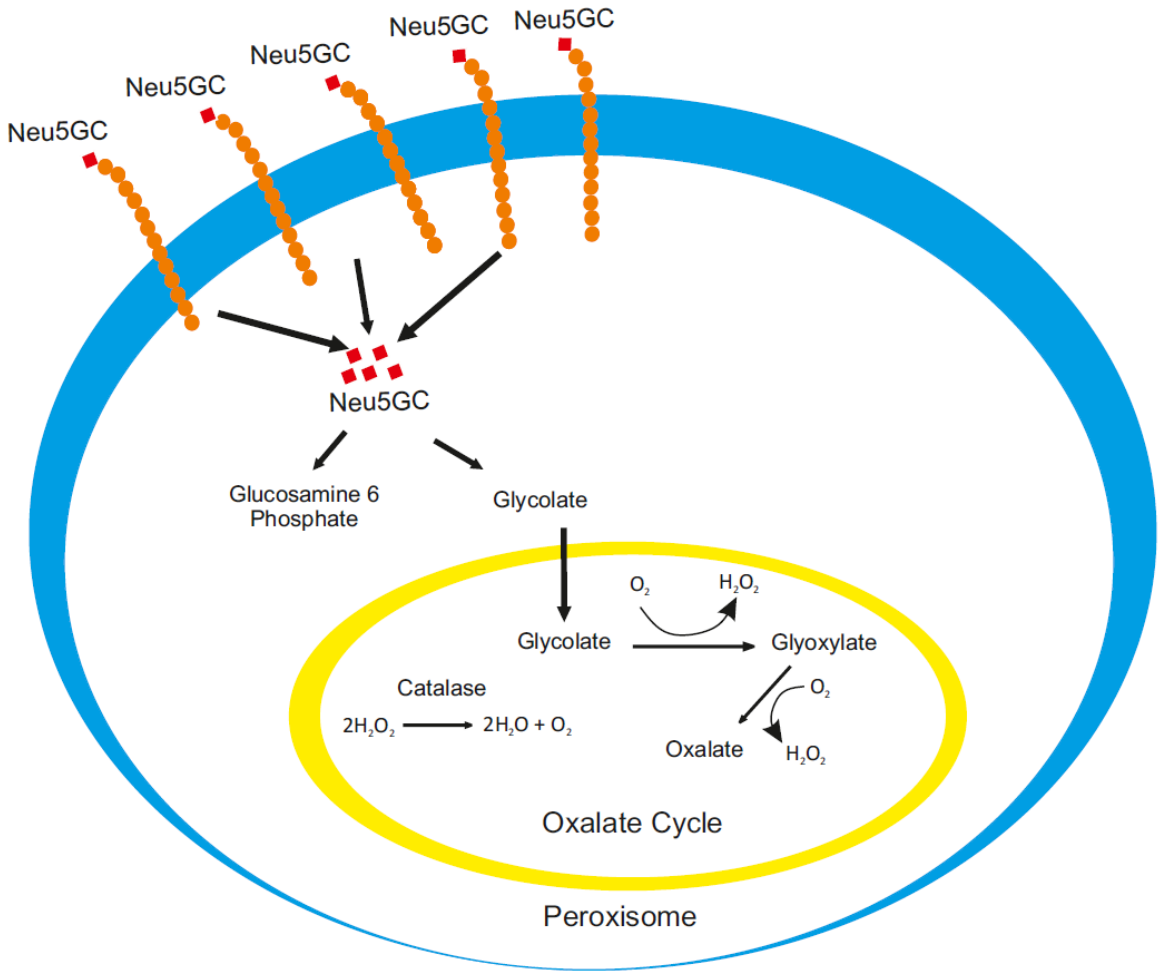

Figure 32 Oxalate cycle in peroxisome produces H_2O_2 from glycolate. From metabolic turnover of internalized Neu5Gc, glycolate is produced and glycolate enters the oxalate cycle. In this cycle, H_2O_2 is produced and neutralized by peroxisomal catalase. This cascade of events depletes the scavenger reservoir of macrophages.

5.4.2.4 Internalized Neu5Gc activates lysosomes and contribute to ROS production

CMAH expression caused increased catalase activity. This elevated response might not only be a result of metabolic products of Neu5Gc, but also through interference of Neu5Gc in other cellular events. Previously, Neu5Gc was shown to be transported to lysosomes where sialic acids is removed from glycoconjugates via neuraminidase acitivity [94]. For this reason, lysosomal activation pattern was analyzed because activity of neuraminidases might have altered the lysosomes. Previous findings in literature and lectin staining results demonstrated that neuraminidases do not possess stronger affinity towards Neu5Gc [112,113,150]. This phenomena could cause accumulation of sialic acid glycoconjugates and might lead to symptoms similar to lysosomal storage disorders (figure 33). Especially, defective or deficient NEU1 activity could be observed because NEU1 is one of the responsible neuraminidases cleaving sialic acids from glycoproteins in lysosomes [156]. LAMP1 is lysosome associated membrane sialylated glycoprotein, involved in several lysosomal storage diseases, and it is one of the substrates of Neu1 [157]. LAMP1 plays an active role in the docking of lysosomes at the plasma membrane [158]. Consequently owing to decreased Neu1 activity, LAMP1 might remain in oversialylated state, and have a prolonged half-life. Accumulation of oversialylated LAMP1 increases the number of LAMP1-marked lysosomes that dock at the plasma membrane. Consequently, these events could cause excessive extracellular release of lysosomal contents like cathepsin B from deficient cells. Released cathepsin B was shown to promote oxidate stress in mitochondria [159]. This mechanism might have contributed to increased ROS production in CMAH expressing macrophages (figure 34). Displaying increased CD68 staining by CMAH expressing macrophages can be considered as another supporting evidence to this concept as CD68 can be considered as activation marker. Moreover, other uprocessed accumulated glycoproteins can further promote activatory signaling of lysosomes which might lead to increase in ROS production.

5.4.3 Neu5Gc as a ligand for CD33

CD33 is a member of the SIGLEC family of molecules having the ability to recognize sialic acids. CD33 is known to bind both sialic acid type, Neu5Gc and Neu5Ac [67].The human CD33 binds preferentially to Neu5Gc glycans rather than Neu5Ac glycans [160], however, the downstream signaling events followed by Neu5Gc binding to CD33 has not been clarified so far. Of note, CD33 can bind to Neu5Ac glycans to some extent [160]. This study showed that binding of Neu5Gc affects downstream signaling and causes activation of macrophages.

5.4.3.1 Neu5Gc activates lysosomes in CD33 dependent manner

Several human pathogens evolved to express sialic acids on their glycocalyx [161]. Thus, those pathogens can be considered as potential ligands for CD33. Several sialylated pathogens have been shown to bind to SIGLECS [162–164]. Receptor mediated endocytosis directs CD33 containing endosomes to lysosomes and sialic acid-CD33 glycoprotein complex is processed with neuraminadases. In my study, I have observed that Neu5Gc bound CD33 activates lysosomes and CMAH expression did not lead to activation of lysosomes in CD33KO background. Thus, CD33 can be accounted as the main carrier of Neu5Gc. In support of this fact, bivalent antibodies directed against CD33 were shown to decrease surface expression of CD33 [165–167]. Since CD33 has higher affinity towards Neu5Gc, binding of Neu5Gc might have triggered receptor mediated endocytosis.

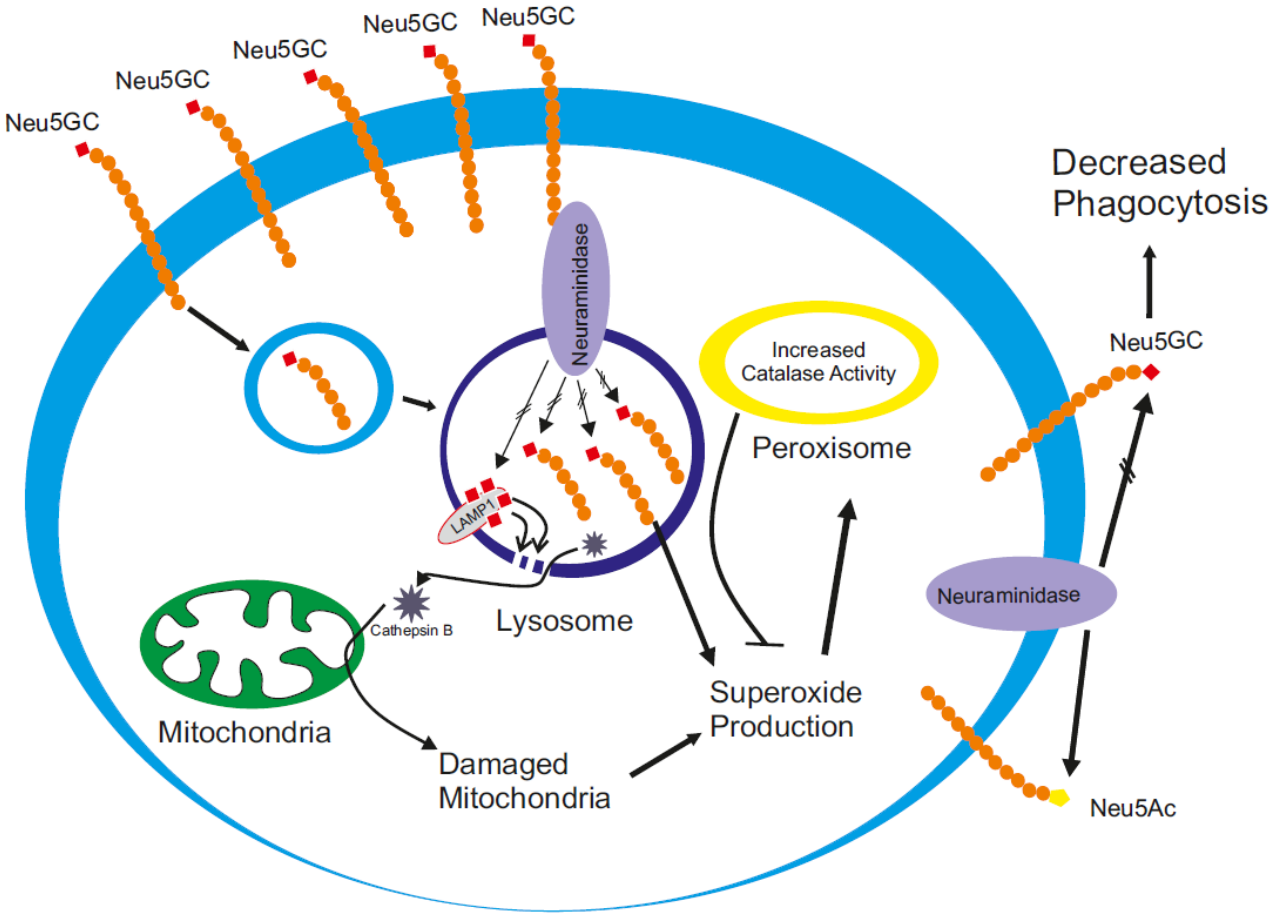

Figure 33 Neu5Gc causes oxidative stress through decreased neuraminidase activity. Internalized glycans are sent to lysosomes for turnover. However, neuraminidases cannot cleave Neu5Gc efficiently. This might lead to glycan accumulation in lysosomes, causing symptoms similar to lysosomal storage disorders. Eventually, hypersialylated LAMP accumulate in lysosomes causing the lysosomal contents leak through the membrane of the lysosomes and damaging mitochondria which is a possible source of ROS. Also, signaling in lysosomes might have contributed to ROS production because of accumulated glycoproteins. However, ROS produced through these mechanisms are eliminated thorugh peroxisomal catalase activity. Decreased neuraminidase activity also affects phagocytosis owing to disrupted priming of macrophages.

5.4.3.2 Binding of Neu5Gc to CD33 disrupts ITIM signaling and increases activation of macrophage

Sialic acid binding domain is located in V set Ig domain of CD33 and sialic acids can bind to CD33 in both cis and trans manner [67]. In this study, cis of sialic acids to CD33 was analyzed. Since CD33 knockout macrophages do not express CD33, they were not included in this experiment. CMAH expression did not alter the cis binding of sialic acids to CD33. In both Neu5Ac and Neu5Gc conditions, the macrophages did

not show any alteration in cis binding. Despite presenting no change in CD33 binding capacity, Neu5Gc could still cause alterations in the intracellular downstream signaling. CD33 counter-regulates the activatory ITAM signaling by the recruitment of SHP1 and SHP2 [71]. For this reason, I checked recruitment of SHP1 to CD33 after CMAH expression. CMAH expressing macrophages showed decreased recruitment of SHP1. However, transcription of SHP1 did not show any alteration after CMAH expression. CD33KO GFP, on the other hand, showed complementary increase in transcription to CD33 loss.

Extracellular signal regulated kinases (ERK) is one of the activatory signaling of macrophages which is regulated by SHP1 [168]. ERK is an important member of the MAPK family, which plays a pivotal role in signal-transduction pathways [169,133]. MAPKs respond to various extracellular stimuli, including growth factors and oxidative stress that have been linked to pathophysiologic processes [170–172]. After observing less recruitment of SHP1 to CD33, phosphorylation status of ERK was analyzed. Although there was slight increase in ERK phosphorylation in WT CMAH compared to WT GFP, the difference was not significant. CD33KO GFP showed increased ERK phosphorylation compared to WT GFP as expected. Since CD33 is an inhibitory molecule, lack of its expression might have led to increased ERK phosphorylation.

Expression of activatory and inhibitory cellular markers of macrophages were also analyzed. Upon ligan binding, TREM2 and CD64 are involved in activation of macrophages [173,174]. Moreover, TREM2 was found to be associated with AD [51,52,174]. Expression of TREM2 and CD64 did not show any difference between WT CMAH and WT GFP. However, CD64 transciption and surface marker expression decreased significantly in CD33KO GFP compared to WT GFP. This phenomena could be explained by feedback regulation of macrophages. Since there is decrease in one of the inhibitory signaling molecules, macrophages might have responded by decreasing one or more of activatory signaling molecules.

As inhibitory molecule, transcription of SIRPα was analyzed in combination with CD33 and CMAH expression. Like CD33, SIRPα is a cell signaling molecule that is predominantly expressed by myeloid origin

cells [131,175,176] and contains a cytoplasmic tail that bears ITIM motifs [177,178]. Transciption of SIRPα did not show any change after CMAH expression. Moreover, CD33KO GFP did not show any significant change compared to WT GFP. Since there is an already increase in SHP1 transcription, CD33KO macrophages might not have responded through intermediate molecule of ITIM signaling rather than changing expression of receptors.

5.4.3.3 Disrupted ITIM signaling and lysosomal activation causes increase in ROS production

A recent study showed that Neu5Gc incorporation was found to be associated with oxidative stress [111]. However, the complete mechanism underlying ROS production has not been clarified so far. My study shows that Neu5Gc incorporation via CMAH expression causes increase in ROS by several ways. Metabolites of Neu5Gc and glycan accumulation were found to increase oxidative stress in CMAH expressing macrophages. However, Neu5Gc could exert its effects not only through metabolites but also through changing activatory and inhibitory signaling.

In this study, role of CD33 in oxidative stress was clarified in cellular level. CMAH expressing macrophages showed CD33 dependent increase in oxidative stress. Previous results of this study showed that SHP1 recruitment to CD33 decreased significantly. Despite the decrease in SHP1 recruitment caused slight increase in ERK phosphorylation, the increase was not significant. This result indicated that there might be other mechanisms increasing oxidative stress.

Findings in lysosomal activation complemented signaling of CD33. Antibody bound CD33 was shown to be directed to lysosomes more in literature [165–167]. Neu5Gc bound CD33 might have triggered similar mechanism. Since neuraminidases would not cleave this complex, it might have triggered other signaling pathways that contribute to increased in number of lysosomes or elevated activation. These mechanisms in total might have given rise to CD33 dependent increase in ROS production (figure 34).

5.5 Altered sialylation in neurodegeneration

Alterations in protein sialylation have been associated with human neurodegenerative disease states, such as prion disease[179], MS[180] , AD[181], and PD[182]. Altough sialylation was found to be related with neurodegeneration, underlying correlation between neurodegeneration with sialylation have not been clarified. Also, previous studies showed that sialylation have impacts on neurodegeneration associated molecules.

5.5.1 Sialylation in Alzheimer's disease

There are reports that have been published about alteration of sialic acid metabolism in AD [183]. Soluble sialyltransferase (enzymes which transfer sialic acids to glycoproteins) activity was reported in a comparative study including 12 AD patients and 12 age-matched controls [184]. This finding was also reproduced in postmortem brains of AD patients and matched controls [185]. Decreased sialyltransferase activity was demonstrated in membrane and soluble fractions of frontal and temporal lobe, but not observed in hippocampus. Moreover, lectin blotting analysis of cerebrospinal fluid proteins showed differences in sialylation between AD patients and healthy individuals [186]. Another lectin blotting study to Cerebrospinal fluid (CSF) of AD patients replicated these results and confirmed reduced binding in AD patients [187]. However, due to cross-reactivity of lectins and limited sample size, these studies could not clearly show which molecules were differentially sialylated in AD.

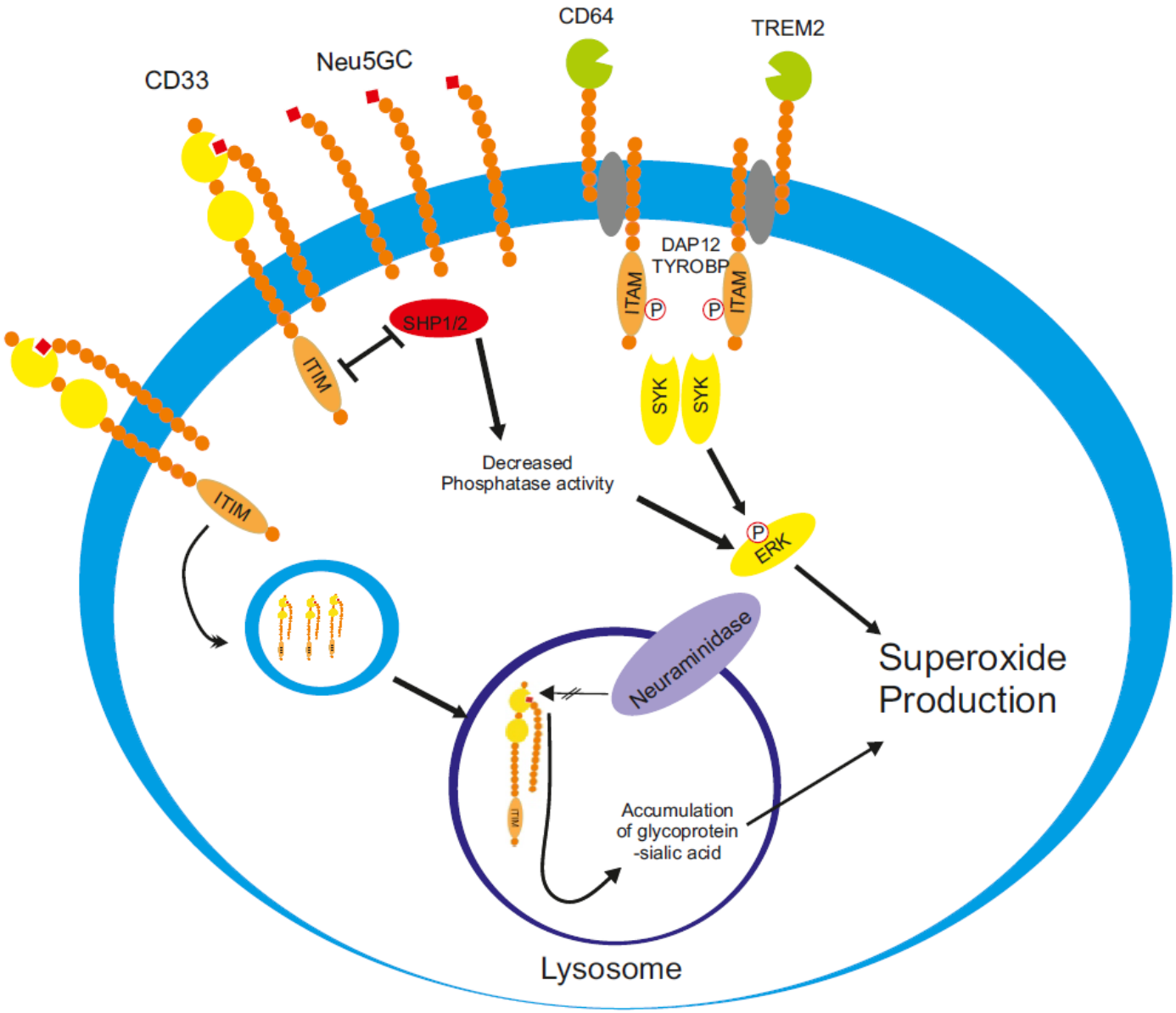

Figure 34 Possible mechanisms underlying CD33 dependent increase in ROS production. Binding of Neu5Gc to CD33 might induce conformational change in CD33, causing less docking of SHP1. Less phosphatase activity of SHP1 could lead to increased phosphorylation of ERK and turn of events cause increase in superoxide production. On the other hand, Neu5Gc bound CD33 is intenalized more into lysosomes and Neu5Gc could not be cleaved of by neuraminidases. Consequently, Neu5Gc bound CD33 molecules could accumulate and activate lysosomes. All of these molecular events might shed light upon the reasons underlying CD33 based increase in ROS production.

One of the most important terminal caping reactions of N-glycans involve addition of terminal sialic acids. Several AD associated molecules were found to N-glycosylated and especially, it is functionally important for APP. It has two potential N-glycosylation sites and elevated sialylation of N-linked glycans of APP was shown to increase secretion of both APP and its metabolites [188–190]. Moreover, mutations in N-glycosylation sites in APP were found to be highly important for AD progression. Deletion of these glycosylation sites in APP resulted in decreased secretion and microsomal localization of APP [191] (figure 36). Also, Swedish and London mutations in APP, known to alter N-Glycosylation sites, were shown to increase total amount of Aβ and Aβ42/ Aβ40 ratio [192]. In addition to N-glycosylation, APP was shown to have three O-glycosylation sites which are Thr291, Thr292 and Thr576 [193]. Although the role of O-glycan is still elusive, there is supporting evidence that O-glycosylated APP is preferentially secreted [194]. Furthermore, APP processing enzyme BACE1 affects sialylation. Several studies have shown that processing of ST6Gal1 by BACE1 is necessary to produce soluble form of this sialyltransferase [195–197]. ST6Gal1 is sialyltransferase which transfers sialic acids to glycoproteins [197]. In this way, BACE1 does not only cleave APP but also by down-regulate sialylation via ST6Gal-I cleavage [190]. Modulation of APP sialylation is also performed in lysosomes through neuraminidase 1 activity [198]. Deficiency in lysosomal sialidase NEU1 leads to occurence of an AD-like amyloidogenic process in mice [199]. Loss of function mutation in NEU1$^{-/-}$ mice caused accumulation and and amyloidogenic processing of hypersialylated APP in lysosomes.

These literature findings strongly suggest that the biosynthetic or the catabolic control of the sialic acids on APP is highly relevant for its β-amyloidogenic processing [157]. Since cleaveage of Neu5Gc from glycoproteins by neuraminidases was proven to be more difficult, I claim that sialylation of APP with Neu5Gc may change its half-life and lead to accumulation of this complex in lysosomes. That might cause accumulated APP to be more prone to β-amyloidogenic cleavage and accelerated production of

neurotoxic APP end-products. This concept could explain the pathogenecity of Neu5Gc through APP in neurons.

Another affected molecule in Alzheimer's disease is tau protein. Interestingly, Tau was found to be N-glycosylated in AD but not in healthy brain [200]. N-glycosylation of tau was found to make it more susceptible to phosphorylation. Thus, it might lead to hyperphosphorylated form of tau which is a hallmark of AD [201,202]. Tau also has multiple O-Glycosylation sites [203] and the level of O-Glycosylated is decreased in AD brain compared to control brain [204]. O-glycosylation was shown to be more protective in AD compared to N-glycosylation since it is less susceptible to phosphorylation [205,206]. Since there is no study about whether Neu5Gc preferes O-Glycosylation or N-glycosylation, I could only speculate that sialic acid Neu5Gc might choose different pathway than Neu5Ac which might have led to more N-Glycosylation.

Sialylation does not only affect AD through misfolded proteins but also through immune activation. Several genome wide association studies have pointed out the importance of CD33, a member of sialic acid binding immunoglobulin like lectins [65,77,78,122]. Moreover, CD33 variant 2 which lacks sialic acid binding domain, was shown to protective against AD [77]. In this study, I clarified CD33 dependent mechanisms of Neu5Gc incorporation *in vitro* culture model. In literature, antibody binding to CD33 causes less surface expression of CD33 in the membrane causing it to be more directed through lysosomes [207]. Similar mechanism seemed to be triggered by Neu5Gc binding because lysosomes were activated in CD33 dependent manner.

5.5.2 Resemblance of CMAH expressing macrophages to microglia in AD

Experimental findings of this study revealed the similarity of CMAH expressing macrophages to microglia in AD. Both of the cell types not only display altered sialylation phenotype, but also increased oxidative stress and decreased phagocytic capacity. Oxidative stress in AD has been shown extensively in microglia [208–213]. The results of this study showed that CMAH expressing macrophages contributed oxidative stress

through its metabolites, accumulated glycans and glycoproteins in lysosomes, and CD33 signaling. Moreover, because of decreased neuraminidase activity, CMAH expressing macrophages could not prime phagocytosis and decreased phagocytosis was observed. All of these findings point out importance of Neu5Gc incorporation in AD. It would be much speculation to claim that Neu5Gc incorporation is the only reason of AD. However, AD related polymorphisms combined with Neu5Gc incorporation might be one of the underlying reasons of neurodegeneration. Moreover, Neu5Gc might have acted as slow poison whose effect could be observable only in aged brain. Since Neu5Gc is having paralysis effect on immune functions, microglia in aged brain with Neu5Gc incorporation might not perform immune functions and contribute to neurodegeneration process.

5.5.3 Connection between red meat consumption and AD

Research conducted in this study combined with literature shows that Neu5Gc incorporation might increase the tendency towards AD. These results are being supported by current findings about prevelance of AD as well. AD prevelance is found to be higher North America and Western Europe [214]. Diet patterns in these countries were found to be strongly associated with AD prevelance. While western diet which is abundant in red meat and milk products has been causing chronic glia activation and more AD prevelance [215], Mediterrenean diet which is rich in fruits and vegetables was found to decrease AD prevelance [216,217]. Since Neu5Gc is encountered aboundantly in red meat and milk products, it is resonable to hypothesize that consuming red meat and milk products increase the prevalence of AD.

6. SUMMARY

Throughout evolutionary processes, organisms gain or lose functions because of emerging mutations. The frameshift mutation emerged in the human *CMAH* gene is one of these loss of function mutations and it caused the human glycocalyx to have distinct phenotype compared to other mammals. Owing to this loss of function mutation, humans lose the ability to process sialic acids as they are not capable of converting N-acetlyneuraminic Acid (Neu5Ac) to N-glycolylneuraminic Acid (Neu5Gc).

The effects of Neu5Gc incorporation to immune cells have not been studied with their impacts on neurodegenerative diseases so far. Aim of this study is to figure out how Neu5Gc incorporation regulates and modifies innate immune cell responses and affects progress of neurodegeneration in *in vitro* culture system. With this purpose, murine *CMAH* gene has been expressed in human THP1 macrophages. Moreover, *CMAH* gene has been expressed in CD33KO macrophages since CD33 is one of the sialic acid binding protein and it has been found to have impacts in progression of Alzheimer's disease.

There were two major outcomes in this study. Firstly, CMAH expression decreased Aβ, debris, and *staphylococcus aureus* bioparticle phagocytosis. The decrease in phagocytosis is not affected by the lack of CD33. This decrease could be explained by difficulty of clearance of Neu5Gc to Neu5Ac. Sialic acids must be cleaved prior to phagocytosis and Neu5Gc could not be cleaved as easy compared to Neu5Ac. Disrupted cleavage of Neu5Gc prior to phagocytosis could be the reason of accumulated Aβ plaques in Alzheimer's disease. Secondly, CMAH expressing macrophages exhibited increase in ROS production via CD33 dependent manner and stimulation with Aβ, debris, and *staphylococcus aureus* bioparticles did not cause increase in further ROS production. The increase in ROS production could be explained by disrupted ITIM signaling, increased lysosomal activation and increased metabolic turnover of Neu5Gc. Lysosomal activation was shown to be CD33 dependent and it could be one of the links to Alzheimer's disease in respect to ROS production.

Another distinct phenotype of CMAH expressing macrophages is their inability to respond and perform immune functions. CMAH expression limited the responses of macrophages to certain level. CD33KO macrophages were known to have increased pro-inflammatory cytokine release, increased Aβ phagocytosis, and elevated response in ROS production after neural debris stimulation. However, when CMAH was expressed in CD33KO macrophages, all of these responses get deteriorated and changes related with CD33KO phenotype reverted. Combined with CMAH expression, CD33KO macrophages displayed decreased proinflammatory cytokine transcription, Aβ phagocytosis and ROS production to external stimuli such as neural debris.

Results of this study might demonstrate the missing connection between Neu5Gc incorporation with macrophage functions in cellular level. Owing to close progeny, these result could shed light upon the connection between CD33 and microglia connection in Alzheimer's disease. Neu5Gc incorporation to macrophages in high levels demonstrated similar phenotype to microglia in Alzheimer's disease which have decreased phagocytic capability and increased oxidative stress in cellular level. However, these results are applicable to only in vitro level and more research in vivo is necessary to reach more conclusive findings. Afterwards, Neu5Gc replacement therapies could be considered as alternative therapy against Alzheimer's disease.

7. ACKNOWLEDGEMENTS

I would like to express my deepest gratitude to Prof. Dr. Harald Neumann for providing me the opportunity to work in his group. I am thankful for his ideas and support that has driven me all these years. He was also the initiator of the collaborations that helped me building up the thesis. I would like to thank Prof. Dr. Walter Witke that kindly agreed to participate as the second referee to the thesis dissertation.

I would like to share my thanks to group of Samanta Cajic, Dr. Erdmann Rapp, and Prof. Veit Hornung for amazing collaboration opportunity. Without their collaboration, this study would not have moved this far.

I would like to thank both former and current members of the Neumann's lab: Akihito, Anahita, Bettina, Christine, Hendrik, Ichiro, Jannis, Jens, Jonas, Omar, Sharon, Rita, Vanessa and Tamara. Especially, I would like to thank Sharon Stursberg for great breaks. I am also grateful to the entire Reconstructive Neurobiolology Institute that contributed in the creation of a great working environment. It was great to work and have fun altogether.

I would like to thank a lot to Assoc. Prof Hasan Deniz and Dr. Liviu Bodea for taking the time to proofread this thesis. Thank you for your useful comments and suggestions.

I also want to thank to my close friends in Bonn who are Ayla, Bahadir, Bane, and Dilek. You made my time much valuable, enjoyable by your presence. It was great to know you.

I want to thank my family, especially my mother, for their endless and unconditional support. Without your presence, I would not complete my PhD for sure.

8. REFERENCES

1. Herculano-Houzel, S. The Human Brain in Numbers: A Linearly Scaled-up Primate Brain . *Front. Hum. Neurosci.* **3,** 31 (2009).

2. Jernigan, T. L. & Stiles, J. Construction of the human forebrain. *Wiley Interdiscip. Rev. Cogn. Sci.* **8,** (2017).

3. Prince, M. *et al. World Alzheimer Report 2015 The Global Impact of Dementia. Alzheimer's Disease International*. (2015).

4. Hirtz, D. *et al.* How common are the 'common' neurologic disorders? *Neurology* **68,** 326–337 (2007).

5. Heppner, F. L., Ransohoff, R. M. & Becher, B. Immune attack: the role of inflammation in Alzheimer disease. *Nat Rev Neurosci* **16,** 358–372 (2015).

6. Regan, K. *et al.* Translating Mendelian and complex inheritance of Alzheimer's disease genes for predicting unique personal genome variants. *J. Am. Med. Inform. Assoc.* **19,** 306–316 (2012).

7. Querfurth, H. W. & LaFerla, F. M. Alzheimer's Disease. *N. Engl. J. Med.* **362,** 329–344 (2010).

8. Brosseron, F., Krauthausen, M., Kummer, M. & Heneka, M. T. Body Fluid Cytokine Levels in Mild Cognitive Impairment and Alzheimer's Disease: a Comparative Overview. *Mol. Neurobiol.* **50,** 534–544 (2014).

9. Hardy, J. The Amyloid Hypothesis of Alzheimer's Disease: Progress and Problems on the Road to Therapeutics. *Science (80-.).* **297,** 353–356 (2002).

10. Chow, V. W., Mattson, M. P., Wong, P. C. & Gleichmann, M. An Overview of APP Processing Enzymes and Products. *Neuromolecular Med.* **12,** 1–12 (2010).

11. Høglund, R. A. & Maghazachi, A. A. Multiple sclerosis and the role of immune cells. *World J. Exp. Med.* **4,** 27–37 (2014).

12. Van Eldik, L. J. *et al.* The roles of inflammation and immune mechanisms in Alzheimer's disease. *Alzheimer's Dement. Transl. Res. Clin. Interv.* **2,** 99–109 (2016).

13. Heneka, M. T., Kummer, M. P. & Latz, E. Innate immune activation in neurodegenerative disease. *Nat Rev Immunol* **14,** 463–477 (2014).

14. Zhang, B. *et al.* Integrated systems approach identifies genetic nodes and networks in late-onset Alzheimer's disease. *Cell* **153,** 707–20 (2013).

15. Tarkowski, E., Andreasen, N., Tarkowski, A. & Blennow, K. Intrathecal inflammation precedes development of Alzheimer's disease. *J. Neurol. Neurosurg. Psychiatry* **74,** 1200–5 (2003).

16. Krstic, D. *et al.* Systemic immune challenges trigger and drive Alzheimer-like neuropathology in mice. *J. Neuroinflammation* **9,** 151 (2012).

17. Rock, R. B. *et al.* Role of microglia in central nervous system infections. *Clin. Microbiol. Rev.* **17,** 942–964 (2004).

18. Davalos, D. *et al.* ATP mediates rapid microglial response to local brain injury in vivo. *Nat. Neurosci.* **8,** 752–758 (2005).

19. Ginhoux, F. *et al.* Fate mapping analysis reveals that adult microglia derive from primitive macrophages. *Science* **330,** 841–5 (2010).

20. Kierdorf, K. *et al.* Microglia emerge from erythromyeloid precursors via Pu.1- and Irf8-dependent pathways. *Nat Neurosci* **16,** 273–280 (2013).

21. Mittelbronn, M., Dietz, K., Schluesener, H. J. & Meyermann, R. Local distribution of microglia in the normal adult human central nervous system differs by up to one order of magnitude. *Acta Neuropathol.* **101,** 249–255 (2001).

22. Gomez-Nicola, D. & Perry, V. H. Microglial Dynamics and Role in the Healthy and Diseased Brain: A Paradigm of Functional Plasticity. *Neurosci.* **21,** 169–184 (2015).

23. Stollg, G. & Jander, S. The role of microglia and macrophages in the pathophysiology of the CNS. *Prog. Neurobiol.* **58,** 233–247 (1999).

24. London, A., Cohen, M. & Schwartz, M. Microglia and monocyte-derived macrophages: functionally distinct populations that act in concert in CNS plasticity and repair. *Front. Cell. Neurosci.* **7,** 34 (2013).

25. Prinz, M. & Priller, J. Microglia and brain macrophages in the molecular age: from origin to neuropsychiatric disease. *Nat. Rev. Neurosci.* **15,** 300–12 (2014).

26. Alliot, F., Godin, I. & Pessac, B. Microglia derive from progenitors, originating from the yolk sac, and which proliferate in the brain. *Dev. Brain Res.* **117,** 145–152 (1999).

27. Glass, C. K. & Saijo, K. Microglial cell origin and phenotypes in health and disease. *Nat. Rev. Immunol.* **11,** 775–787 (2011).

28. Barger, S. W. & Harmon, a D. Microglial activation by Alzheimer amyloid precursor protein and modulation by apolipoprotein E. *Nature* **388,** 878–81 (1997).

29. Combs, C. K., Johnson, D. E., Karlo, J. C., Cannady, S. B. & Landreth, G. E. Inflammatory mechanisms in Alzheimer's disease: inhibition of beta-amyloid-stimulated proinflammatory responses and neurotoxicity by PPARgamma agonists. *J. Neurosci.* **20,** 558–567 (2000).

30. Itagaki, S., McGeer, P. L., Akiyama, H., Zhu, S. & Selkoe, D. Relationship of microglia and astrocytes to amyloid deposits of Alzheimer disease. *J. Neuroimmunol.* **24,** 173–82 (1989).

31. Gandy, S. & Heppner, F. L. Microglia as dynamic and essential components of the amyloid hypothesis. *Neuron* **78,** 575–7 (2013).

32. Ahmed, M. *et al.* Structural conversion of neurotoxic amyloid-beta(1-42) oligomers to fibrils. *Nat.*

Struct. Mol. Biol. **17,** 561–567 (2010).

33. Liu, Y. *et al.* LPS receptor (CD14): A receptor for phagocytosis of Alzheimer's amyloid peptide. *Brain* **128,** 1778–1789 (2005).

34. Stewart, C. R. *et al.* CD36 ligands promote sterile inflammation through assembly of a Toll-like receptor 4 and 6 heterodimer. *Nat. Immunol.* **11,** 155–61 (2010).

35. Sheedy, F. J. *et al.* CD36 coordinates NLRP3 inflammasome activation by facilitating intracellular nucleation of soluble ligands into particulate ligands in sterile inflammation. *Nat. Immunol.* **14,** 812–20 (2013).

36. Bamberger, M. E., Harris, M. E., McDonald, D. R., Husemann, J. & Landreth, G. E. A cell surface receptor complex for fibrillar beta-amyloid mediates microglial activation. *J. Neurosci.* **23,** 2665–2674 (2003).

37. Koenigsknecht, J. Microglial Phagocytosis of Fibrillar Beta-Amyloid through a Beta1 Integrin-Dependent Mechanism. *J. Neurosci.* **24,** 9838–9846 (2004).

38. Khoury, J. El *et al.* Scavenger receptor-mediated adhesion of microglia to [beta]-amyloid fibrils. *Nature* **382,** 716–719 (1996).

39. Du Yan, S. *et al.* Amyloid-beta peptide-receptor for advanced glycation endproduct interaction elicits neuronal expression of macrophage-colony stimulating factor: a proinflammatory pathway in Alzheimer disease. *Proc Natl Acad Sci* **94,** 5296–301 (1997).

40. Fu, H. *et al.* Complement Component C3 and Complement Receptor Type 3 Contribute to the Phagocytosis and Clearance of Fibrillar Aβ by Microglia. *Glia* **60,** 993–1003 (2012).

41. Krabbe, G. *et al.* Functional impairment of microglia coincides with Beta-amyloid deposition in mice with Alzheimer-like pathology. *PLoS One* **8,** e60921 (2013).

42. Hickman, S. E., Allison, E. K. & El Khoury, J. Microglial Dysfunction and Defective -Amyloid Clearance Pathways in Aging Alzheimer's Disease Mice. *J. Neurosci.* **28,** 8354–8360 (2008).

43. Yan, P. *et al.* Characterizing the Appearance and Growth of Amyloid Plaques in APP/PS1 Mice. *J. Neurosci.* **29,** 10706–10714 (2009).

44. Mawuenyega, K. G. *et al.* Decreased clearance of CNS beta-amyloid in Alzheimer's disease. *Science* **330,** 1774 (2010).

45. Grathwohl, S. A. *et al.* Formation and maintenance of Alzheimer's disease beta-amyloid plaques in the absence of microglia. *Nat. Neurosci.* **16,** 164–167 (2010).

46. Griffin, W. S. T. *et al.* Brain interleukin 1 and S-100 immunoreactivity are elevated in Down syndrome and Alzheimer disease. *Proc. Natl. Acad. Sci. U. S. A.* **86,** 7611–7615 (1989).

47. Patel, N. S. *et al.* Inflammatory cytokine levels correlate with amyloid load in transgenic mouse models of Alzheimer's disease. *J. Neuroinflammation* **2,** 9 (2005).

48. vom Berg, J. *et al.* Inhibition of IL-12/IL-23 signaling reduces Alzheimer's disease-like pathology and cognitive decline. *Nat Med* **18,** 1812–1819 (2012).

49. Fillit, H. *et al.* Elevated circulating tumor necrosis factor levels in Alzheimer's disease. *Neurosci. Lett.* **129,** 318–320 (1991).

50. Jonsson, T. *et al.* Variant of TREM2 Associated with the Risk of Alzheimer's Disease. *N. Engl. J. Med.* **368,** 107–116 (2012).

51. Guerreiro, R. *et al.* TREM2 variants in Alzheimer's disease. *N. Engl. J. Med.* **368,** 117–27 (2013).

52. Frank, S. *et al.* TREM2 is upregulated in amyloid plaque-associated microglia in aged APP23 transgenic mice. *Glia* **56,** 1438–1447 (2008).

53. Hickman, S. E. *et al.* The microglial sensome revealed by direct RNA sequencing. *Nat Neurosci* **16,** 1896–1905 (2013).

54. Bradshaw, E. M. *et al.* CD33 Alzheimer's disease locus: altered monocyte function and amyloid biology. *Nat. Neurosci.* **16,** 848–850 (2013).

55. Hollingworth, P. *et al.* Common variants at ABCA7, MS4A6A/MS4A4E, EPHA1, CD33 and CD2AP are associated with Alzheimer's disease. *Nat. Genet.* **43,** 429–35 (2011).

56. Jiang, T. *et al.* CD33 in Alzheimer's disease. *Mol. Neurobiol.* **49,** 529–35 (2014).

57. Yu, Z., Maoui, M., Wu, L., Banville, D. & Shen, S.-H. mSiglec-E, a novel mouse CD33-related siglec (sialic acid-binding immunoglobulin-like lectin) that recruits Src homology 2 (SH2)-domain-containing protein tyrosine phosphatases SHP-1 and SHP-2. *Biochem. J.* **353,** 483–492 (2001).

58. Thambisetty, M. *et al.* Effect of Complement CR1 on Brain Amyloid Burden During Aging and Its Modification by APOE Genotype. *Biol. Psychiatry* **73,** 422–428 (2013).

59. Takahashi, K., Rochford, C. D. P. & Neumann, H. Clearance of apoptotic neurons without inflammation by microglial triggering receptor expressed on myeloid cells-2. *J. Exp. Med.* **201,** 647–657 (2005).

60. Hsieh, C. L. *et al.* A role for TREM2 ligands in the phagocytosis of apoptotic neuronal cells by microglia. *J. Neurochem.* **109,** 1144–1156 (2009).

61. Kleinberger, G. *et al.* TREM2 mutations implicated in neurodegeneration impair cell surface transport and phagocytosis. *Sci. Transl. Med.* **6,** 243ra86 LP-243ra86 (2014).

62. Jay, T. R. *et al.* TREM2 deficiency eliminates TREM2+ inflammatory macrophages and ameliorates pathology in Alzheimer's disease mouse models. *J. Exp. Med.* **212,** 287 LP-295 (2015).

63. Wang, Y. *et al.* TREM2 lipid sensing sustains the microglial response in an Alzheimer's disease model. *Cell* **160,** 1061–1071 (2015).

64. Powell, L. D. & Varki, A. I-type Lectins. *J. Biol. Chem.* **270,** 14243–14246 (1995).

65. Nguyen, D. H., Ball, E. D. & Varki, A. Myeloid precursors and acute myeloid leukemia cells express multiple CD33-related Siglecs. *Exp. Hematol.* **34,** 728–735 (2006).

66. Crocker, P. R., Paulson, J. C. & Varki, A. Siglecs and their roles in the immune system. *Nat. Rev. Immunol.* **7,** 255–266 (2007).

67. Linnartz-Gerlach, B., Mathews, M. & Neumann, H. Sensing the neuronal glycocalyx by glial sialic acid binding immunoglobulin-like lectins. *Neuroscience* **275,** 113–124 (2014).

68. Crocker, P. R. & Varki, a. Siglecs in the immune system. *Immunology* **103,** 137–45 (2001).

69. Angata, T. & Brinkman-Van der Linden, E. I-type lectins. *Biochim. Biophys. Acta* **1572,** 294–316 (2002).

70. Jandus, C., Simon, H.-U. & von Gunten, S. Targeting siglecs--a novel pharmacological strategy for immuno- and glycotherapy. *Biochem. Pharmacol.* **82,** 323–32 (2011).

71. Huang, Z. *et al.* The effect of phosphatases SHP-1 and SHIP-1 on signaling by the ITIM- and ITAM-containing Fcgamma receptors FcgammaRIIB and FcgammaRIIA. *J. Leukoc. Biol.* **73,** 823–829 (2003).

72. Linnartz, B. & Neumann, H. Microglial activatory (immunoreceptor tyrosine-based activation motif)- and inhibitory (immunoreceptor tyrosine-based inhibition motif)-signaling receptors for recognition of the neuronal glycocalyx. *Glia* **61,** 37–46 (2013).

73. Lorenz, U. SHP-1 and SHP-2 in T cells: two phosphatases functioning at many levels. *Immunol. Rev.* **228,** 342–359 (2009).

74. Garnache-Ottou, F. *et al.* Expression of the myeloid-associated marker CD33 is not an exclusive factor for leukemic plasmacytoid dendritic cells. *Blood* **105,** 1256–1264 (2005).

75. Cao, H. & Crocker, P. R. Evolution of CD33-related siglecs: regulating host immune functions and escaping pathogen exploitation? *Immunology* **132,** 18–26 (2011).

76. Carrasquillo, M. M. *et al.* Replication of EPHA1 and CD33 associations with late-onset Alzheimer's disease: a multi-centre case-control study. *Mol. Neurodegener.* **6,** 54 (2011).

77. Malik, M. *et al.* CD33 Alzheimer's risk-altering polymorphism, CD33 expression, and exon 2 splicing. *J. Neurosci.* **33,** 13320–5 (2013).

78. Naj, A. C. *et al.* Common variants at MS4A4/MS4A6E, CD2AP, CD33 and EPHA1 are associated with late-onset Alzheimer's disease. *Nat. Genet.* **43,** 436–441 (2011).

79. Varki, A. *et al. Essentials of Glycobiology*. (2009).

80. Warren, L. The distribution of sialic acids in natural. *Comp. Biochem. Physiol. B* **10,** 153–171 (1963).

81. Lewis, A. L. *et al.* Innovations in host and microbial sialic acid biosynthesis revealed by

phylogenomic prediction of nonulosonic acid structure. *Proc. Natl. Acad. Sci. U. S. A.* **106,** 13552–13557 (2009).

82. Du, J. *et al.* Metabolic glycoengineering: Sialic acid and beyond. *Glycobiology* **19,** 1382–1401 (2009).

83. Schauer, R. Biosynthese der 7V-Glykoloylneuraminsäure durch eine von Ascorbinsäure bzw. NADPH abhängige TV-Acetyl-hydroxylierende „TV-AcetylneuraminatrOz-Oxidoreduktase" in Homogenaten der Unterkieferspeicheldrüse vom Schwein. *Hoppe. Seylers. Z. Physiol. Chem.* **351,** 783–791 (1970).

84. Scheinthal, B. M. & Bettelheim, F. A. Multiple forms of sialic acids. *Carbohydr. Res.* **6,** 257–265 (1968).

85. Castronuovo, G., Elia, V., Perez-Casas, S. & Velleca, F. Efficiency of hydroxyl groups in promoting hydrophobic interactions. A calorimetric study of ternary aqueous solutions of alkan-1-ols and alkane-m,n-diols. *J. Mol. Liq.* **88,** 163–173 (2000).

86. Kawano, T. *et al.* Molecular Cloning of Cytidine Monophospho-N-acetylneuraminic Acid Hydroxylase. Regulation of Species- and Tissue-Specific Expression of N-Glycolylneuraminic Acid. *J. Biol. Chem.* **270,** 16458–16463 (1995).

87. Hedlund, M. *et al.* N-glycolylneuraminic acid deficiency in mice: implications for human biology and evolution. *Mol. Cell. Biol.* **27,** 4340–4346 (2007).

88. Irie, A., Koyama, S. & Kawasaki, T. The Molecular Basis for the Absence of N -Glycolylneuraminic Acid in Humans. *J. Biol. Chem.* **273,** 15866–15871 (1998).

89. Hayakawa, T. *et al.* Alu-mediated inactivation of the human CMP- N-acetylneuraminic acid hydroxylase gene. *Proc Natl Acad Sci* **107,** 21300–21305 (2001).

90. Callinan, P. A. *et al.* Alu Retrotransposition-mediated Deletion. *J. Mol. Biol.* **348,** 791–800 (2005).

91. Deininger, P. L. & Batzer, M. A. Alu Repeats and Human Disease. *Mol. Genet. Metab.* **67,** 183–193 (1999).

92. Schlenzka, W. *et al.* CMP-N-acetylneuraminic acid hydroxylase: The first cytosolic Rieske iron-sulphur protein to be described in Eukarya. *FEBS Lett.* **385,** 197–200 (1996).

93. Tangvoranuntakul, P. *et al.* Human uptake and incorporation of an immunogenic nonhuman dietary sialic acid. *Proc. Natl. Acad. Sci. U. S. A.* **100,** 12045–50 (2003).

94. Bardor, M., Nguyen, D. H., Diaz, S. & Varki, A. Mechanism of uptake and incorporation of the non-human sialic acid N-glycolylneuraminic acid into human cells. *J. Biol. Chem.* **280,** 4228–4237 (2005).

95. Samraj, A. N., Läubli, H., Varki, N. & Varki, A. Involvement of a non-human sialic acid in human cancer. *Front. Oncol.* **4,** 33 (2014).

96. Davies, L. R. L. *et al.* Metabolism of vertebrate amino sugars with N-glycolyl groups: Resistance of ??2-8-linked N-glycolylneuraminic acid to enzymatic cleavage. *J. Biol. Chem.* **287,** 28917–28931 (2012).

97. Davies, L. R. L. & Varki, A. Why Is N-Glycolylneuraminic Acid Rare in the Vertebrate Brain? *Top. Curr. Chem.* **366,** 31–54 (2013).

98. Schnaar, R. L. Glycosphingolipids in cell surface recognition. *Glycobiology* **1,** 477–485 (1991).

99. Klenk, E. & Langerbeins, H. Über die Verteilung der Neuraminsäure im Gehirn. *Hoppe-Seyler Z. Physiol. Chem.* **50,** 185–193 (1941).

100. Wang, B., Miller, J. B., McNeil, Y. & McVeagh, P. Sialic acid concentration of brain gangliosides: Variation among eight mammalian species. *Comp. Biochem. Physiol.* **119,** 435–439 (1998).

101. Cariappa, A. *et al.* B cell antigen receptor signal strength and peripheral B cell development are regulated by a 9-O-acetyl sialic acid esterase. *J. Exp. Med.* **206,** 125–138 (2009).

102. Naito, Y. *et al.* Germinal Center Marker GL7 Probes Activation-Dependent Repression of N-Glycolylneuraminic Acid, a Sialic Acid Species Involved in the Negative Modulation of B-Cell Activation. *Mol. Cell. Biol.* **27,** 3008–3022 (2007).

103. Kavaler, S. *et al.* Pancreatic beta-cell failure in obese mice with human-like CMP-Neu5Ac hydroxylase deficiency. *FASEB J.* **25,** 1887–1893 (2011).

104. Padler-Karavani, V. *et al.* Human xeno-autoantibodies against a non-human sialic acid serve as novel serum biomarkers and immunotherapeutics in cancer. *Cancer Res.* **71,** 3352–3363 (2011).

105. Pham, T. *et al.* Evidence for a novel human-specific xeno-auto-antibody response against vascular endothelium. *Vasc. Biol.* **114,** 5225–5235 (2009).

106. Taylor, R. E. *et al.* Novel mechanism for the generation of human xeno-autoantibodies against the nonhuman sialic acid N-glycolylneuraminic acid. *J. Exp. Med.* **207,** 1637–46 (2010).

107. Hedlund, M., Padler-karavani, V., Varki, N. M. & Varki, A. Evidence for a human-specific mechanism for diet and antibody-mediated inflammation. *Proc Natl Acad Sci* **105,** 18936–18941 (2008).

108. Pearce, O. M. T. *et al.* Inverse hormesis of cancer growth mediated by narrow ranges of tumor-directed antibodies. *Proc Natl Acad Sci* **111,** 5998–6003 (2014).

109. Samraj, A. N. *et al.* A red meat-derived glycan promotes inflammation and cancer progression. *Proc Natl Acad Sci* **112,** 542–547 (2015).

110. Ghaderi, D., Taylor, R. E., Padler-karavani, V., Diaz, S. & Varki, A. letters Implications of the presence of N -glycolylneuraminic acid in recombinant therapeutic glycoproteins. *Nat. Biotechnol.* **28,** 863–867 (2010).

111. Kwon, D. N., Park, W. J., Choi, Y. J., Gurunathan, S. & Kim, J. H. Oxidative stress and ROS

metabolism via down-regulation of sirtuin 3 expression in Cmah-null mice affect hearing loss. *Aging (Albany. NY).* **7,** 579–594 (2015).

112. Buchlis, G. *et al.* Enhanced T Cell Function in a Mouse Model of Human Glycosylation. *J. Immunol.* **191,** 228–237 (2013).

113. Okerblom, J. J. *et al.* Loss of CMAH during Human Evolution Primed the Monocyte − Macrophage Lineage toward a More Inflammatory and Phagocytic State. *J. Immunol.* **198,** 2366–2373 (2017).

114. Ghaderi, D. *et al.* Sexual selection by female immunity against paternal antigens can fix loss of function alleles. *Proc Natl Acad Sci* **108,** 17743–17748 (2011).

115. Ma, F. *et al.* A mouse model for dietary xenosialitis – Antibodies to xenoglycan can reduce fertility. *J. Biol. Chem.* **291,** 18222–18231 (2016).

116. Kwon, D. *et al.* CMP-Neu5Ac Hydroxylase Null Mice as a Model for Studying Metabolic Disorders Caused by the Evolutionary Loss of Neu5Gc in Humans. **2015,** (2015).

117. Kwon, D., Chang, B. & Kim, J. MicroRNA Dysregulation in Liver and Pancreas of CMP-Neu5Ac Hydroxylase Null Mice Disrupts Insulin / PI3K-AKT Signaling. *Biomed Res. Int.* **2014,** (2014).

118. Chandrasekharan, K. *et al.* A Human-Specific Deletion in Mouse Cmah Increases Disease Severity in the mdx Model of Duchenne Muscular Dystrophy. *Sci. Transl. Med.* **2,** (2010).

119. Martin, P. T., Camboni, M., Xu, R., Golden, B. & Chandrasekharan, K. N-Glycolylneuraminic acid deficiency worsens cardiac and skeletal muscle pathophysiology in α-sarcoglycan-deficient mice. *Glycobiology* **23,** 833–843 (2013).

120. Martin, P. T. *et al.* A Comparative Study of N-glycolylneuraminic Acid (Neu5Gc) and Cytotoxic T Cell (CT) Carbohydrate Expression in Normal and Dystrophin-Deficient Dog and Human Skeletal Muscle. *PLoS One* **9,** 14–20 (2014).

121. Is, O. Role of CD33 and CMAH in Modulation of Microglial Responses. (University of Bonn, 2013).

122. Griciuc, A. *et al.* Alzheimer's disease risk gene CD33 inhibits microglial uptake of amyloid beta. *Neuron* **78,** 631–43 (2013).

123. Deriy, L. V *et al.* Disease-causing Mutations in the Cystic Fibrosis Transmembrane Conductance Regulator Determine the Functional Responses of Alveolar Macrophages. *J. Biol. Chem.* **284,** 35926–35938 (2009).

124. Miksa, M., Komura, H., Wu, R., Shah, K. G. & Wang, P. A Novel Method to Determine the Engulfment of Apoptotic Cells by Macrophages using pHrodo Succinimidyl Ester. *J. Immunol. Methods* **342,** 71–77 (2009).

125. Seyrantepe, V. *et al.* Regulation of phagocytosis in macrophages by neuraminidase 1. *J. Biol. Chem.* **285,** 206–215 (2010).

126. Shibuya, N. *et al.* The elderberry (Sambucus nigra L.) bark lectin recognizes the Neu5Ac(alpha 2-

6)Gal/GalNAc sequence. *J. Biol. Chem.* **262,** 1596–1601 (1987).

127. Slauch, J. M. How does the oxidative burst of macrophages kill bacteria? Still an open question. *Mol. Microbiol.* **80,** 580–583 (2011).

128. Rothe, G. & Valet, G. Flow cytometric analysis of respiratory burst activity in phagocytes with hydroethidine and 2',7'-dichlorofluorescin. *J. Leukoc. Biol.* **47,** 440–448 (1990).

129. Carter, W. O., Narayanan, P. K. & Robinson, J. P. Intracellular hydrogen peroxide and superoxide anion detection in endothelial cells. *J. Leukoc. Biol.* **55,** 253–258 (1994).

130. Claude, J., Linnartz-Gerlach, B., Kudin, A. P., Kunz, W. S. & Neumann, H. Microglial CD33-Related Siglec-E Inhibits Neurotoxicity by Preventing the Phagocytosis-Associated Oxidative Burst. *J. Neurosci.* **33,** 18270–18276 (2013).

131. Barclay, A. N. & Brown, M. H. The SIRP family of receptors and immune regulation. *Nat. Rev. Immunol.* **6,** 457–464 (2006).

132. Guilliams, M., Bruhns, P., Saeys, Y., Hammad, H. & Lambrecht, B. N. The function of Fc?? receptors in dendritic cells and macrophages. *Nat. Rev. Immunol.* **14,** 94–108 (2014).

133. Seger, R. & Krebs, E. G. The MAPK signaling cascade. *FASEB J.* **9,** 726–735 (1995).

134. Schrader, M. & Fahimi, H. D. Peroxisomes and oxidative stress. *Biochim. Biophys. Acta - Mol. Cell Res.* **1763,** 1755–1766 (2006).

135. Hume, D. A. Applications of myeloid-specific promoters in transgenic mice support in vivo imaging and functional genomics but do not support the concept of distinct macrophage and dendritic cell lineages or roles in immunity. *J. Leukoc. Biol.* **89,** 525–538 (2011).

136. Schnaar, R. L., Gerardy-Schahn, R. & Hildebrandt, H. Sialic Acids in the Brain: Gangliosides and Polysialic Acid in Nervous System Development, Stability, Disease, and Regeneration. *Physiol. Rev.* **94,** 461–518 (2014).

137. Franz, C. K., Rutishauser, U. & Rafuse, V. F. Polysialylated Neural Cell Adhesion Molecule Is Necessary for Selective Targeting of Regenerating Motor Neurons. *J. Neurosci.* **25,** 2081 LP-2091 (2005).

138. Rutishauser, U. Polysialic acid in the plasticity of the developing and adult vertebrate nervous system. *Nat. Rev. Neurosci.* **9,** 26–35 (2008).

139. Hildebrandt, H., Mühlenhoff, M., Weinhold, B. & Gerardy-Schahn, R. Dissecting polysialic acid and NCAM functions in brain development. *J. Neurochem.* **103,** 56–64 (2007).

140. Sato, C. & Kitajima, K. Disialic, oligosialic and polysialic acids: distribution, functions and related disease. *J. Biochem.* **154,** 115–136 (2013).

141. Sumida, M. *et al.* Rapid Trimming of Cell Surface Polysialic Acid (PolySia) by Exovesicular Sialidase Triggers Release of Preexisting Surface Neurotrophin. *J. Biol. Chem.* **290,** 13202–13214 (2015).

142. Varki, A. Multiple changes in sialic acid biology during human evolution. *Glycoconj. J.* **26,** 231–245 (2009).

143. Chou, H. H. *et al.* A mutation in human CMP-sialic acid hydroxylase occurred after the Homo-Pan divergence. *Proc Natl Acad Sci* **95,** 11751–6 (1998).

144. Chou, H.-H. *et al.* Inactivation of CMP-N-acetylneuraminic acid hydroxylase occurred prior to brain expansion during human evolution. *Proc Natl Acad Sci* **99,** 11736–11741 (2002).

145. Malykh, Y. N. *et al.* Distribution and localization of CMP-N-acetylneuraminic acid hydroxylase and N-glycolylneuraminic acid-containing glycoconjugates in porcine lymph node and peripheral blood lymphocytes*. *Eur. J. Cell Biol.* **80,** 48–58 (2001).

146. Martin, M. J., Rayner, J. C., Gagneux, P., Barnwell, J. W. & Varki, A. Evolution of human-chimpanzee differences in malaria susceptibility: Relationship to human genetic loss of N-glycolylneuraminic acid. *Proc Natl Acad Sci* **102,** 12819–12824 (2005).

147. Suzuki, Y. *et al.* Sialic Acid Species as a Determinant of the Host Range of Influenza A Viruses. *J. Virol.* **74,** 11825–11831 (2000).

148. Hentrich, K. *et al.* Streptococcus pneumoniae Senses a Human-like Sialic Acid Profile via the Response Regulator CiaR. *Cell Host Microbe* **20,** 307–317 (2017).

149. Mogensen, T. H. Pathogen recognition and inflammatory signaling in innate immune defenses. *Clin. Microbiol. Rev.* **22,** 240–273 (2009).

150. Nystedt, J. *et al.* Human CMP-N-Acetylneuraminic Acid Hydroxylase Is a Novel Stem Cell Marker Linked to Stem Cell-Specific Mechanisms. *Stem Cells* **28,** 258–267 (2010).

151. Bergfeld, A. K., Pearce, O. M. T., Diaz, S. L., Pham, T. & Varki, A. Metabolism of vertebrate amino sugars with N-glycolyl groups: elucidating the intracellular fate of the non-human sialic acid N-glycolylneuraminic acid. *J. Biol. Chem.* **287,** 28865–81 (2012).

152. Hopkins, A. P., Hawkhead, J. A. & Thomas, G. H. Transport and catabolism of the sialic acids N-glycolylneuraminic acid and 3-keto-3-deoxy-d-glycero-d-galactonononic acid by Escherichia coli K-12. *FEMS Microbiol. Lett.* **347,** 14–22 (2013).

153. Baker, P. R. S., Cramer, S. D., Kennedy, M., Assimos, D. G. & Holmes, R. P. Glycolate and glyoxylate metabolism in HepG2 cells. *Am. J. Physiol. Cell Physiol.* **287,** 1359–1365 (2004).

154. Schwarz, F. *et al.* Siglec receptors impact mammalian lifespan by modulating oxidative stress. *Elife* **4,** e06184 (2015).

155. Lajaunias, F., Dayer, J.-M. & Chizzolini, C. Constitutive repressor activity of CD33 on human monocytes requires sialic acid recognition and phosphoinositide 3-kinase-mediated intracellular signaling. *Eur. J. Immunol.* **35,** 243–51 (2005).

156. D'Avila, F. *et al.* Identification of lysosomal sialidase NEU1 and plasma membrane sialidase NEU3 in human erythrocytes. *J. Cell. Biochem.* **114,** 204–211 (2013).

157. D'Azzo, A., Machado, E. & Annunziata, I. Pathogenesis, emerging therapeutic targets and treatment in sialidosis. *Expert Opin. Orphan Drugs* **3,** 491–504 (2015).

158. Yogalingam, G. *et al.* Neuraminidase 1 Is a Negative Regulator of Lysosomal Exocytosis. *Dev. Cell* **15,** 74–86 (2008).

159. Zhao, M., Antunes, F., Eaton, J. W. & Brunk, U. T. Lysosomal enzymes promote mitochondrial oxidant production, cytochrome c release and apoptosis. *Eur. J. Biochem.* **270,** 3778–3786 (2003).

160. Padler-Karavani, V. *et al.* Rapid evolution of binding specificities and expression patterns of inhibitory CD33-related Siglecs in primates. *FASEB J.* **28,** 1280–93 (2014).

161. McMillan, S. J. & Crocker, P. R. CD33-related sialic-acid-binding immunoglobulin-like lectins in health and disease. *Carbohydr. Res.* **343,** 2050–2056 (2008).

162. Carlin, A. F., Lewis, A. L., Varki, A. & Nizet, V. Group B streptococcal capsular sialic acids interact with siglecs (immunoglobulin-like lectins) on human leukocytes. *J. Bacteriol.* **189,** 1231–1237 (2007).

163. Jones, C., Virji, M. & Crocker, P. R. Recognition of sialylated meningococcal lipopolysaccharide by siglecs expressed on myeloid cells leads to enhanced bacterial uptake. *Mol. Microbiol.* **49,** 1213–1225 (2003).

164. Avril, T., Wagner, E. R., Willison, H. J. & Crocker, P. R. Sialic Acid-Binding Immunoglobulin-Like Lectin 7 Mediates Selective Recognition of Sialylated Glycans Expressed on Campylobacter jejuni Lipooligosaccharides . *Infect. Immun.* **74,** 4133–4141 (2006).

165. Laszlo, G. S. *et al.* Cellular determinants for preclinical activity of a novel CD33/CD3 bispecific T-cell engager (BiTE) antibody, AMG 330, against human AML. *Blood* **123,** 554–561 (2014).

166. Van Der Velden, V. H. J. *et al.* Targeting of the CD33-calicheamicin immunoconjugate Mylotarg (CMA-676) in acute myeloid leukemia: In vivo and in vitro saturation and internalization by leukemic and normal myeloid cells. *Blood* **97,** 3197–3204 (2001).

167. Scheinberg, D. A. *et al.* A phase I trial of monoclonal antibody M195 in acute myelogenous leukemia: Specific bone marrow targeting and internalization of radionuclide. *J. Clin. Oncol.* **9,** 478–490 (1991).

168. Štefanová, I. *et al.* TCR ligand discrimination is enforced by competing ERK positive and SHP-I negative feedback pathways. *Nat. Immunol.* **4,** 248–254 (2003).

169. Bokemeyer, D., Sorokin, A. & Dunn, M. J. Multiple intracellular MAP kinase signaling cascades. *Kidney Int.* **49,** 1187–1198 (1996).

170. Ishida, T., Haneda, M., Maeda, S., Koya, D. & Kikkawa, R. Stretch-induced overproduction of fibronectin in mesangial cells is mediated by the activation of mitogen-activated protein kinase. *Diabetes* **48,** 595 LP-602 (1999).

171. Kusuhara, M., Chait, A., Cader, A. & Berk, B. C. Oxidized LDL Stimulates Mitogen-Activated Protein

Kinases in Smooth Muscle Cells and Macrophages. *Arterioscler. Thromb. Vasc. Biol.* **17,** 141 LP-148 (1997).

172. Huwiler, A., Fabbro, D. & Pfeilschifter, J. Platelet-derived growth factor stimulates de-novo synthesis of mitogen-activated protein kinase in renal mesangial cells. *Eur. J. Biochem.* **227,** 209–213 (1995).

173. Vogel, D. Y. S. *et al.* Human macrophage polarization in vitro: Maturation and activation methods compared. *Immunobiology* **219,** 695–703 (2014).

174. Turnbull, I. R. *et al.* Cutting Edge: TREM2 Attenuates Macrophage Activation. *J. Immunol.* **177,** 3520–3524 (2006).

175. Per-Arne, O. Role of CD47 and Signal Regulatory Protein Alpha (SIRPα) in Regulating the Clearance of Viable or Aged Blood Cells. *Transfus. Med. Hemotherapy* **39,** 315–320 (2012).

176. Seiffert, B. M. *et al.* Human Signal-Regulatory Protein Is Expressed on Normal, But Not on Subsets of Leukemic Myeloid Cells and Mediates Cellular Adhesion Involving Its Counterreceptor CD47. *Blood* **94,** 3633–3644 (1999).

177. Liu, D.-Q. *et al.* Signal Regulatory Protein α Negatively Regulates β2 Integrin-Mediated Monocyte Adhesion, Transendothelial Migration and Phagocytosis. *PLoS One* **3,** e3291 (2008).

178. Veillette, A., Thibaudeaut, E. & Latour, S. High expression of inhibitory receptor SHPS-1 and its association with protein-tyrosine phosphatase SHP-1 in macrophages. *J. Biol. Chem.* **273,** 22719–22728 (1998).

179. Bate, C. & Williams, A. Neurodegeneration induced by clustering of sialylated glycosylphosphatidylinositols of prion proteins. *J. Biol. Chem.* **287,** 7935–7944 (2012).

180. Yu, X., Dennison, K., Pointon, T. & Vollmer, T. Reduced Level of Sialylated IgG Antibody in the CSF of Patients with Multiple Sclerosis (P4.135). *Neurology* **82,** (2014).

181. Salminen, A. & Kaarniranta, K. Siglec receptors and hiding plaques in Alzheimer's disease. *J. Mol. Med.* **87,** 697–701 (2009).

182. van Kamp, G. J., Mulder, K., Kuiper, M. & Wolters, E. C. Changed transferrin sialylation in Parkinson's disease. *Clin. Chim. Acta* **235,** 159–167 (1995).

183. Schedin-Weiss, S., Winblad, B. & Tjernberg, L. O. The role of protein glycosylation in Alzheimer disease. *FEBS J.* **281,** 46–62 (2014).

184. Maguire, T. M., Gillian, A. M., O'Mahony, D., Coughlan, C. M. & Breen, K. C. A decrease in serum sialyltransferase levels in Alzheimer's disease. *Neurobiol. Aging* **15,** 99–102 (1994).

185. Maguire, T. M. & Breen, K. C. A decrease in neural sialyltransferase activity in Alzheimer's disease. *Dement. Geriatr. Cogn. Disord.* **6,** 185–190 (1995).

186. Fodero, L. R. *et al.* Wheat germ agglutinin-binding glycoproteins are decreased in Alzheimer's

disease cerebrospinal fluid. *J. Neurochem.* **79,** 1022–1026 (2001).

187. Taniguchi, M. *et al.* Sugar Chains of Cerebrospinal Fluid Transferrin as a New Biological Marker of Alzheimer's Disease. *Dement. Geriatr. Cogn. Disord.* **26,** 117–122 (2008).

188. Tienari, P. J. *et al.* The beta-amyloid domain is essential for axonal sorting of amyloid precursor protein. *EMBO J.* **15,** 5218–5229 (1996).

189. McFarlane, I., Georgopoulou, N., Coughlan, C. M., Gillian, A. M. & Breen, K. C. The role of the protein glycosylation state in the control of cellular transport of the amyloid β precursor protein. *Neuroscience* **90,** 15–25 (1999).

190. Nakagawa, K. *et al.* Sialylation enhances the secretion of neurotoxic amyloid-β peptides. *J. Neurochem.* **96,** 924–933 (2006).

191. Yazaki, M. *et al.* Mutation of potential N-linked glycosylation sites in the Alzheimer's disease amyloid precursor protein (APP). *Neurosci. Lett.* **221,** 57–60 (1996).

192. Akasaka-Manya, K. *et al.* Increased bisecting and core-fucosylated N-glycans on mutant human amyloid precursor proteins. *Glycoconj. J.* **25,** 775–786 (2008).

193. Perdivara, I. *et al.* Elucidation of O-Glycosylation Structures of the β-Amyloid Precursor Protein by Liquid Chromatography−Mass Spectrometry Using Electron Transfer Dissociation and Collision Induced Dissociation. *J. Proteome Res.* **8,** 631–642 (2009).

194. Kitazume, S. *et al.* Brain endothelial cells produce amyloid {beta} from amyloid precursor protein 770 and preferentially secrete the O-glycosylated form. *J. Biol. Chem.* **285,** 40097–40103 (2010).

195. Kitazume, S., Saido, T. C. & Hashimoto, Y. Alzheimer's beta-secretase cleaves a glycosyltransferase as a physiological substrate. *Glycoconj. J.* **20,** 59–62 (2004).

196. Kitazume, S. *et al.* In vivo cleavage of alpha2,6-sialyltransferase by Alzheimer beta-secretase. *J. Biol. Chem.* **280,** 8589–8595 (2005).

197. Kitazume, S. *et al.* Characterization of α2,6-sialyltransferase cleavage by Alzheimer's β-secretase (BACE1). *J. Biol. Chem.* **278,** 14865–14871 (2003).

198. d'Azzo, A. & Bonten, E. Molecular Mechanisms of Pathogenesis in a Glycosphigolipid and a Glycoprotein Storage Disease. *Biochem. Soc. Trans.* **38,** 1453–1457 (2010).

199. Annunziata, I. *et al.* Lysosomal NEU1 deficiency affects amyloid precursor protein levels and amyloid-β secretion via deregulated lysosomal exocytosis. *Nat. Commun.* **4,** (2013).

200. Sato, Y., Naito, Y., Grundke-Iqbal, I., Iqbal, K. & Endo, T. Analysis of N-glycans of pathological tau: possible occurrence of aberrant processing of tau in Alzheimer's disease. *FEBS Lett.* **496,** 152–160 (2001).

201. Liu, F. *et al.* Role of glycosylation in hyperphosphorylation of tau in Alzheimer's disease. *FEBS Lett.* **512,** 101–106 (2002).

202. Liu, F., Zaidi, T., Iqbal, K., Grundke-Iqbal, I. & Gong, C.-X. Aberrant glycosylation modulates phosphorylation of tau by protein kinase A and dephosphorylation of tau by protein phosphatase 2A and 5. *Neuroscience* **115,** 829–837 (2002).

203. Arnold, C. S. *et al.* The microtubule-associated protein tau is extensively modified with O-linked N-acetylglucosamine. *J. Biol. Chem.* **271,** 28741–28744 (1996).

204. Liu, F. *et al.* Reduced O-GlcNAcylation links lower brain glucose metabolism and tau pathology in Alzheimer's disease. *Brain* **132,** 1820–1832 (2009).

205. Li, X., Lu, F., Wang, J.-Z. & Gong, C.-X. Concurrent alterations of O-GlcNAcylation and phosphorylation of tau in mouse brains during fasting. *Eur. J. Neurosci.* **23,** 2078–2086 (2006).

206. Liu, F., Iqbal, K., Grundke-Iqbal, I., Hart, G. W. & Gong, C.-X. O-GlcNAcylation regulates phosphorylation of tau: A mechanism involved in Alzheimer's disease. *Proc. Natl. Acad. Sci.* **101,** 10804–10809 (2004).

207. Walter, R. B., Raden, B. W., Kamikura, D. M., Bernstein, I. D. & Cooper, J. A. Lysosomal Degradation of CD33, the Target for the Anti-Leukemia Immunoconjugate, Gemtuzumab Ozogamicin: Evidence for Cbl-Mediated Monoubiquitination. *Blood* **106,** 2469 LP-2469 (2005).

208. Van Muiswinkel, F. L., Veerhuis, R. & Eikelenboom, P. Amyloid β Protein Primes Cultured Rat Microglial Cells for an Enhanced Phorbol 12-Myristate 13-Acetate-Induced Respiratory Burst Activity. *J. Neurochem.* **66,** 2468–2476 (1996).

209. Klegeris, A., Walker, D. G. & Mcgeer, P. L. Activation of Macrophages by Alzheimer β Amyloid Peptide. *Biochem. Biophys. Res. Commun.* **199,** 984–991 (1994).

210. Aluise, C. D. *et al.* Preclinical Alzheimer Disease: Brain Oxidative Stress, Aβ Peptide & Proteomics. *Neurobiol. Dis.* **39,** 221–228 (2010).

211. Vitek, M. P. *et al.* Advanced glycation end products contribute to amyloidosis in Alzheimer disease. *Proc. Natl. Acad. Sci.* **91,** 4766–4770 (1994).

212. Smith, C. D. *et al.* Excess brain protein oxidation and enzyme dysfunction in normal aging and in Alzheimer disease. *Proc. Natl. Acad. Sci.* **88,** 10540–10543 (1991).

213. Bowling, A. C. & Beal, M. F. Bioenergetic and oxidative stress in neurodegenerative diseases. *Life Sci.* **56,** 1151–1171 (1995).

214. Ferri, C. P. *et al.* Global prevalence of dementia: a Delphi consensus study. *Lancet* **366,** 2112–7 (2005).

215. Graham, L. C. *et al.* Chronic consumption of a western diet induces robust glial activation in aging mice and in a mouse model of Alzheimer's disease. *Sci. Rep.* **6,** 1–13 (2016).

216. N., S. S. *et al.* Physical activity, diet, and risk of Alzheimer disease. *JAMA* **302,** 627–637 (2009).

217. Scarmeas, N., Stern, Y., Mayeux, R. & Luchsinger, J. A. Mediterranean diet, Alzheimer disease,

and vascular mediation. *Arch Neurol* **63,** 1709–1717 (2006).

9. DECLARATION

I, hereby confirm that this work submitted is my own. This thesis has been written independently and with no other sources and aids than stated. The presented thesis has not been submitted to another university and I have not applied for a doctorate procedure so far.

Hiermit versichere ich, dass die vorgelegte Arbeit – abgesehen von den ausdrücklich bezeichneten Hilfsmitteln – persönlich, selbständig und ohne Benutzung anderer als der angegebenen Hilfsmittel angefertigt wurde. Aus anderen Quellen direkt oder indirekt übernommenen Daten und Konzepte sind unter Angabe der Quelle kenntlich gemacht worden.

Die vorliegende Arbeit wurde an keiner anderen Hochschule als Dissertation eingereicht. Ich habe früher noch keinen Promotionsversuch unternommen.

Bonn, February 2018

Ozkan Is